Order Number 9215030

A study of 1/f noise in the normal state of high-T_c superconductors

Misra, Anupam Kumar, Ph.D.

University of Hawaii, 1991

U·M·I

300 N. Zeeb Rd.
Ann Arbor, MI 48106

A STUDY OF 1/f NOISE IN THE NORMAL STATE OF HIGH-T_c SUPERCONDUCTORS

A DISSERTATION SUBMITTED TO THE GRADUATE DIVISION OF THE UNIVERSITY OF HAWAII IN PARTIAL FULFILLMENT OF THE REQUIREMENTS FOR THE DEGREE OF

DOCTOR OF PHILOSOPHY

IN

PHYSICS

DECEMBER 1991

BY

Anupam Kumar Misra

Dissertation Committee:

James R. Gaines, Chairperson
Vincent Z. Peterson
Peter P. Crooker
Chester A. Vause III
John W. Gilje

ACKNOWLEDGEMENTS

I wish to express my sincere appreciation to my advisor, Prof. James R. Gaines, for his valuable advice, encouragement and support during the entire stages of my graduate work and significantly for accepting me as his graduate student. I am grateful to Dr. Yi Song who introduced me to this field of study, supervised my work, and provided invaluable help and support from the beginning of my research to its completion. Working with him has been an important part of my life; I have learned and will continue to learn much from him.

A very special thanks goes to Antonio Querubin, who is recognized as the computer expert of the department, for his valuable contributions in maintaining the computer systems and other electronic devices in the lab. He was always available and willing to help, in spite of his very busy schedule. I am also thankful to other members of the group: X. D. Chen, Yue Cao, Chian Chiu Li, Fred Matsunaga, and Judy Nakamura for their contributions in operating the lab and maintaining a friendly atmosphere. Judy saved time and energy by handling the paper work essential to this research. Fred, a wise and gentle person, taught me many things through his experience and a keen knowledge of vacuum systems. I wish him a very long and healthy life.

I am very thankful to Roy Tom and Melvin Matsunaga for their expert technical work. They built many parts of the equipments and their contribution in maintaining and installing equipments is highly appreciated.

I am indebted to a number of people: Christopher J. Bushing and Jane S. Tribble (who are members of SOEST, X-ray diffraction facility), and Donald McGee (member of SOEST, Analytical Electron Microscope Laboratory) for letting me use their facilities and helping me in various ways. A special thanks goes to Tina M. Weatherby of Biological

Electron Microscope Facility, PBRC for training me to use their scanning electron microscope. X-ray diffraction on single crystals were done in Roger E. Cramer's lab (chemistry dept.) by Philip Palatano and the photographs of the single crystals were taken by the expert photographer of HIG, Mr. Tom Tatnall.

Thin film samples were supplied by Albert H. Cardona of Superconductor Technologies, Inc., California. His contribution is an important part of this study.

I am also grateful to Chuck Hayes who made it possible for me to attend the University of Hawaii and helped me in many ways. I am thankful to my dissertation committee : Dr. Vincent Peterson, Dr. Peter Crooker, Dr. Chester Vause, and Dr. John Gilje for giving their precious time and advice for the improvement of this work. I would like to express my sincere thanks to Prof. John Gilje, who kept us out of danger by providing valuable information on the chemical properties (especially the toxic nature) of various chemicals.

Finally, I am grateful to my parents, brothers, sister and friends for their moral support and love.

ABSTRACT

1/f noise measurements were done on two classes of materials, $Tl_2Ba_2Ca_{n-1}Cu_nO_{4+2n}$ (n=2,3) and $Y_1Ba_2Cu_3O_x$, that exhibit superconductivity above 77K. In $Tl_2Ba_2Ca_{n-1}Cu_nO_{4+2n}$ materials, 1/f noise was measured on thin films and bulk samples. The measurements on the bulk samples of these materials are the first reported. The obtained experimental results on these samples indicate that 1/f noise is not an intrinsic property of high-T_c superconductors. Two important facts were discovered. First, a very low noise level was observed in the thin film samples and second, in the superconducting transition region, no enhanced noise was observed for some samples. Both these results, which are important from both physics and engineering point of views, are reported for the first time.

In $Y_1Ba_2Cu_3O_x$ material, measurements of 1/f noise were done on single crystals in order to obtain more fundamental results. The measurements on the single crystals are the first reported. The measurements were performed in two crystallographic directions, ab-planes and c-axes, of the crystals. Noise level and its temperature dependence were found to be similar in both the directions, in spite of a very different resistivity behavior, in the normal state of the material. In the superconducting transition region, anisotropic behavior of 1/f noise was observed. The noise was found to be enhanced by several orders of magnitude along the c-axis of the crystal and no such enhancement of noise was observed in the ab-plane of the crystal. The anisotropic behavior of 1/f noise is the first reported. Possible explanations for the observed anisotropic behavior of noise are discussed along with various models. The plausible sources of 1/f noise in these materials are then argued to be related to tunneling conduction mechanism and thermally activated vortex motion.

TABLE OF CONTENTS

ACKNOWLEDGEMENTS iv

ABSTRACT vi

LIST OF TABLES xi

LIST OF FIGURES xii

I INTRODUCTION 1

1.1 Motivation 1

1.2 Outline of the thesis 2

1.3 Definitions and mathematical background 3

1.4 Introduction to noise 8

1.4.1 Thermal noise 8

1.4.2 Shot noise 9

1.4.3 Generation-Recombination noise 10

1.4.4 1/f noise 10

References 12

II THEORETICAL MODELS OF 1/f NOISE 14

2.1 General properties of 1/f noise 14

2.2 Hooge's empirical formula 17

2.3 Thermal fluctuation model 19

2.4 The McWhorter model 22

2.5 The Dutta, Dimon, and Horn model 24

2.6 Two component model by Mantese 27

2.7 Quantum model by Handel 29

References 30

III SAMPLE PREPARATION 32

3.1 Preparation of bulk samples of $Tl_2Ba_2Ca_{n-1}Cu_nO_{4+2n}$ (n=2,3) 32

3.2 Preparation of $Tl_2Ba_2Ca_1Cu_2O_8$ thin films 39

References 42

IV SINGLE CRYSTAL GROWTH OF $Y_1Ba_2Cu_3O_x$ 43

4.1 Introduction 43

4.2 Experimental details 44

4.3 Experimental results 46

4.3.1 Effect of starting materials 46

4.3.2 Effect of the starting stoichiometry 47

4.3.3 Geometrical factors 57

4.3.4 The choice of crucibles 59

4.3.5 Effect of the highest heating temperature 62

4.3.6 Effect of the cooling rate 64

4.3.7 Effect of the plateau temperature 66

4.3.8 Re-baking for better yield 66

4.4 Discussion 67

4.5 Conclusion 71

References 72

V EXPERIMENTAL SETUP 74

5.1 Resistivity measurement 74

5.2 Susceptibility measurement 78

5.3 1/f noise measurement 83

5.4 Error analysis 89

References 98

VI EXPERIMENTAL RESULTS 99

6.1 1/f noise in bulk samples of $Tl_2Ba_2Can\text{-}_1Cu_nO_{4+2n}$ 102

6.1.1 1/f noise in bulk samples of $Tl_2Ba_2Ca_1Cu_2O_8$ 102

6.1.2 /f noise in bulk sample of $Tl_2Ba_2Ca_2Cu_3O_{10}$ 108

6.2 1/f noise in $Tl_2Ba_2Ca_1Cu_2O_8$ thin films 110

6.3 1/f noise in $Y_1Ba_2Cu_3O_{7-\delta}$ single crystals 117

References 130

VII DISCUSSION 132

7.1 Self consistency of experimental results 133

7.1.1 Noise in thin films 133

7.1.2 Noise in bulk samples 134

7.1.3 Conclusions based on the experimental results 136

7.2 Comparison of the data with models 138

7.2.1 Comparison with Hooge's empirical formula 138

7.2.2 Comparison with thermal fluctuation model 139

7.3 1/f noise in the normal state (tunneling mechanism) 141

7.3.1 MIM junctions model 141

7.3.2 Success of MIM junction model 145

7.3.3 Mantese's two component model 146

7.3.4 Justification for the existence of MIM juctions 148

7.3.5 The source of 1/f noise: point defects vs twin boundaries 149

7.4 1/f noise in the superconducting state : vortex motion..... 151

7.4.1 Limitations of experimental techniques for noise measurements..... 151

7.4.2 Magnetic 1/f noise vs electric 1/f noise..... 153

7.4.3 Magnetic flux model..... 154

7.5 1/f noise in the transition region (anisotropic behavior)..... 155

7.5.1 Thermally activated flux motion & 1/f noise..... 157

7.5.2 Anisotropic 1/f noise: difference in activation energies..... 157

7.5.3 Enhanced noise: comparison with thermal fluctuation model.... 160

7.5.4 The effect of twin boundaries: anisotropic 1/f noise..... 161

7.5.5 Flux lattice melting and 1/f noise..... 163

7.6 Conclusions..... 164

References..... 166

LIST OF TABLES

3.1 Thermal history and results of resistivity measurement of TlBaCaCuO samples..38

4.1 Details of heating procedure and type of crystal grown..... 52

4.2 Value of resistivity for as grown crystals..... 56

4.3 Effect of highest heating temperature on crystal growth..... 63

LIST OF FIGURES

3.1 Arrangement of alumina crucibles for preparation of $Tl_2Ba_2Ca_{n-1}Cu_nO_{4+2n}$..... 36

3.2 SEM photograph of several $Tl_2Ba_2Ca_1Cu_2O_8$ thin films..... 40

3.3 SEM photograph showing the microstructure of a $Tl_2Ba_2Ca_1Cu_2O_8$ thin film..... 41

4.1 Y_2O_3-BaO-CuO ternary phase diagram 48

4.2 A plate-like crystal of size 6.1x4.8x0.05mm^3 grown from $Y_{1,4.33,8}$ 49

4.3 The other side of the crystal shown in Fig. 4.2..... 49

4.4 Block crystals grown from $Y_{1,4.33,8}$..... 50

4.5 Plate-like crystals grown from composition $Y_{1,6,13}$..... 50

4.6 Block-like crystals grown from composition $Y_{1,6,13}$..... 51

4.7 Plate like crystal of size 7.3x7x0.14mm^3 grown from $Y_{1,6,13}$..... 51

4.8 Normalized electrical resistance in the ab-planes vs temperature for as grown crystals..... 54

4.9 Normalized c-axis electrical resistance vs temperature for as grown crystals. 55

4.10 Geometrical arrangement of crucible and powder for crystal growth..... 58

4.11 Normalized resistance vs temperature for an oxygen annealed crystal grown in alumina crucible..... 60

4.12 Energy dispersive spectrum of a $Y_1Ba_2Cu_3O_x$ single crystal..... 61

4.13 Thickness of plate-like crystals vs cooling rate..... 65

4.14 Normalized resistance vs temperature for as grown crystal, grown on gold.... 69

4.15 Normalized resistance vs temperature for an oxygen annealed crystal, grown on gold..... 70

5.1 Four-probe method for resistivity measurement..... 75

5.2 Circuit diagram for the susceptibility measurement..... 79

5.3 Susceptibility vs temperature for a $Tl_2Ba_2Ca_2Cu_3O_{10}$ bulk sample..... 80

5.4 Susceptibility vs temperature for a $Y_1Ba_2Cu_3O_x$ single crystal..... 81

5.5 DC four-probe cross-correlation method for noise measurement..... 84

5.6 Noise spectral density $S_v(f)$ vs frequency for $Y_1Ba_2Cu_3O_x$ single crystal..... 87

5.7 Schematic diagram for two-probe and four-probe methods..... 90

5.8 Resistance as a function of temperature for $Y_1Ba_2Cu_3O_x$ single crystal for different values of driving current..... 92

5.9 The difference between the sample temperature and thermal sensor as a function of driving current..... 94

5.10 The resistance vs temperature data of Fig. 5.8 replotted as a function of corrected temperature..... 95

5.11 The normalized noise spectral density, with error bars, vs temperature..... 96

6.1 The electrical resistivity as a function of temperature for bulk samples of $Tl_2Ba_2Ca_1Cu_2O_8$..... 101

6.2 The normalized noise spectral density Sn for bulk samples of $Tl_2Ba_2Ca_1Cu_2O_8$ as a function of temperature..... 103

6.3 The electrical resistivity as a function of temperature for bulk samples of $Tl_2Ba_2Ca_2Cu_3O_{10}$..... 106

6.4 The normalized noise spectral density Sn for bulk samples of $Tl_2Ba_2Ca_2Cu_3O_{10}$ as a function of temperature..... 107

6.5 The electrical resistivity measured on thin films of $Tl_2Ba_2Ca_1Cu_2O_8$ as a function of temperature..... 109

6.6 Normalized 1/f noise spectral density S_v/V^2 vs sample temperature for thin film sample A..... 111

6.7 Normalized 1/f noise spectral density S_v/V^2 vs sample temperature for thin film sample B..... 112

6.8 Normalized resistance as a function of temperature for single crystals of $Y_1Ba_2Cu_3O_x$ in the ab-planes..... 116

6.9 Normalized 1/f noise spectral density S_V/V^2 vs sample temperature for single crystals of $Y_1Ba_2Cu_3O_x$ in the ab-planes 118

6.10 Normalized resistance as a function of temperature for single crystals of $Y_1Ba_2Cu_3O_x$ along the c-axes 121

6.11 Normalized 1/f noise spectral density S_V/V^2 vs sample temperature for single crystals of $Y_1Ba_2Cu_3O_x$ along the c-axes 122

6.12 Normalized resistance and noise spectral density as a function of temperature for single crystal of $Y_1Ba_2Cu_3O_x$ (sample 2) 125

6.13 Normalized resistance and noise spectral density as a function of temperature for single crystal of $Y_1Ba_2Cu_3O_x$ (sample 3) 126

6.14 The normalized noise spectral density Sn for bulk, thin film and single crystal samples as a function of temperature 128

7.1 Normalized noise density calculated from Voss-Clarke model 140

7.2 A schematic diagram of the metal-insulator-metal junction 142

7.3 Normalized noise density calculated from the MIM model 144

7.4 An Arrhenius plot for single crystal of $Y_1Ba_2Cu_3O_x$ (sample 2) 156

7.5 1/f noise spectral density and square of temperature derivative of resistance as a function of temperature 158

7.6 1/f noise spectral density and temperature derivative of resistance as a function of temperature 159

CHAPTER 1

INTRODUCTION

1.1 Motivation

The phenomenon of noise is important in science since it sets lower limits to the reliability of any measurement. Understanding the behavior of noise and its sources is crucial in designing any electronic device. For example, in the case of sound amplifiers, circuits are designed to have minimum noise in the audio-frequency range. The noises outside the audio-frequency range are not crucial for the sound amplifier. A knowledge of frequency dependence of various noises is essential to suit the above purpose. The study of fluctuation is also of interest to fundamental physics since it relates the fluctuating quantities with the equilibrium state properties of a system. For example, existence of Brownian motion is essential in attaining the thermal equilibrium and then maintaining it. Apart from its importance to science, noise has its influence on our daily life; our hearing power and health are affected by the noise level. Signal-to-noise ratio determines our choice of stereo, television, home, radio station, telephone company etc.

Most electrical noises are well understood with their theories predicting the experimental results and helping us in designing electronic devices with low noise levels. However, there is one exception -- 1/f noise --, which often causes trouble at low frequencies. At low frequencies ($f << 1000$Hz), 1/f noise is the dominant source of electronic noise, its value being several orders of magnitude higher than other electronic noises. The electrical 1/f noise occurs in contacts, thin films, resistors, semiconductors, metals, superconductors, and in nearly all electronic devices. In spite of such omnipresence and half a century of research on 1/f noise, there is no accepted

theory explaining 1/f noise. Experimentally, the source (or sources) of 1/f noise has not been singled out.

The recent discovery of high Tc superconductors [1] showing superconductivity well above the boiling point of liquid nitrogen [2] has raised great interest in these materials because of their potential technical applications. A study of noise in these materials is important and critical in determining their suitability for use in certain devices. In the past, studies of 1/f noise in high Tc superconductors have given negative results, characterizing these materials as highly noisy [3,4]. Previous studies of 1/f noise on superconducting materials have supported one type of theoretical model of 1/f noise based on thermal fluctuations. Since this model has been found to be inadequate in other systems, a careful study of 1/f noise in these materials was needed to understand the phenomenon of 1/f noise. Study of 1/f noise in high Tc superconductors is also of interest from a technological point of view.

1.2 Outline of the thesis

This thesis summarizes research on the study of 1/f noise in the normal state of high Tc superconductors. 1/f noise was studied on two classes of high Tc superconductors which show superconductivity above the boiling point of liquid nitrogen: $Y_1Ba_2Cu_3O_7$ and $Tl_2Ba_2Ca_{n-1}Cu_nO_{4+2n}$. In the Tl-based superconductors the measurements were done on bulk and thin film samples. In the $Y_1Ba_2Cu_3O_7$, study of 1/f noise was done on single crystal samples in order to get more fundamental results.

In the remainder of this chapter (section 1.3), I briefly discuss the general mathematical background and definition of various terms generally encountered in the study of noise. More detailed theories of various types of noise and discussion of

mathematical theorems can be found in the references 5 to 7. In section 1.4, a general introduction to various types of noise, commonly observed in conductors, is given.

Chapter 2 describes the various existing theoretical models of 1/f noise. A brief note on the properties of 1/f noise is given in the beginning of this chapter. Sample preparation techniques for Tl-based superconductors are discussed in chapter 3. An extensive study of crystal growth of $Y_1Ba_2Cu_3O_7$ is given in chapter 4. The results obtained from the crystal growth study are summarized in this chapter itself. The results are useful for growing good, large single crystals of $Y_1Ba_2Cu_3O_7$. Experimental setups for the measurement of resistivity, susceptibility and 1/f noise are described in chapter 5. At the end of this chapter, the analysis of various errors is included. Experimental data and results are given in chapter 6 and finally, the discussion of the results and conclusion of this thesis is given in chapter 7.

1.3 Definitions and mathematical background

The instantaneous value of a quantity x showing fluctuations can be written as

$$x(t) = \langle x \rangle + \Delta x(t) \qquad (1)$$

where <x> is the average value of x and $\Delta x(t)$ is the amount of deviation from the average value of x at time t. For statistically stationary noise $\langle \Delta x \rangle = 0$ and $\langle (\Delta x)^2 \rangle$=constant, where <> represents the time average.

A variable x(t) can be expanded in a Fourier series if it is strictly periodic with a time constant $T = 1/f_o$, where f_o is the fundamental frequency of x(t). In this case, the fourier coefficients would be completely known numbers and would define the frequency spectrum of the variable x(t). If, on the other hand, the given variable is a more or less random function of time, then the fourier coefficients would themselves be statistical in

nature. To apply the concept of periodicity to such a function, one must consider the time interval infinitely large i.e. $T\to\infty$. One can use the Fourier integral formalism followed by ensemble averaging to determine the average spectral content of random fluctuation. The Fourier transform and its inverse are defined as

$$X(\omega) = \int_{-\infty}^{\infty} x(t)\, \exp(-i\omega t)\, dt \qquad (2)$$

$$x(t) = \frac{1}{2\pi}\int_{-\infty}^{\infty} X(\omega)\, \exp(i\omega t)\, d\omega \qquad (3)$$

A natural interpretation of $X(\omega)$ is that it is the amplitude spectrum of $x(t)$, giving a measure of the contribution to $x(t)$ from waves with angular frequencies between ω and $\omega+d\omega$.

Suppose now that a noise process is observed over the interval [-T/2, T/2], so that outside this time interval its ordinate values can be regarded as zero. Using Parseval's Theorem

$$\int_{-\infty}^{\infty} x_1(t)x_2^*(t)\, dt = \frac{1}{2\pi}\int_{-\infty}^{\infty} X_1(\omega)X_2^*(\omega)\, d\omega \qquad (4)$$

we can write

$$\int_{-\infty}^{\infty} [x_T(t)]^2\, dt = \frac{1}{2\pi}\int_{-\infty}^{\infty} |X_T(\omega)|^2\, d\omega \qquad (5)$$

where the subscript T refers to the time interval in which the fluctuations are non-zero. The above equation (5) is known as Plancherel's theorem or the Energy theorem. Each side of equation (5) equals the total energy of the fluctuations. The average power in the noise process is the total energy divided by T, which as $T\to\infty$ becomes

$$\lim_{T\to\infty} \frac{1}{T}\int_{-\infty}^{\infty} [x_T(t)]^2\, dt = \lim_{T\to\infty} \frac{1}{2\pi}\int_0^{\infty} \frac{2|X_T(\omega)|^2}{T}\, d\omega \qquad (6)$$

since $x_T(t)$ is real, the integral on the right hand side of equation (6) has been limited to positive frequencies and a factor of 2 incorporated. The term $2|X_T(\omega)|^2/T$ has dimensions of power per hertz. The average power spectral density of the stationary process $x_T(t)$ is then defined as the ensemble average

$$S_x(\omega) = \lim_{T\to\infty} \overline{\frac{2|X_T(\omega)|^2}{T}} \qquad (7)$$

where the overbar represents the ensemble average. From Parseval's theorem (equation (4)) one can write

$$\int_{-\infty}^{\infty} x_T(t+\tau)x_T(t)\, dt = \frac{1}{2\pi}\int_{-\infty}^{\infty} |X_T(\omega)|^2 \exp(i\omega\tau)\, d\omega \qquad (8)$$

which can be written in terms of power spectral density, by dividing both sides by T, ensemble averaging and taking the limit as $T\to\infty$

$$\lim_{T\to\infty} \frac{1}{T}\int_{-\infty}^{\infty} \overline{x_T(t+\tau)x_T(t)}\, dt = \lim_{T\to\infty} \frac{1}{2\pi}\int_0^{\infty} \overline{\frac{2|X_T(\omega)|^2}{T}} \cos(\omega\tau)\, d\omega \qquad (9)$$

where the left hand side of the above equation is the ensemble averaged autocorrelation function $\overline{K_x(\tau)}$, which is equal to the autocorrelation function of any one of the member functions of the ensemble, provided the process is stationary. The above equation is then written in the form

$$K_x(\tau) = \frac{1}{2\pi}\int_0^{\infty} S_x(\omega) \cos(\omega\tau) d\omega \qquad (10)$$

The inverse of above Fourier transform relation is

$$S_x(\omega) = 4\int_0^{\infty} K_x(\tau)\cos(\omega\tau)d\tau \qquad (11)$$

Equations (10) and (11) constitute the Wiener-Khintchine theorem [8].

The autocorrelation function $K(\tau)$ is a measure of the statistical correlation between the value of the fluctuating variable x at time t_1 and its value at time $t_1+\tau$. One of the important properties of the autocorrelation function is that in a stationary ensemble, the autocorrelation function depends only on the time interval τ. In general, the autocorrelation function is defined as

$$K(t_1,t_1+\tau) \equiv \overline{x(t_1)\cdot x(t_1+\tau)} = K(\tau) \qquad \text{(independent of } t_1) \qquad (12)$$

The quantity K(0) is identically equal to the mean square value of the variable x at time t_1 and must be positive, and $K(0) \geq |K(\tau)|$ for all τ. As τ becomes large in comparison with the characteristic time τ^* of the process, the values of $x(t_1)$ and $x(t_1+\tau)$ become uncorrelated, that is

$$K(\tau) \equiv \overline{x(t_1)\cdot x(t_1+\tau)} \rightarrow \overline{x(t_1)} \cdot \overline{x(t_1+\tau)} = 0 \qquad \text{for } \tau>>\tau^* \qquad (13)$$

We shall now examine some special cases to illustrate the use of the Wiener-Khintchine theorem:

(1) If the variable x(t) is extremely irregular, then the autocorrelation function $K(\tau)$ would extend over a negligibly small range of the time interval τ. Then

$$K(\tau) = c\,\delta(\tau) \qquad (14)$$

where c is a constant. From the Wiener-Khintchine theorem, the average power spectral density will be

$$S_x(\omega) = 4\int_0^{\infty} c\delta(\tau)\cos(\omega\tau)\,d\tau = 2c \qquad (15)$$

hence the spectrum is independent of frequency. A frequency independent average power density spectrum is called "white".

(2) On the other hand, if the variable x(t) is extremely regular and hence predictable, then the correlation function would extend over considerably large value of τ. In the simplest case of a monochromatic variable of characteristic frequency ω_o, the correlation function is given by

$$K(\tau) = K(0)\cos(\omega_0\tau) \qquad (16)$$

for which

$$S(\omega) = K(0)\,\delta(\omega-\omega_0) \qquad (17)$$

The power spectrum then appears in the form of a peak located at the characteristic frequency.

(3) Consider a relaxation process, which is usually encountered in solid state devices, and is characterized by the decay equation

$$\frac{d\Delta x}{dt} = -\frac{\Delta x}{\tau^*} \qquad (18)$$

where τ^* is the decay constant. Solution of the decay equation is of the form

$$\Delta x(t) = \Delta x(0)\exp(\frac{-t}{\tau^*}) \qquad (19)$$

The autocorrelation function is then given by

$$K_x(\tau) = K_x(0)\exp(\frac{-\tau}{\tau^*}) \qquad (20)$$

where $K_X(0) = \overline{(\Delta x)^2}$ is the variance of the process. The power spectral density of the process is given by

$$S_X(\omega) = \overline{(\Delta x)^2}\ \frac{4\tau^*}{1 + \omega^2\tau^{*2}} \qquad (21)$$

This type of spectrum is called Lorentzian. It is flat when $\omega << 1/\tau^*$ and it rolls off as $1/\omega^2$ when $\omega >> 1/\tau^*$.

In general, the power spectrum $S(\omega)$ of a fluctuating variable x(t) is completely determined by the autocorrelation function $K(\tau)$ of the same variable.

1.4 Introduction to noise

In most materials and electronic devices, various kinds of noise processes are observed. The most commonly encountered types of noise are thermal noise, shot noise, generation-recombination noise and 1/f noise. The first three types of noise are well understood and their detailed theories can be found in references 5 and 6. A brief introduction of these types of noise is given below:

1.4.1 Thermal noise

Thermal noise arises from random velocity fluctuations of the charge carriers in a material. The mechanism is said to be the Brownian motion of charge carriers due to thermal energy. The mechanism of the Brownian motion is vital in formulating and solving problems as to how "a physical system, which is not in a state of equilibrium, finally approaches a state of equilibrium," while "a physical system which is already in the state of equilibrium, persist in that state." Thermal noise is even present when a system is in thermal equilibrium with its surrounding. Thermal noise may be regarded as the mechanism by which the state of thermal equilibrium is maintained : on average, a random departure from the equilibrium state is followed by a relaxation back towards it.

In the equilibrium state, the thermal motion of charge carrier has an average energy of kT/2, where k is the Boltzmann's constant, T is temperature. The relaxation time is extremely fast ($\tau \approx 10^{-12}$s), so that at all frequencies, $f << 10^{12}$Hz, the power spectrum of thermal noise is white. By considering a simple LC circuit with a random frequency-independent thermal noise source, Nyquist [9] was able to derive the spectral density of the thermal noise in the limit $f << (kT/h)$ as

$$S_{v,thermal} = 4kTR$$

where h is Planck's constant and R is sample resistance. The thermal noise can not be reduced by whatever method of sample preparation is used. However, since its value is easily determined and is independent of frequency, it does not create any problem when studying other types of noise.

1.4.2 Shot noise

Shot noise is generated when charge carriers pass through an energy gap. Shot noise is a non-equilibrium form of noise and was first discussed by Schottky [10], who used the analogy of small shot pattering into a container. Shot noise is frequently encountered in solid state devices, whenever a current flows across a potential barrier such as the depletion region of a p-n junction. The nature of shot noise is easily understood in a thermionic diode in which electrons are randomly emitted from the cathode and then drift across to the anode under the influence of the electric field. The current associated with the stream of electrons fluctuates randomly about a mean level due to the random, discrete nature of the emission process. Because of the very short transit time τ^* of the electrons ($\approx 10^{-9}$s), the spectral density of shot noise is independent of frequency in the low frequency region ($f << 1/\tau^*$) and is given by

$$S_I = 2eI$$

where e is the electron charge and I is the current. Both thermal noise and shot noise have similar waveforms but the physical origins of the noise are distinct.

1.4.3 Generation-Recombination noise

In intrinsic materials, processes involving generation and recombination of free electrons and free holes occur. In addition to these processes, there is continuous trapping and detrapping of charge carriers due to the number of trap levels usually present in semiconductors. As a result, the total number of free charge carriers fluctuates. Such fluctuations in the number of charge carriers can be represented by the equation

$$\frac{d\Delta N}{dt} = -\frac{\Delta N}{\tau^*}$$

where ΔN is the fluctuation in number of carriers and τ^* is the life time of the added carriers ($\approx 10^{-5}$s). The spectral density of generation-recombination noise is Lorentzian, given by

$$S_N(\omega) = \overline{(\Delta N)^2}\ \frac{4\tau^*}{1+\omega^2\tau^{*2}}$$

It is flat when $\omega << 1/\tau^*$ and it rolls off as $1/\omega^2$ when $\omega >> 1/\tau^*$.

1.4.4 1/f noise

1/f noise is also called flicker noise. It has a power spectral density which varies as $1/f^{\alpha}$, where α lies between 0.8 and 1.4. The name "1/f noise" comes from the shape of the power spectrum. This spectral shape has been observed over a wide frequency range from 10^{-6} Hz to 10^{6} Hz. At very high frequencies, 1/f noise is usually masked by the thermal noise; hence at these frequencies its existence is difficult to establish.

Noise obeying the inverse frequency power law is known to exist in a wide range

of physical and non-physical systems. Among the physical systems it is observed in practically all electronic materials and devices, semiconductors, metals, resistors, superconductors, electrolytic solutions, thermionic tubes and Josephson junctions. Among the non-physical systems it has been observed in connection with earthquakes, thunderstorms [11], height of the floods of river Nile [12], human heartbeat, brain-waves [13], and music [14]. All the noises obeying the inverse frequency power law are usually called 1/f noise, irrespective of the where the phenomenon occurs. A common name of "1/f noise" should not be taken to imply the existence of a common physical mechanism giving rise to 1/f noise. At present, the physical origin of 1/f noise is not understood. However 1/f noise in simple systems has been empirically found to have the form

$$S_V(f) \approx \frac{V^2}{\Omega f^{\alpha}}$$

where V is the voltage, Ω is the sample volume and α is a constant with a value close to 1.

1/f noise was first observed by Johnson [15] in 1925. In the past 1/f noise was also called "contact noise". However 1/f noise is not a spurious effect associated with faulty contacts. 1/f noise is usually measured by four-probe measurements, where the two terminals maintaining the dc level are independent of the pair sensing the fluctuation. In this way, contacts are eliminated as a possible source of noise. In addition, contact resistance is usually kept much lower than the sample resistance.

Since the 1/f noise spectral density is proportional to the square of the sample voltage, it is easily measured in the case of bulk resistors. However in bulk metals, 1/f noise is too small to be easily detected. To overcome this problem, 1/f noise in good conductors is usually measured on thin-film samples. In pure metals, thin films are

needed to maximize the quantity V^2/Ω; the voltage can not be increased by using a very high current which causes heating effects.

1/f noise has been found to be the dominant type of electrical noise at low frequencies, its magnitude being several orders of magnitude larger than the thermal noise. Because of this large magnitude 1/f noise is considered to be detrimental for solid-state devices operating at low frequencies.

A more detailed review of 1/f noise can be found in the literature [16 to 19].

References:

[1] J. G. Bednorz and K. A. Muller, Z. Phys. B 64 (1986) 189.

[2] M. K. Wu et al., Phys. Rev. Lett. 58 (1987) 908.

[3] J.A. Testa, Y. Song, X.D. Chen, J. Golben, S.I. Lee, B.R. Patton, and J.R. Gaines, Phys. Rev. B 38, 2922 (1988).

[4] A. Maeda, Y. Nakayama, S. Takebayashi, and K. Uchinokura, Physica C 160, 443 (1989).

[5] R. K. Pathria, "Statistical Mechanics", Pergaman Press, New York (1972) chapter 13.

[6] A. van der Ziel, "Noise in solid state devices and circuits", John Wiley & sons (1986).

[7] A. Ambrozy, "Electronic Noise", McGraw-Hill International Book Company (1982).

[8] N. Wiener, Acta Math 55 (1930) 117; A. Khintchine, Math. Ann. 109 (1934) 604.

[9] H. Nyquist, Phys. Rev. 32 (1928) 110.

[10] W. Schottky, Ann. d. Phys. 57 (1918) 541.

[11] S. Machlup, Proc. 6th Int. Conf. on Noise in Physical Systems held at the National Bureau of Standards, Gaithersburg, MD USA April 6 (1981) 157.

[12] M. Gardner, Scientific American, 238(4) (1978) 16.

[13] T. Musha, Proc. 6th Int. Conf. on Noise in Physical Systems held at the National Bureau of Standards, Gaithersburg, MD USA April 6 (1981) 143.

[14] R. F. Voss & J. Clarke, J. Acoust. Soc. Am. 63 (1978) 258.

[15] J. B. Johnson, Phys. Rev. 26 (1925) 71.

[16] P. Dutta et al., Rev. of Mod. Phys. 53 (1981) 497.

[17] M. B. Weissman, Rev. of Mod. Phys. 60 (1988) 537.

[18] M. J. Kirton et al., Advances in Phys. 38(4) (1989) 367.

[19] F. N. Hooge et al., Rep. Prog. Phys. 44 (1981) 479.

CHAPTER 2

THEORETICAL MODELS OF 1/f NOISE

This chapter contains seven sections. In section 2.1, some of the general properties of 1/f noise are discussed. In the remaining sections (2.2 to 2.7) various models of 1/f noise are discussed briefly. Details of these models can be found in the respective references.

2.1 General properties of 1/f noise

One of the main concern for the theoretical modeling of 1/f noise is that the integral :

$$\int_0^\infty (1/f^\alpha)\, df$$

which represents the total noise power, is divergent at both limits for $\alpha = 1$. Thus, for the process to be stationary, it is necessary for cut off frequencies to exist. Experimentally no low frequency limit for 1/f noise has been found. Measurements were performed by Calyanides [1] on semiconductors down to a frequency of 5×10^{-7} Hz but no significant departure from 1/f law was observed. At very high frequencies, 1/f noise is lost in the background noise. The existence of a high frequency limit is possible and may be associated with the response time of the mechanism producing the noise. So far, no physical reason has been found for the existence of a low frequency limit. However, the actual experimental measurements of 1/f noise are limited in frequencies either directly by filtering or indirectly by a limited observation time. The spectral density of a band-limited 1/f noise x(t) can be represented by :

$$\langle S_x(\omega) \rangle = \frac{c}{\omega} \qquad \text{for } \omega_1 \le \omega \le \omega_2$$

$$= 0 \qquad \text{otherwise}$$

where ω_1 and ω_2 are the lower and upper angular frequency limits of the measured noise and c is a constant. The integrated power in the spectrum between ω_1 and ω_2 is :

$$P_x(\omega_1,\omega_2) = \frac{1}{2\pi}\int_{\omega_1}^{\omega_2} \frac{c}{\omega}\, d\omega = \frac{c}{2\pi} \ln\left(\frac{\omega_2}{\omega_1}\right)$$

Above result shows that for a fixed frequency ratio ω_2/ω_1, the integrated power is constant. This property of 1/f noise is known as scale invariance.

The autocorrelation function of x(t) is given by Wiener-Khintchine theorem as

$$\langle K_x(\tau) \rangle = \frac{c}{2\pi}\int_{\omega_1}^{\omega_2} \frac{1}{\omega} \cos \omega\tau \, d\omega$$

which can be written as by the change of variable

$$\langle K_x(\tau) \rangle = \frac{c}{2\pi}\left(\int_{\infty}^{\omega_2\tau} \frac{1}{\omega\tau} \cos \omega\tau \, d(\omega\tau) - \int_{\infty}^{\omega_1\tau} \frac{1}{\omega\tau} \cos \omega\tau \, d(\omega\tau)\right)$$

where the cosine integral behaves as logarithmic function in the limit $\tau \to 0$. In such a limit

$$\langle K_x(0) \rangle = \frac{c}{2\pi} \ln\left(\frac{\omega_2}{\omega_1}\right)$$

Both the autocorrelation function and total power spectral density converge to a limiting value. Since the autocorrelation function depends only on the delay time τ and not on the absolute times, a band limited 1/f noise is stationary. In fact, by mathematically modifying the spectra in a small undetectable way, one can change a non-stationary process to a stationary status. The real problem is not with the mathematics of 1/f noise

but in identifying the physical mechanisms which are responsible for producing 1/f noise.

Another important characteristic of 1/f noise is its I_o^2 dependence. If a constant current I_o is passing through a resistor, then the fluctuation in voltage is caused by the fluctuation in the resistance given by

$$\Delta R(t) = R(t) - R_0$$

where R_o is the average value of the resistance. By Ohm's law, the voltage fluctuation is then given by

$$\Delta V(t) = I_0 \, \Delta R(t)$$

and the spectral density is given by

$$S_V(f) = I_o^2 \, S_R(f) = \frac{V_o^2}{R_o^2} S_R(f)$$

where $V_o = I_o R_o$ is the average voltage across the resistor. The I_o^2 dependence indicates that the dc current flow does not generate the resistance fluctuation but it is necessary to have an observable noise voltage, similar to the case of Ohm's law where current does not generate the resistance but is necessary to measure it. However $\Delta R(t)$ may depend on I_o if there is significant heating of the resistor due to dc current or if the resistor is nonlinear or has poor contacts. In these cases deviation from the quadratic current dependence is expected.

The resistance of a resistor containing N electrons with mobility μ is given by $R=L^2/q\mu N$, where L is the length of the resistor and q is the electron charge. The fluctuation in the resistance can be directly obtained if there is a fluctuation in either N or μ. When N fluctuates, one talks about the number fluctuation. A number fluctuation can be due to various reasons. Most commonly, a number fluctuation is observed if

trapping-detrapping of charge carriers takes place. A fluctuation in mobility is commonly observed due to fluctuation in the temperature and hence in the kinetic energy of the electrons. In order to explain the observed 1/f noise spectra, the fluctuations in mobility would have to show characteristic times which are very long, greater than one second, but it is physically not possible to have such a large characteristic time. The mean free time of a carrier is of the order of picoseconds. However, a charge can be trapped for much longer period of time and number fluctuation is physically reasonable to explain the 1/f spectra.

Indirectly, fluctuations in resistance can also be obtained if there are fluctuations in the temperature of the sample. In such a case, resistance fluctuations are related to thermal fluctuations through the temperature coefficient of resistivity of the sample. Another possibility for resistance to fluctuate is due to the scattering of charge particles by defects. 1/f noise is generated when charged particles are accelerated or decelerated. In such a situation some of the particles emit a very low frequency radiation (bremsstrahlung). The bremsstrahlung part of the beam interferes with the rest of the original electron beam and modulates it, thereby producing noise.

2.2 Hooge's empirical formula

It was generally believed for many years that 1/f noise is exhibited by continuous semiconductor materials but not by homogeneous metal films. Then in 1969, Hooge et al. [2] reported observations of 1/f noise in continuous thin gold films. After reviewing previous measurements he proposed [3] that the 1/f noise in all homogeneous materials can be represented by the empirical formula :

$$S_V(f) = \frac{\gamma V^2}{N f^{\alpha}}$$

Where $S_v(f)$ is the power spectral density of the voltage fluctuation, V is the sample voltage, N is the total number of charge carriers in the sample, f is the frequency, α is a constant close to 1 and $\gamma \cong 2 \times 10^{-3}$ is a universal constant showing only a very weak temperature dependence. The empirical formula correctly describes the following well established facts for simple systems such as bulk metals :

1) $S_v \propto V^2$

2) $S_v \propto N^{-1} \propto$ (sample volume)$^{-1}$

3) $S_v \propto f^{-\alpha}$

Hooge [3] has tabulated a vast amount of data on both metals and semiconductors which show room-temperature noise in agreement with the empirical formula. The original claim that the law applies to all homogeneous materials has since been modified to include only those cases where lattice scattering is negligible [4]. According to Hooge [5], if the impurity scattering is significant then the constant γ in the empirical formula should be reduced by a factor $[\mu_{imp}^2 \div (\mu_{imp}+\mu_{lat})^2]$ where μ_{imp} and μ_{lat} are the mobilities associated with impurity and lattice scattering, respectively.

Despite the considerable success by Hooge's empirical formula, there is evidence that γ is not a universal constant. The strong dependence of the noise in semiconductors on the oxide state of the surface [6], a very different magnitude of noise in bismuth [7], temperature dependence of noise in metals [8], and 1/f noise in copper whiskers [9] with high value of γ, are in disagreement with the empirical formula. The empirical formula explain neither the physical mechanism responsible for producing the noise nor does it give a theoretical justification for the value of the constant γ.

2.3 Thermal fluctuation model

The most developed model where resistance fluctuations are caused by equilibrium thermal fluctuations is due to Voss and Clarke [10]. When a resistor is in thermal equilibrium with its surroundings at mean temperature T_o, it experiences temperature fluctuations due to thermal energy exchange with the environment. These temperature fluctuations in turn give rise to a resistance fluctuation as a function of time $\Delta R(t)$, about the mean resistance R_o through the temperature coefficient of resistance $\beta = (1/R_o)(dR/dT)$, by the relation :

$$\Delta R(t) = \beta R_o \Delta T(t)$$

Where $\Delta T(t)$ is the average temperature fluctuation taken over the volume of the sample. The average temperature fluctuation is related to the energy fluctuation by $\Delta E = C_v \Delta T$, where Cv is the heat capacity of the system. For a canonical ensemble, an average of the energy fluctuations of a system in contact with a heat bath is given by $\langle(\Delta E)^2\rangle = kT^2C_v$, where k is the Boltzmann constant. By using the above two equations one can get :

$$\langle(\Delta T)^2\rangle = kT^2/C_v$$

For a constant current, the mean square voltage fluctuation is then given by :

$$\langle\Delta V^2\rangle = I^2 \langle\Delta R^2\rangle$$

$$= (V^2/R_o^2)\, \beta^2 R_o^2 \langle\Delta T^2\rangle$$

$$= V^2 \beta^2 kT^2/C_v$$

Since $C_v \propto N$, above equation has the same voltage and volume dependence as in the empirical formula of Hooge.

Following Voss and Clarke, one can write a Langevin diffusion equation for the local temperature T(x,t) :

$$\frac{\partial T}{\partial t} = D\nabla^2 T + \frac{1}{c}\nabla\cdot\mathbf{F}$$

where D is the thermal diffusity, c is the heat capacity per unit length, and **F** is an uncorrelated random driving term satisfying :

$$\langle \mathbf{F}(\mathbf{x}+\mathbf{s},t+\tau)\cdot\mathbf{F}(\mathbf{x},t)\rangle \propto \delta(\mathbf{s})\delta(\tau)$$

The temperature fluctuation spectrum is :

$$S(\omega) = \int \langle T(t+\tau)\, T(t)\rangle \cos(\omega\tau)\, d\tau$$

The resulting power spectrum decays with frequency. Voss and Clarke found that for a sample with dimensions $2L_1 x 2L_2 x 2L_3$ where $L_1 >> L_2 >> L_3$, four frequency regions can be identified, separated by the three frequencies $\omega_1 = D/[2(L_1)^2]$, $\omega_2 = D/[2(L_2)^2]$ and $\omega_3 = D/[2(L_3)^2]$.

The shapes of the spectra in these regions are :

$S_T(\omega) \propto \omega^{-3/2}$ for $\omega >> \omega_3$

$\propto \omega^{-1/2}$ for $\omega_3 >> \omega >> \omega_2$

$\propto [\text{ constant - ln } \omega\ ]$ for $\omega_2 >> \omega >> \omega_1$

$= \text{constant}$ for $\omega_1 >> \omega$

Thus the standard Langevin diffusion equation yields no explicit 1/f region. However a 1/f dependent region can be created phenomenologically (but without justification based on any microscopic model) by replacing the Langevin equation by :

$$\frac{\partial T}{\partial t} = D\nabla^2 T + \frac{1}{c} P(\mathbf{x},t)$$

where $P(\mathbf{x},t)$ is uncorrelated in space and time like **F**. The $\nabla\cdot\mathbf{F}$ term represented a

random flow of energy within the system, whereas the P(**x**,t) term causes a fluctuation in the energy of the system by acting as a random energy source which adds or subtracts energy from the system. From the modified Langevin equation, a 1/f region is created between the frequencies ω_1 and ω_2, with

$S_T(\omega) \propto \omega^{-3/2}$ for $\omega >> \omega_2$

$\propto \omega^{-1}$ for $\omega_2 > \omega > \omega_1$

= constant for $\omega_1 >> \omega$

and in the 1/f region the spectral density of voltage fluctuations is given as :

$$S_v(f) = \frac{V^2 \beta^2 k T^2}{C_v [\, 3 + 2 \ln (\frac{L_1}{L_2}) \,] f}$$

The presence of β in the above equation is significant. Voss and Clarke found no detectable 1/f noise in manganin, which has a temperature coefficient of resistance very close to zero, in agreement with the theoretical prediction from the above model. Further experimental support was reported by Clarke [11], who measured noise in iin films at the superconducting transition, where $\beta \cong 155\ K^{-1}$ is extremely large compared with the room temperature value of approximately $5 \times 10^{-3}\ K^{-1}$. The measured noise was found to be in agreement with the predicted values. According to the above model, the temperature fluctuation in metal films should show a degree of spatial coherence with correlation length of $(D/f)^{-1/2}$ where D is the thermal diffusity of the film. Correlation measurements on a bismuth film at room temperature by Voss and Clarke are in good agreement with the theoretical prediction.

There are many shortcomings in this model. It does not give rise to an explicit 1/f region of significant extent. It leads to a low frequency roll off, which is generally not observed. It also predicts a monotonic temperature dependence weaker than that

observed. Despite the initial success of the model, recent investigations have led to the conclusion that in general thermal fluctuations are not responsible for the observed spectra in metals and semiconductors. The case of superconducting tin films may be special in the sense that the voltage fluctuations are strongly coupled through the temperature coefficient of resistivity to the temperature fluctuation.

The absence of 1/f noise in manganin, which provided strong support for the temperature fluctuation model, has been questioned by Hooge who reports [12] contact noise on solid manganin bars and found nothing unusual about the observed spectrum. Dutta et al. [13] found that the temperature dependence of the noise power changes behavior at high temperature of 400 K for silver and copper films. The observed peak structure in the noise level of these films cannot be predicted by the thermal fluctuation model. In addition, recent experiments have been unable to measure the spatial coherence predicted for the noise. Schofield et al. [14] took two gold films separated by an electrically insulating layer so thin that the thermal fluctuations in one film were strongly correlated with those in the other film. Thus if 1/f noise were due to thermal fluctuations, the noise in the two films should have been strongly correlated. The experiments showed that there was essentially no causal connection between the 1/f noise in the two films and the coherence coefficient was two orders of magnitude smaller than that predicted.

2.4 The McWhorter model

A simple model that gives a 1/f noise spectrum in a natural way was proposed by McWhorter in 1957 [6]. The model is still among the most popular and successful models of 1/f noise. The model, which was originally meant for the semiconductors, is

based on the idea that the density of charge carriers is modulated by trapping and detrapping from surface states causing the resistance to fluctuate. If a population of traps with a distribution of trapping times is present, then the overall spectrum is the summation of the relaxation spectra from each species of trap and this sum can show a 1/f dependence over a limited range of frequency determined by the spread of the lifetimes. The spectral density of the number fluctuation due to a given species of trap with time constant τ is of the form [15] :

$$\frac{4\tau}{1+\omega^2\tau^2}$$

Introducing a distribution function $D(\tau)$ to represent the spread of characteristic time, gives the power spectral density of the total number fluctuation n(t) as :

$$\langle S_n(\omega)\rangle = 4\,\langle n^2(t)\rangle \int_0^\infty \frac{\tau}{1+\omega^2\tau^2}\, D(\tau)\, d\tau$$

McWhorter assumed that the distribution of trapping times arises from the tunnelling of charge from the surface to traps, hence the time constants are of the form :

$$\tau = \tau_o \exp(\gamma d)$$

where τ_o and γ are constants ($\gamma \cong 10^{-8}$ cm^{-1}), and d is the depth of the trap from the surface. For a homogeneous distribution of traps between depths d_1 and d_2 (corresponding to time constants τ_1 and τ_2) the distribution function follows from the above equation and is given as :

$$D(\tau)\, d\tau = \frac{d\tau}{\tau \ln\left(\frac{\tau_2}{\tau_1}\right)} \qquad \text{for } \tau_1 \le \tau \le \tau_2$$

$$= 0 \qquad \text{otherwise}$$

Then the power spectral density of number fluctuation will be :

$$\langle S_n(\omega)\rangle = \frac{4\langle n^2(t)\rangle}{\ln\left(\frac{\tau_2}{\tau_1}\right)} \int_{\tau_1}^{\tau_2} \frac{d\tau}{1+\omega^2\tau^2}$$

$$= \frac{4\langle n^2(t)\rangle}{\ln\left(\frac{\tau_2}{\tau_1}\right)} \frac{[\tan^{-1}\omega\tau_2 - \tan^{-1}\omega\tau_1]}{\omega}$$

In the frequency range where $\omega\tau_2 >> 1$ and $0 \leq \omega\tau_1 \leq 1$, the two trigonometric functions in the numerator approximate to $\pi/2$ and zero, respectively; giving approximate 1/f frequency dependence. The above surface-effect model can be recast into a form which can give a bulk effect [16], by making the assumption [17] $\langle n^2(t)\rangle = \beta N$, where β is a constant and N is the total number of carriers. The voltage fluctuation is then given by :

$$\frac{S_v(\omega)}{V^2} = \frac{S_n(\omega)}{N^2} = \frac{2\pi\beta}{N \ln\left(\frac{\tau_2}{\tau_1}\right)\omega}$$

The above equation is similar to Hooge's empirical formula as :

$$S_v(f) = \left(\frac{\beta}{\ln\left(\frac{\tau_2}{\tau_1}\right)}\right)\frac{V^2}{N f}$$

A difficulty with the model concerns the range of time constants required to give the 1/f noise over an extensive range of frequency. For example, for the spectrum to be in the 1/f shape for four decades, one needs $\tau_2/\tau_1 = 10^6$. In certain specific devices, such as the MOSFET, it is possible to invoke a physical mechanism which could account for relaxation times distributed between, say, 10^{-5}s and 10^8s, but in general this is not the case.

2.5 The Dutta, Dimon and Horn model

The effect of the substrate on the temperature dependence of 1/f noise in thin

metal films was investigated by Dutta et al. [13]. Two interesting features of the noise were revealed : (i) above room temperature the substrate has little effect on the 1/f spectra of silver and copper films and (ii) below room temperature, in the case of copper films, the 1/f noise is substrate dependent. The experimental results and several contradictions in previously existing data (e.g. correlation experiments) were explained [18] in terms of two types of 1/f noise existing simultaneously :

(a) Type A noise : a background noise that is weakly temperature dependent. Both its magnitude and its temperature dependence are affected by the nature of the substrate. The possible source of this noise is temperature fluctuations due to thermal conduction between metal film and substrate. This noise can be explained by the Voss-Clarke thermal fluctuation model.

(b) Type B noise : a strongly temperature dependent noise that is characteristic of the metal, independent of the substrate and dominant at high temperatures. The source of this noise is thermally activated random processes and not thermal fluctuations.

The source of type B noise was explained by a random-fluctuation model by Dutta, Dimon and Horn [19] developed from the McWhorter model. Following the McWhorter model, the spectral density for a random process with characteristic time τ is given as :

$$S(\omega) \approx \int_0^\infty \frac{\tau}{1+\omega^2\tau^2} D(\tau)\, d\tau$$

where $D(\tau)$ is the distribution of characteristic times within the sample. Since now the characteristic times are due to thermally activated processes, instead of tunnelling (as in the case of the McWhorter model), the expression for τ is given by :

$$\tau = \tau_o \exp(\frac{E}{kT})$$

where τ_o^{-1} is the attempt frequency for random processes in crystals and is roughly equal to 10^{14} Hz (of the order of the phonon frequency), E is a thermal activation energy, k is the Boltzmann constant and T is the temperature of the sample. The above integration is rewritten as :

$$S(\omega) \approx \int \frac{\tau_o \exp(\frac{E}{kT})}{1 + \omega^2\tau_o^2 \exp(\frac{2E}{kT})} D(E)dE$$

It was noted by Dutta et al. [18] that for the spectrum to be of 1/f shape, it is necessary only that D(E) vary slowly compared to kT. The above integration can then be carried out after expanding D(E) in a Taylor series around $E_o = -kT \ln(\omega\tau_o)$, the value of E at which the function $[\tau_o \exp(E/kT)]/[1+\omega^2\tau_o^2 \exp(2E/kT)]$ peaks.

If D(E) varies more slowly with E than with kT, only the first term in the Taylor expansion is necessary. The integration then yields :

$$S(\omega,T) \approx \frac{kT}{\omega} D(E_o)$$

Because of the temperature and frequency dependence of E_o, $S(\omega,T)$ is actually a rather complex function of the frequency ω and the temperature T. The structure of dependence of S on T depends on the temperature dependence of D(E).

In summary, the above model is based on following three assumptions:

(a) The excess noise is due to a superimposition of random processes whose characteristic times are thermally activated.

(b) The distribution of activation energies D(E) may have any shape as long as it varies slowly over any $\Delta E \approx kT$.

(c) The attempt frequency τ_o^{-1} is much larger than the frequencies at which the noise is measured.

The model does not refer to any specific type of random process responsible for the source of noise. Processes such as vacancy-interstitial formation and recombination, diffusion of all types, and trapping and detrapping of charge carriers satisfy the criteria listed above.

2.6 Two component model by Mantese

The two component model by Mantese [20] uses the effective medium theory to explain the behavior of 1/f noise in metal-insulator composites. One of the important properties of metal-insulator composite conductors is the increase by many orders of magnitude of the electrical resistivity ρ as the metal volume fill fraction x is reduced below a critical value x_c. The resistivity spectral density $S_\rho(f)$ shows even stronger dependence on x and increases with decreasing x [21,22]. The shape of the noise spectrum however, remains unchanged with $S_\rho(f) \propto 1/f^\alpha$ with $0.8 \leq \alpha \leq 1.2$ over the entire range of x [21].

For $x>>x_c$ the composites consist of a metallic continuum with inclusions of the insulators and electrical conduction is dominated by charge transport along the metallic continuum. For $x<<x_c$ the microstructure is inverted with small metal islands dispersed in the dielectric matrix and electrical conduction occurs by thermally assisted charge tunneling [23]. At $x \cong x_c$ both the metallic conduction and thermally assisted tunneling contribute to conduction.

In this model, thin film composites were modeled as a regular array of cells of volume V. Within each cell the metal is assumed to be continuous and to have a volume xV; hence the macroscopic metal volume fraction is also assumed to describe the volume of metal per cell. The probability that two neighboring cells are connected by metal

components is given by f(x); satisfying the constraints : f(1) = 1, f(0) = 0, $f(x_c)$ = 1/3. The pairs of connected metal particles are assumed to have resistivity ρ_M appropriate to metallic conduction with the fraction of metallic resistors equal to f(x). Near-neighbor metal particles separated by insulator are replaced by resistor of resistivity ρ_T appropriate to tunneling through the insulating barrier. The number of such tunneling resistors is equal to 1-f(x). The model neglects the distributions in insulating barrier thickness, particle sizes and shapes to which tunneling can be quite sensitive. The model calculates the resistivity for a simple cubic lattice (coordination number z = 6) as a solution to the equation:

$$1 = \frac{3f}{2+\frac{\rho}{\rho_M}} + \frac{3(1-f)}{2+\frac{\rho}{\rho_T}}$$

where f = f(x) is the probability that two neighboring cells are connected by metallic resistors with resistivity ρ_M. The tunneling resistivity is taken to be of the usual form $\rho_T(x) = \rho_0 \exp[\chi t(x)]$ which depends exponentially on the tunnel barrier thickness t(x). ρ_0 and χ are used as adjustable parameters (χ=0.5 Å^{-1} and ρ_0=8x10^{-5} Ωcm), in determining the resistivity. Model calculates the 1/f noise in the resistivity by the equation:

$$\frac{s}{(1+\gamma)} = f(x)\frac{(g_M^2 s_M + \gamma g^2 s)}{(g_M + \gamma g)^2} + [1-f(x)]\frac{(g_T^2 s_T + \gamma g^2 s)}{(g_T + \gamma g)^2}$$

where $g = \rho^{-1}$, $g_M = \rho_M^{-1}$, $g_T = \rho_T^{-1}$, $\gamma = (z-2)/2$,

$$s_M = \frac{S_{\rho_M}(x)}{\rho_M^2(x)}, \quad s_T = \frac{S_{\rho_T}(x)}{\rho_T^2(x)}.$$

Clearly $s = s_M$ for x = 1.0 and $s = s_T$ for x = 0, since f(0) = 0 and f(1) = 1.

The primary effect of the tunnel resistors for $x \equiv x_c$ is to eliminate the divergence in $\rho(x)$ at x_c. Below x_c, the tunnel resistors dominates the resistivity. The calculated noise shows a sharp rise with decreasing x and then a saturation for $x << x_c$. The results from the model are consistent with the experimental measurements [21] of both $\rho(x)$ and $s(x)$ on Pt-Al_2O_3 composite over the full range of x, including the metallic conduction threshold at x_c. The consequences of neglecting the tunnel paths entirely can be calculated by setting $\rho_T = \infty$ and $s_T = 0$. It is found that for $x > x_c$, the resistivity is virtually unchanged if one neglects the tunnel paths entirely, but the noise deviates substantially from the experimental data. The model then points out that it is the tunnel junction which are responsible for the noise, even for $x >> x_c$.

2.7 Quantum model by Handel

To explain the existence of 1/f noise in wide range of systems, Handel [24,25] proposed a quantum theory of 1/f noise. In this model, 1/f noise is generated when charged particles are accelerated or decelerated. In such a situation some of the particles emit very low-frequency radiation (bremsstrahlung). The bremsstrahlung part of the beam interferes with the rest of the original electron beam and modulates it, thereby producing noise. This noise spectrum is proportional to the number N of quanta emitted per second. Since the low-frequency bremsstrahlung has a constant spectrum in energy and hf is the quantum energy, N will be proportional to 1/f, hence the generated noise has a 1/f spectrum. 1/f noise due to bremsstrahlung should therefore occur in all devices in which particles are accelerated or decelerated. Since the energy of the emitted photon can be arbitrarily small, the energy of the electrons in the solid can fluctuate at

very low frequencies ($\approx 10^{-4}$Hz). This energy fluctuation leads to fluctuation in the current. The model derives the following equation for the current fluctuation :

$$\langle (\delta I)^2 \rangle_f = \frac{1}{2} \kappa \alpha \langle A \rangle \frac{I^2}{f N}$$

where κ is a corrective factor which takes into account the correlations between carriers. For $\kappa = 1$ no correlations are present. $\alpha = 1/137$ is the fine structure constant and <A> is an average over the scattering angle. The value of the constant ($= \kappa \alpha \langle A \rangle / 2$) is shown by Handel to be equal to 2×10^{-3}, which coincides with the experimental value obtained by Hooge. Hence the above equation has a spectral density which exactly agrees with the Hooge's empirical formula in both magnitude and frequency dependence. However the agreement between theory and experiment is an accident because Handel's model is a zero-temperature theory for a beam of electrons which can emit low energy photons. However, most electrons in metal at zero temperature can not emit low energy photons because all the nearby states are occupied. Also, since experimental results on many systems do not coincide with Hooge' constant, it will be hard to explain these results on the basis of Handel's model. Existence of 1/f noise due to bremsstrahlung is not always observed, possibly because it is masked by stronger 1/f noise processes.

References:

[1] M. A. Caloyanides, J. Appl. Phys. 45 (1974) 307.

[2] F. N. Hooge and A. M. H. Hoppenbrouwers, Physica C 45, (1969) 386.

[3] F. N. Hooge et al., Phys. Lett. A 29, (1969) 139.

[4] F. N. Hooge et al., J. Appl. Phys. 50, (1979) 8087.

[5] F. N. Hooge et al., Phys. Lett. 66A, (1978) 315.

[6] A. L. McWhorter, In Semiconducting Surface Physics, edited by R. H. Kington (University of Pennsylvania, Philadelphia) (1957) 207.

[7] R. F. Voss et al., Phys. Rev. B, 13 (1976) 556.

[8] J. W. Eberhard et al., Phys. Rev. B, 18 (1978) 6681.

[9] P. Dutta et al., Solid State Comm. 21, (1977) 679.

[10] R. F. Voss et al., Phys. Rev. B 13 (1976) 556.

[11] J. Clarke et al., Phys. Rev. Lett. 34 (1975) 1217.

[12] F. N. Hooge et al., Physica 83B, (1976) 14.

[13] P. Dutta et al., Solid State Comm. 27, (1978) 1389.

[14] J. H. Schofield, Proc. 6th Int. Conf. on noise in physical systems held at the National Bureau of Standards, Gaithersberg, MD USA, april (1981) 147.

[15] M. J. Buckingham, Noise in electronic sys. and dev., Halsted Press (1983) 197.

[16] A. Vander Ziel et al., Adv. in Elect. and Phys. 49 (1979) 225.

[17] F. M. Klaassen et al., IEEE Trans. Electron. Devices, ED-18, (1971) 887.

[18] P. Dutta et al., Rev. of Mod. Phys. 53 #3 (1981) 497.

[19] P. Dutta et al., Phys. Rev. Lett. 43 (1979) 646.

[20] J. V. Mantese et al., Phy. Rev. B, 33 #12 (1986) 7897.

[21] J. V. Mantese et al., Phy. Rev. Lett. 55 (1985) 2212.

[22] C. C. Chen et al., Phy. Rev. Lett. 54 (1985) 2529.

[23] B. Abeles et al. Adv. Phys. 24 (1975) 407.

[24] P. H. Handel, Phy. Rev. Lett. 34 #24 (1975) 1492.

[25] P. H. Handel, Phy. Rev. A 22 (1980) 745.

CHAPTER 3

SAMPLE PREPARATION

This chapter consists of two sections. In the first section a sample preparation procedure for bulk samples of Tl-based superconductors is discussed along with various safety procedures. In the second section preparation of thin films of $Tl_2Ba_2Ca_1Cu_2O_8$ is discussed briefly.

3.1 Preparation of bulk samples of $Tl_2Ba_2Ca_{n-1}Cu_nO_{4+2n}$ (n=2,3)

The synthesis of high Tc superconducting bulk samples is based on a general method of making perovskites ceramics, i.e., mixing the constituents, usually in oxide form, and firing the mixture at high temperature. Two of the most common methods used for the preparation of high Tc superconductors are solid state reaction and coprecipitation. The solid state reaction method involves simple mixing, grinding, and baking oxide forms of constituents. The coprecipitation method mixes the constituents in their nitrate form in water solution and then precipitates them out of solution in their corresponding carbonate forms. Mixing of constituents is on the atomic level in the coprecipitate form, and this method usually gives a more homogeneous sample. However, in the case of Tl-based superconductors, the coprecipitate method is found to be a failure [1] ; thallium samples prepared by the coprecipitation method were found to exhibit semiconducting behavior. The solid state reaction method is a much simpler method than the coprecipitation method; bulk samples of yttrium or bismuth-based superconductors can be easily prepared. However, one needs to be extra careful when

preparing thallium-based superconductors because of thallium's toxic nature.

Thallium and most of its compounds are toxic. Symptoms of acute toxicity include vomiting, weakness, coma, loss of hair, and death [2]. Mixtures of 2% thallium salts and 98% inert substances are effective rat killers. Thallium salts are usually odorless and tasteless, giving no warning of their presence. Their contact with skin and eye is dangerous. Thallium is also highly volatile, which makes the handling of this substance more difficult. Tl-based insecticide and rodenticide have been prohibited in the U.S. since 1975. Thallium has been used in treating ringworm and other skin infections; however, its use has been limited because of the narrow margin between toxicity and therapeutic benefits.

Because of the volatile and toxic nature of thallium, it is necessary that synthesis of Tl-based superconductors be carried out in a closed air tight system. In our experiments, all samples were prepared in a closed quartz tube furnace. In order to prevent any thallium leak, samples can be sealed in quartz capsules containing oxygen gas. A box furnace, which is usually used for the synthesis of other superconductors, is definitely not recommended because of the possibility of serious contamination and health hazards. A step-by-step method for synthesis of Tl-superconductor is given below. Useful hints for reducing the thallium leak are also given along with the procedure.

The first step in the sample preparation is the choice of proper starting materials. The conventional solid state reaction method approach of mixing and heating the constituent oxides namely Tl_2O_3, CaO, BaO and CuO in a proper stoichiometry ratio, was found to be a failure for the synthesis of Tl-based superconductors [3]. The result is a consequence of the highly volatile nature of Tl_2O_3. To overcome this problem of

losing thallium atoms, Tl-superconductors are normally made by the precursor method. In this method, all other stable chemicals are reacted together by sintering--that is, before incorporating any thallium oxide. Raw powders of $BaCO_3$, $CaCO_3$ and CuO were thoroughly mixed in 2:2:3 and 2:1:2 stoichiometric ratios for the synthesis of $Tl_2Ba_2Ca_2Cu_3O_{10}$ and $Tl_2Ba_2Ca_1Cu_2O_8$ compounds respectively. The mixtures were sintered in air at 940 °C for 48 hours with an intermediate grinding. The intermediate grinding step is important for producing a more uniform precursor. The original paper by Z. Z. Sheng and A. M. Hermann [4] describing the synthesis of Tl-based superconductors has recommended the use of $BaCu_3O_4$ as a precursor compound. According to the authors, $BaCu_3O_4$ has the lowest melting point among the Ba-Cu oxides and molten $BaCu_3O_4$ is extremely fluid [5]. It is believed by the authors that melt-solid reactions take place more completely then do typical solid state reactions. However, both types of precursors listed above give similar results. Among the two available choices of Tl-oxide compounds, namely Tl_2O and Tl_2O_3; Tl_2O_3 is preferred over Tl_2O. This is because Tl_2O_3 has a much higher melting point (717 °C) than Tl_2O (300 °C); and hence will be more stable and less volatile.

The second step is weighing of chemicals. To overcome the problem of Tl-loss during the synthesis Tl_2O_3 powder is mixed with the precursor in a 1.1 to 1 ratio. Thallium loss can come in two ways : (i) due to volatile nature of thallium oxide, thallium atoms escape from the sample and react with the surrounding; (ii) due to its low melting point, Tl_2O_3 melts and seeps out of the sample. To overcome these problems the starting powder is pressed into a dense pellet. This step is different from the processing of other high Tc superconductors, in which powder is baked before making a

pellet. The pellet is then wrapped tightly in gold foil to reduce Tl-leakage. Even after following the above procedure there is a significant Tl-loss. Tl-weight loss can be estimated by weighing the pellet before and after the sintering step. Depending on the duration of sintering, temperature of sintering and other factors controlling the leakage of thallium, the Tl-loss will be a variable parameter [6].

After wrapping the pellet in gold foil, the sample is either sealed inside a quartz capsule containing oxygen gas or enclosed by several alumina crucibles as shown in figure 3.1. Sealing the pellet in a quartz tubing requires extra precaution since the quartz tube can be sealed only at very high temperatures (≈ 1500 °C), and it is possible that the sample gets heated by the exchange gas. In such a case the researcher will be exposed to thallium vapors. On the other hand if alumina crucibles are used to enclose the sample then oxygen gas must be flowed through a properly sealed tube furnace. The outcoming gas must exhaust to open atmosphere, outside the building.

In the next step, the crucible is inserted in a preheated furnace which is heated to 900 °C. This step is different from the normal process of synthesizing yttrium or bismuth based superconductors, in which samples are heated slowly from room temperature to the sintering temperature. A preheated furnace is useful in quickly reacting thallium oxide with the precursor at the sintering temperature. A slowly heated sample will lose most of its thallium atoms below the sintering temperature because of the low melting point of thallium oxide. The duration of sintering for Tl-samples is also kept smaller than that followed in the conventional method for preparing yttrium or bismuth samples. Usually Tl-samples are sintered only for 5 to 20 minutes. After the first sintering, samples are quickly cooled by either turning off the furnace or by quenching the sample in liquid nitrogen. A quenching process is risky because the very hot sample is exposed to the open atmosphere for few seconds. In our experiments,

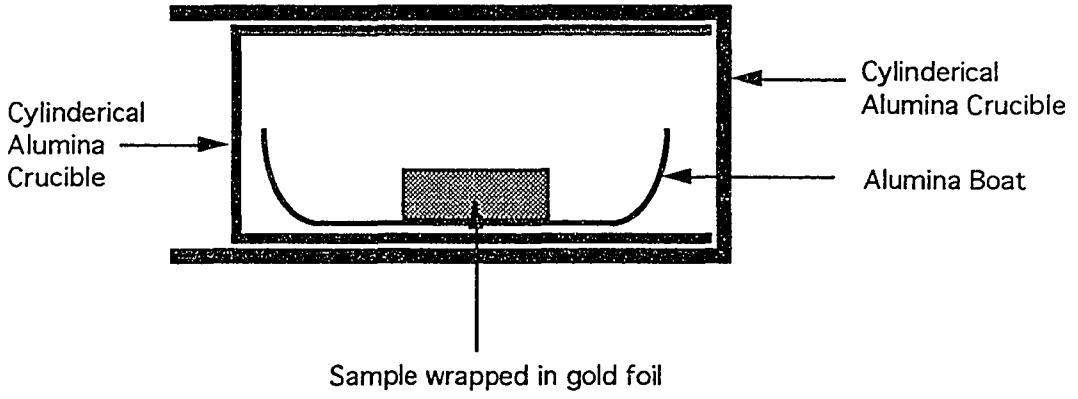

Fig. 3.1 : Arrangement of alumina crucibles for preparation of $Tl_2Ba_2Ca_{n-1}Cu_nO_{4+2n}$ (n=2,3). Three crucibles are used to enclosed the sample, which is wrapped in a gold foil, to reduce the risk of Tl-leakage.

all samples were prepared by turning off the furnace; which is safer than the quenching method.

After the first sintering procedure, it is generally believed that samples are safer to handle. This is because the Tl-superconducting phases are stable. However, there is no confirmed report on the non-toxicity of Tl-superconductors. After the first sintering, samples do show superconductivity at high temperatures (≈ 80 K to 100 K) but they usually have high normal state resistivity, suggesting that the inter-grain connection is poor. This behavior is shown in fig 6.1 (chapter 6) in which normal state resistivity is plotted for two samples of $Tl_2Ba_2Ca_1Cu_2O_8$ as a function of temperature. Sample 1 was measured after first sintering step. Sample 2 went through a second sintering step. It can be seen that the resistivity of sample 1 is 10 times larger than that of sample 2. Also, sample 2 is a 103 K superconductor whereas sample 1 is only an 80 K superconductor. From the plot it is obvious that the second sintering is important for the preparation of good samples with higher $T_{c,zero}$.

Before sintering the sample for the second time, the sample is grounded into powder form and pressed in a pellet. This is done to make the sample more homogeneous. Second sintering is done in exactly the same way as first sintering by inserting the sample wrapped in gold foil in a preheated furnace. However, since thallium has already reacted with the precursor the chemical is more stable; hence the second sintering can be done for the longer time. For our samples, the duration of second sintering was between 2 to 4 hours. After the second sintering, samples were cooled to room temperature in oxygen atmosphere by turning off the furnace. Table 3.1 shows the details of sample preparation. The sintering temperatures and the durations of sintering are given along with the normal state resistivity values at 200 K and $T_{c,zero}$ for four

Table 3.1 : Thermal history and results of resistivity measurements of samples. The notations 2212 and 2223 represent $Tl_2Ba_2Ca_1Cu_2O_8$ and $Tl_2Ba_2Ca_2Cu_3O_{10}$ respectively.

Sample	Composition	1st Sintering	2nd Sintering	ρ(200°C) (mΩcm)	$T_{c,zero}$ (K)
1	2212	900°C/10min	No 2nd sintering	17.25	80
2	2212	900°C/20min	900°C/2h	1.48	103
3	2223	900°C/10min	880°C/2h	0.75	106
4	2223	900°C/10min	900°C/4h	3.55	119

samples. The resistivity vs temperature plot for sample 3 and 4, which have the stoichiometry $Tl_2Ba_2Ca_2Cu_3O_{10}$ is shown in fig 6.3.

Due to the risk involved in making Tl-superconductors, only a few good samples were made. Study of the effect of parameters like sintering temperature, sintering-duration etc. on the quality and property of the sample was purposely avoided. Such a study would require a large number of samples to be made and hence is not safe for the health of the people working in the lab.

3.2 Preparation of $Tl_2Ba_2Ca_1Cu_2O_8$ thin films

Thin films of $Tl_2Ba_2Ca_1Cu_2O_8$ were made by Dr. Albert H. Cardona of Superconductor Technologies, Inc., Santa Barbara, CA 93111. The preparation method is briefly discussed in the following paragraph.

$Tl_2Ba_2Ca_1Cu_2O_8$ thin films were prepared in a two-step process of deposition and thermal annealing. The first step was laser ablation transport, in which material from a single target of thallium, calcium, barium, and copper oxides was vaporized by a pulsed 248 nm excimer laser beam. Noncrystalline films with thicknesses of about 1 μm were deposited at room temperature onto precleaned $LaAlO_3$ substrates in 20 mTorr of oxygen with a laser energy of 3 - 5 J/cm^2. The films were then annealed by heating at about 860 °C for 2 - 6 min. An overpressure of Tl_2O and O_2 was used to control the thallium content of the film. Films made by this process have x-ray diffraction patterns showing almost exclusively the $Tl_2Ba_2Ca_1Cu_2O_8$ phase, with dc critical current densities of J_c (77 K) = 0.5 - 1 x 10^6 A/cm^2. Microstructural analysis show mostly c-axis normal epitaxy, with occasional a-axis normal plates.

Fig. 3.2 : SEM photograph of several $Tl_2Ba_2Ca_1Cu_2O_8$ thin films on a $LaAlO_3$ substrate. The samples have a 4-probe bridge geometry (with the probed portion typically 300 µm long and 25 µm wide). They are patterned from the films by conventional photolithography and a wet chemical etch.

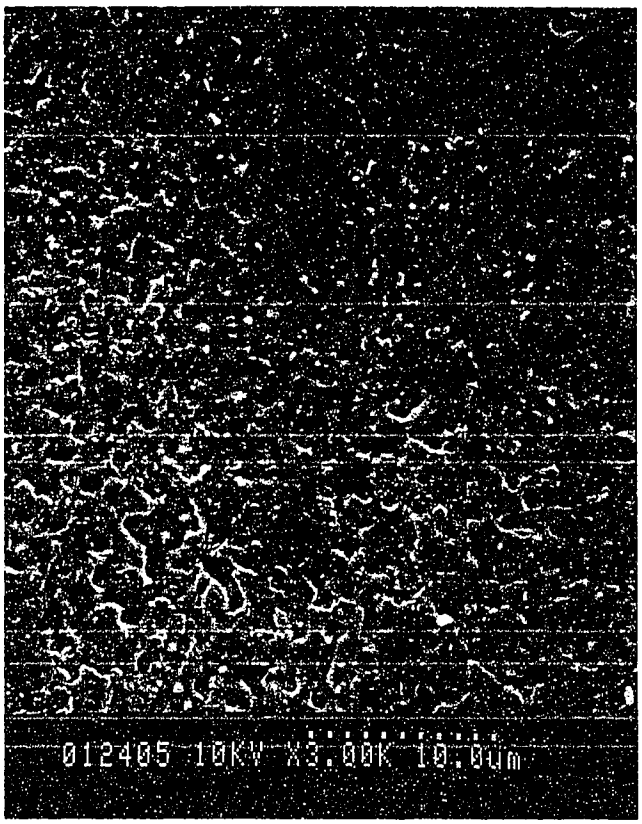

Fig. 3.3 : SEM photograph showing the microstructure of a $Tl_2Ba_2Ca_1Cu_2O_8$ thin film sample. The grains are well connected and grain size is of the order of several microns. Several voids of size 1μm can also be seen in the sample. The scale and the magnification (X3000) used in taking the picture is indicated at the bottom of the picture.

These measurements and characterization of films were done by Dr. Cardona. The samples have a geometry of 4-probe bridges (with the probed portion typically 300 μm long and 25 μm wide) and they are patterned from the films by conventional photolithography and a wet chemical etch. Gold pads are evaporated onto the sample and electrical leads for the resistance and the noise power measurement are attached to the gold pads by a bonding machine. The contact resistance at each point is usually less than 15% of the sample resistance. Fig. 3.2 shows the overall picture of several patterned thin film samples. The picture was taken with the help of SEM. The technical help of Mrs. Tina M. Weatherby and the use of the SEM at Biological Electron Microscope Facility, PBRC is gratefully acknowledged. Fig. 3.3 shows the SEM picture of the grain structure of thin film sample B. The grains are well connected and grain size is of the order of several microns. Several voids of size 1 μm can also be seen in the sample. The scales and the magnifications used in taking these pictures are indicated at the bottom of the pictures.

References:

[1] R. S. Liu et.al. Jpn. J. Appl. Phys. 27(7), L1206 (1988).

[2] E. Browning "Toxicity of industrial metals", Appleton-Century-Crofts, New York, 2nd ed. (1969), p317-322.

[3] I. K. Gopalakrishnan et.al. Appl. Phys. Lett. 53(5) (1988) p414.

[4] Z. Z. Sheng et. al., Nature 332 (1988) 138.

[5] A. M. Hermann et.al. Appl. Phys. Lett. 51 (1987) 1854.

[6] N. L. Wu et.al. Physica C 161 (1989) 302.

CHAPTER 4

SINGLE CRYSTAL GROWTH OF $Y_1Ba_2Cu_3O_x$

This chapter describes the growth of single crystals of $Y_1Ba_2Cu_3O_x$. The study of crystal growth of $Y_1Ba_2Cu_3O_x$ was done independently and some of the results are reported here for the first time. The chapter consists of five sections. Section 4.1 gives a general introduction of crystal-growth of $Y_1Ba_2Cu_3O_x$. In section 4.2, a general description of the crystal growth process is briefly given. Results of the effects of various factors such as, highest temperature of heating, cooling rate, plateau temperature, choice of crucible, starting stoichiometry, geometrical factors, etc., on the crystal growth of $Y_1Ba_2Cu_3O_x$ are given in section 4.3. The experimental results are discussed in section 4.4. Growth of single crystals using gold crucibles is described in this section. Conclusion of this chapter is briefly described in section 4.5.

4.1 Introduction

Since the discovery of high temperature superconductivity in copper oxide materials, a great deal of activity has revolved around understanding the basic physical properties of these materials. Single crystals are required in order to investigate their intrinsic physical properties. The main objective of this study is to understand the phenomenon of 1/f noise in high Tc superconductors. In order to understand this fundamental phenomenon it was necessary to do measurements of noise on single crystals of a high Tc superconducting material. From the study of 1/f noise on single crystals of $Y_1Ba_2Cu_3O_x$ some new results have been obtained by us.

Single crystals of $Y_1Ba_2Cu_3O_x$ have been grown by two different flux methods: one based on excess CuO+BaO [1] and the other on mixed alkali-halides [2]. In general, crystals grown from the CuO+BaO flux are smaller than those grown from the halide-flux, but to date the former are superior in quality. Crystals grown from the CuO+BaO flux normally have regular shapes and optically flat surfaces, in contrast with those grown from the halide flux which usually have more inclusions, microcracks, and poorer crystallinity [3]. In the past, much work has been devoted to developing practical recipes for the growth of $Y_1Ba_2Cu_3O_x$ crystals [1,2] but a systematic analysis of the effects of various factors in the growth process has been lacking.

We have performed extensive studies on the growth process and the optimization of growth conditions for large size $Y_1Ba_2Cu_3O_x$ single crystals of good quality, using the CuO+BaO flux method. Our experiments show that $Y_1Ba_2Cu_3O_x$ single crystals can be grown from a wide range of stoichiometries of the starting materials. The governing factors in the growth of $Y_1Ba_2Cu_3O_x$ crystals are found to be heating temperature, cooling rates, and growth environment.

4.2 Experimental details

Single crystals of $Y_1Ba_2Cu_3O_x$ were grown by the CuO+BaO flux method. Various components as the starting materials were used, including raw powders of CuO, $BaCO_3$, Y_2O_3 (all of 99.9% purity, from Alfa Chemical Co., USA), precursor $BaCuO_2$, and bulk powders of $Y_1Ba_2Cu_3O_x$ [4-5]. The precursor $BaCuO_2$ was prepared in advance by mixing $BaCO_3$ and CuO in a 1 : 1 molecular ratio and heating the mixture at 920 °C for 12 hours in air. Another component, a bulk powder of $Y_1Ba_2Cu_3O_x$ which exhibits

superconductivity, was separately synthesized by the solid-state reaction method [6], by mixing Y_2O_3, $BaCO_3$, and CuO in the stoichiometric ratio 1:2:3 and sintering at 950 °C for 24 hours with intermediate grinding. The mixture was slowly cooled, with a cooling rate of 200 °C/h, to 500 °C in flowing oxygen. It was annealed in oxygen at 500 °C for 12 hours and slowly cooled to room temperature. The powder was found to be superconductive at 91 K.

The starting materials were mixed in various stoichiometric ratios, namely $Y_1Ba_4Cu_{10}O_x$ (which will be referred to as $Y_{1,4,10}$ for the rest of this chapter, and similar notations will be used for other stoichiometric compositions), $Y_{1,6,13}$, $Y_{1,6.3,12.5}$, $Y_{1,4.33,8}$, $Y_{1,3.25,5.75}$, and $Y_{1,9,23}$. Powders were ground in a mortar-pestle for at least 15 minutes until fine uniform mixtures were obtained. Portions of the mixture weighing 3 to 4 grams were loaded in alumina crucibles with capacities of 10 ml (boat) and 13 ml (rectangular tray) and heated in air at various temperatures ranging from 970 °C to 1100 °C. After staying at these temperatures for several hours, samples were cooled to lower temperature (900 °C) with a cooling rate ranging from 0.5 °C/h to 6 °C/h. From this lower temperature, samples were cooled to room temperature at a higher cooling rate (from 20 °C/h to 100 °C/h). The exact heating procedures and their effects will be discussed in detail in Section 4.3. After the heating process, crucibles were removed from the furnace and free standing crystals, in most cases, could be easily picked up with tweezers. Crucibles were never broken into pieces in order to remove the crystals.

Electrical leads for the resistivity measurement were connected to crystals with gold contacts. The crystal surfaces were cleaned by dipping the crystals in a solution of 1%Br (by volume) in ethanol [7] for 40 to 60 seconds before thoroughly rinsing in pure ethanol. Four gold pads were evaporated on to the crystal surface. The samples

were then annealed in air at 500 °C for 1 hour. This annealing process was found to be necessary to further reduce the contact resistance between the gold pads and the crystal surface. While an etching process using the bromine solution does clean the surface of the crystal, but once the crystal is exposed to the atmosphere a thin carbon dioxide layer forms on the crystal surface. This CO_2-layer separates the gold pads from the surface of the crystal. An annealing process is used in order to get the gold to diffuse through the insulating CO_2-layer. In order to have a much lower contact resistance one should clean the crystal in a vacuum system with sputtering and then deposit gold pads while maintaining the vacuum. Thin gold wires were attached to the gold pads with silver epoxy. The resulting contact resistance at each contact is less than 1 Ω. The electrical resistance as a function of temperature was measured using the standard dc four probe technique (discussed in chapter 5).

4.3 Experimental results

A variety of factors were explored in the crystal growth process in order to optimize the crystal growth. These factors can be divided into two groups: (1) those related to materials and the environment (including the effect of various starting components, the effect of the overall starting stoichiometry, the geometrical arrangement of powders, and the choice of crucibles) and (2) those related to the thermal treatment (including the highest heating temperature, the cooling rate, the plateau temperature, and the effect of re-baking). The growth factors and the experimental results are discussed in detail below.

4.3.1 Effect of the starting materials

To study the role of starting materials on crystal growth, samples were

fabricated from two different combinations of various starting components. The first batch was composed of the precursor $BaCuO_2$, $Y_1Ba_2Cu_3O_x$ in bulk powder form, and CuO powder. The second batch contained powders of Y_2O_3, $BaCO_3$, and CuO [8]. Crystal growth results show that there is no apparent advantage of using $Y_1Ba_2Cu_3O_x$ and the precursor as the starting materials. Crystals obtained in the above two batches prepared from different starting components are approximately of the same size and the batches yield nearly equal numbers of crystals that are bigger than 2 mm in length. Since the heating temperature in most cases is much higher than the melting point of $Y_1Ba_2Cu_3O_x$ (990°C) [9] and $Y_1Ba_2Cu_3O_x$ melts incongruently [10], there is no advantage in having $Y_1Ba_2Cu_3O_x$ as a starting component. On the other hand, a process using Y_2O_3, $BaCO_3$, and CuO in raw powdered form as the starting materials saves time since neither the precursor nor $Y_1Ba_2Cu_3O_x$ has to be prepared in advance.

4.3.2 Effect of the starting stoichiometry

To investigate the relationship between the starting stoichiometric composition and crystal quality [3,8,10,11], four different overall compositions of the starting materials were studied with cooling rates ranging from 0.5 °C/h to 6 °C/h: $Y_{1,4,10}$, $Y_{1,6.3,12.5}$, $Y_{1,4.33,8}$ and $Y_{1,3.25,5.75}$. The positions of these stoichiometric compositions in the phase diagram near 1000 °C [10] are shown in Fig. 4.1. It can be seen that all the compositions are well inside the region of partial melting. It is found that at cooling rates higher than or equal to 3 °C/h, plate-like crystals with sizes larger than 2x2 mm^2 are obtained for compositions which are rich in flux (i.e., $Y_{1,4,10}$ and $Y_{1,6,13}$). At the same cooling rates, no crystals larger than 1x1 mm^2 are obtained for the compositions $Y_{1,4.33,8}$ and $Y_{1,3.25,5.75}$ which are not so rich in flux. On the other hand at

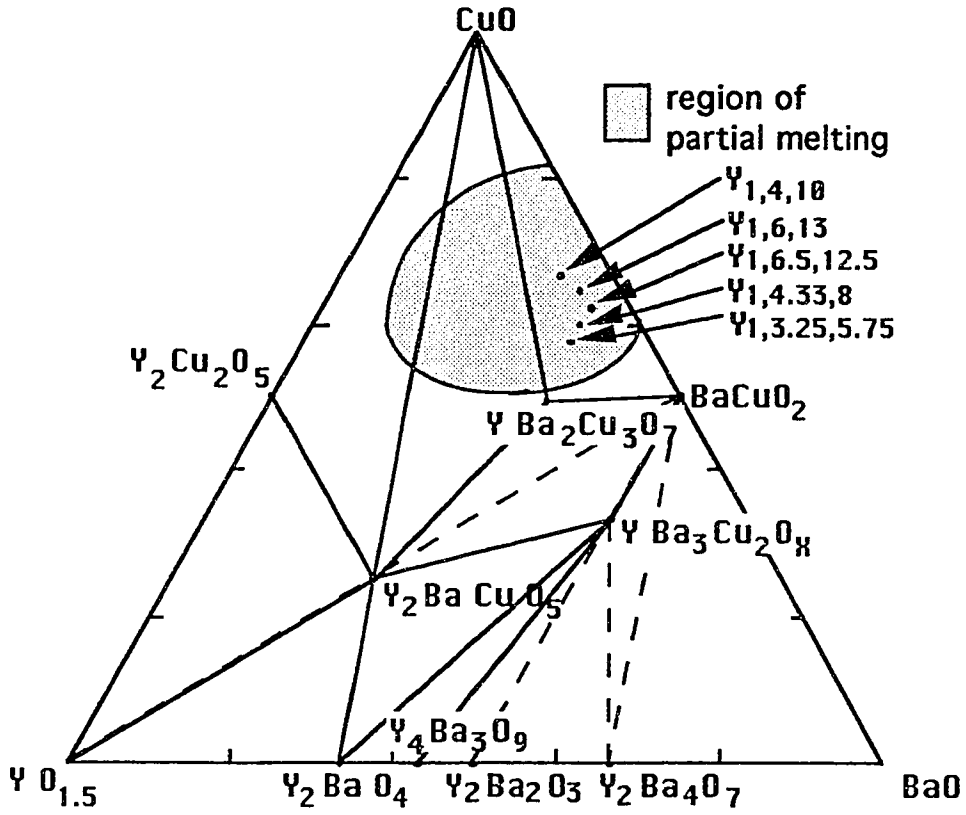

Fig. 4.1: Y_2O_3-BaO-CuO ternary phase diagram near 1000°C (reference 10).

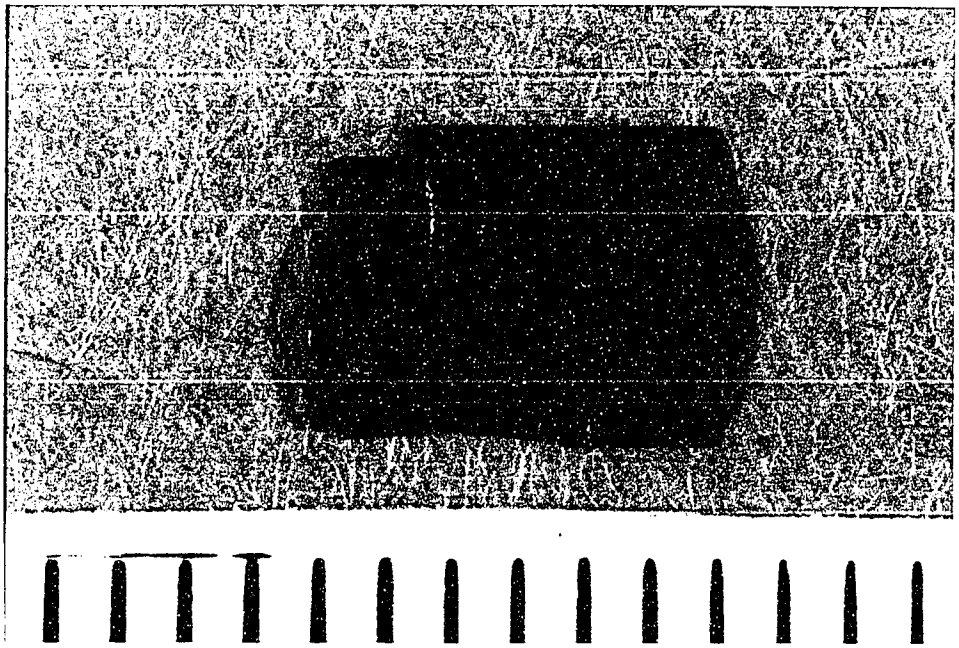

Fig. 4.2 : A plate-like crystal of size 6.1x4.8x0.05 mm^3 grown from $Y_{1,4.33,8}$ composition. The crystal is resting on a cardboard piece (in the background). The distance between the two marks is 1mm (this is the same for Fig. 4.2 through Fig. 4.7).

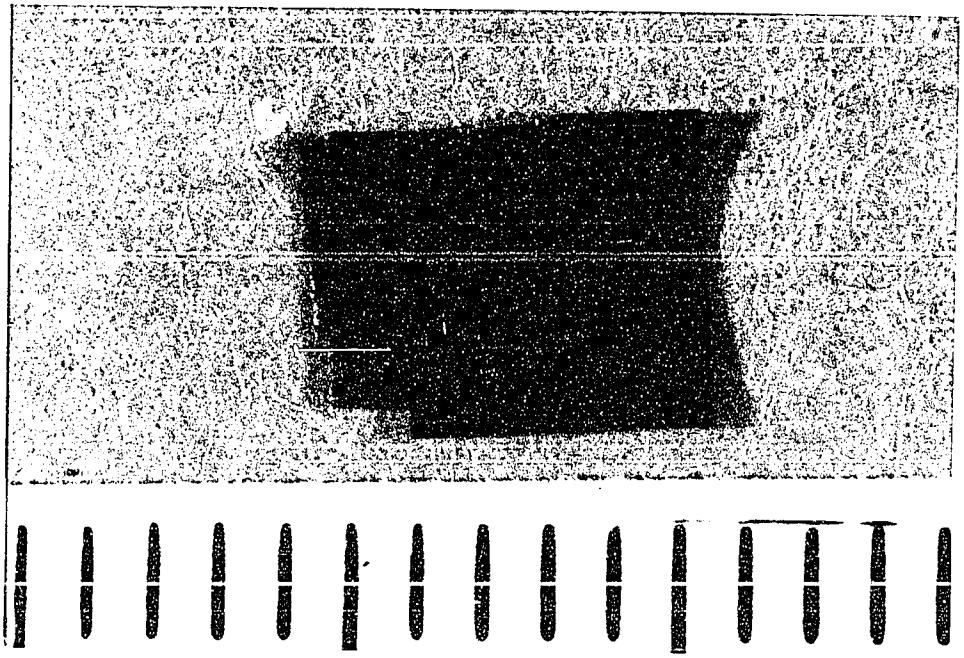

Fig. 4.3: The other side of the crystal shown in Fig 4.2. Both sides of the crystals are equally clean and free from flux material.

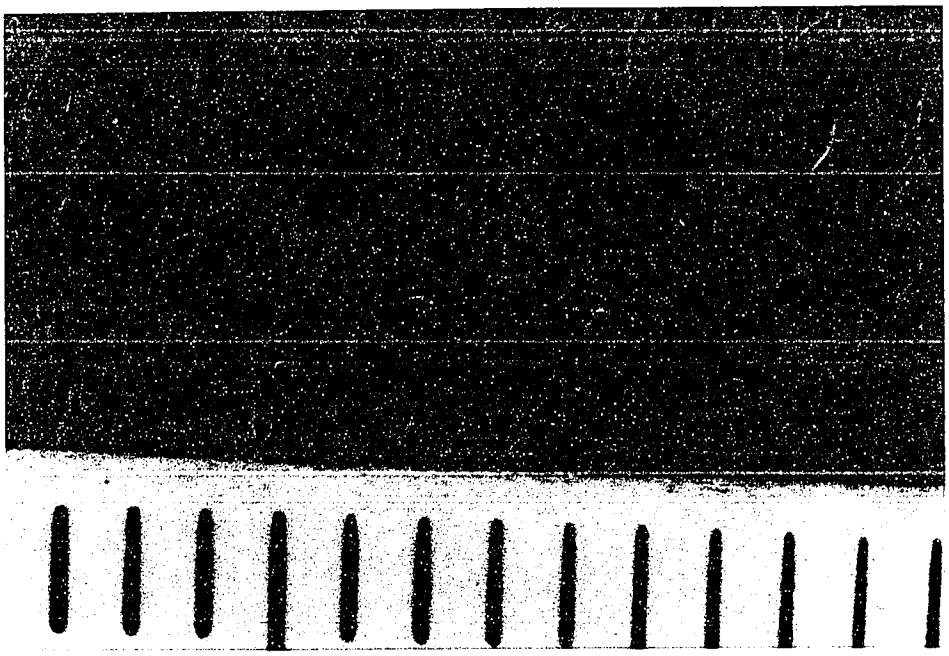

Fig. 4.4 : Block-like crystals grown in the same crucible as plate crystal shown in Fig. 4.2, from stoichiometry $Y_{1,4.33,8}$.

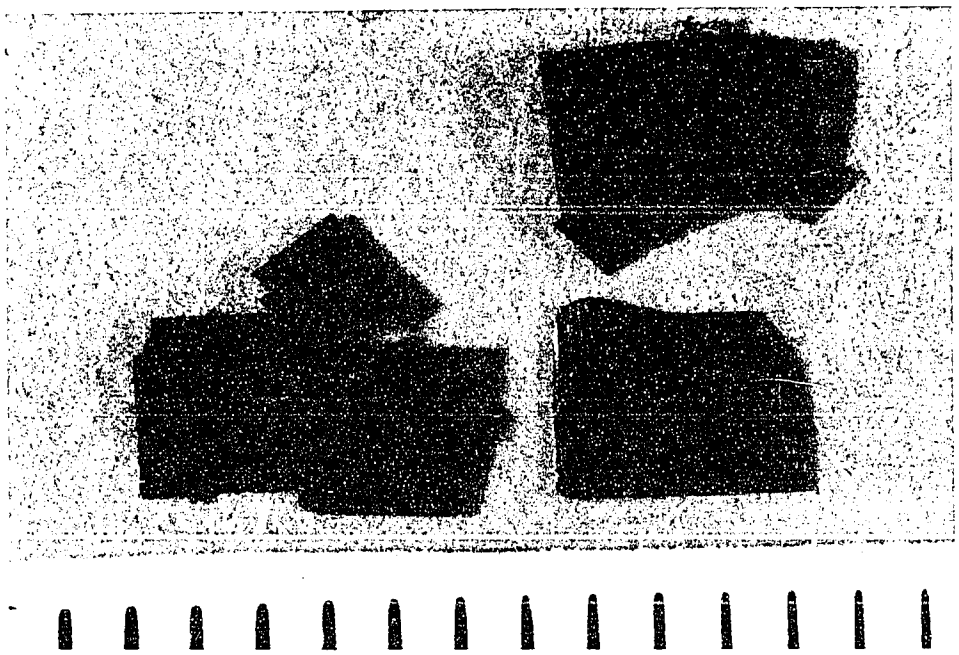

Fig. 4.5 : Plate-like crystals grown from composition $Y_{1,6,13}$.

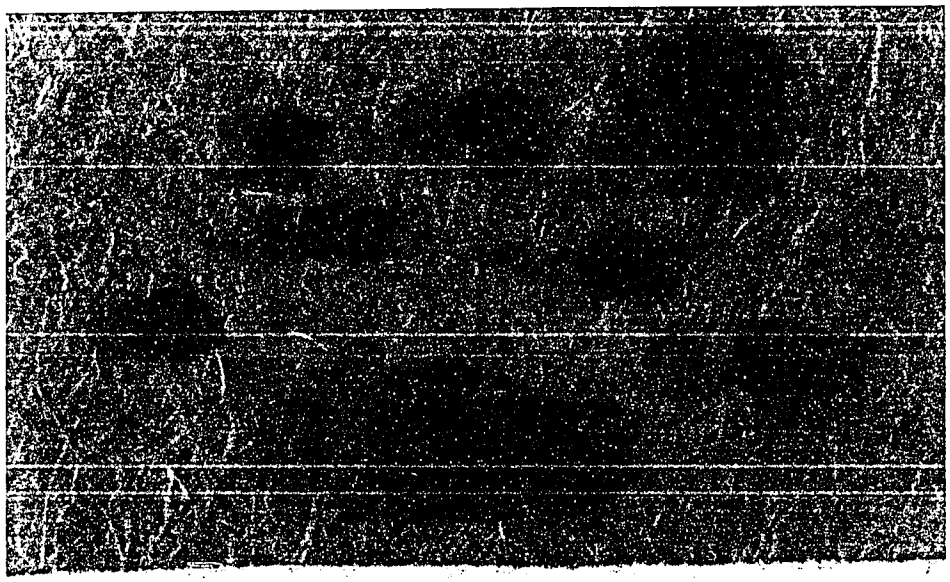

Fig. 4.6 : Block-like crystals grown from the composition $Y_{1,6,13}$.

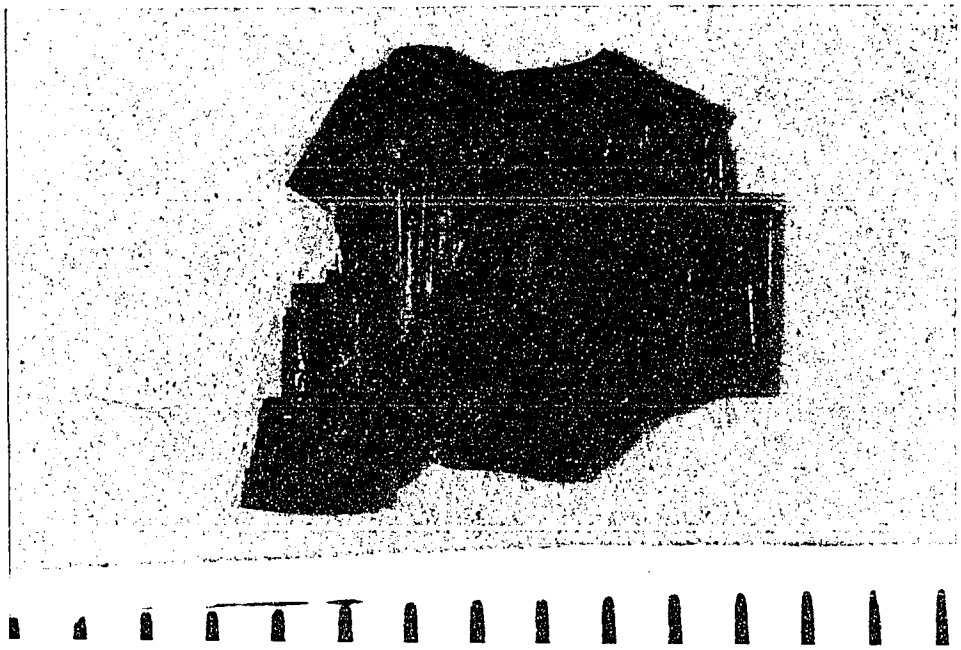

Fig. 4.7 : A plate crystal of size 7.3x7.0x0.14 mm^3 grown from $Y_{1,6,13}$.

Table 4.1: Details of heating procedure and type of crystal grown

Heating Procedure	Compositions	Results
a) 1010°C (1h)-2°C/h-989°C(48h)-1°C/h-900°C	$Y_{1,6,13}$	Thick plate crystals of size 4x3mm^2 and block crystal of 1mm size
	$Y_{1,4.33,8}$	Plate crystal of size 6x5mm^2 and block crystals of 1mm size
b) 1010°C(1h)-2°C/h-980°C(48h)-1°C/h-900°C	$Y_{1,6,13}$	Thin plates of size 5x5,4x4mm^2 and block crystals of size upto 1.5mm
	$Y_{1,4.33,8}$	Plate crystals of size 5x4mm^2 and block crystals of size 1mm
c) 989°C(48h)-1°C/h-900°C	$Y_{1,6,13}$	Thick plates of size 5x6mm^2
	$Y_{1,4.33,8}$	Small blocks of size 0.5mm
d) 1020°C(2h)-4°C/h-900°C	$Y_{1,4,10}$	Thin plates of size 4x4mm^2
	$Y_{1,4.33,8}$	Block crystals of size less than .5mm
e) 1020°C(2h)-2°C/h-900°C	$Y_{1,4,10}$	Thin plates of size 3x3mm^2
	$Y_{1,4.33,8}$	Block crystals of size less than 1mm
f) 970°C(12h)-1°C/h-900°C	$Y_{1,4,10}$	Plates of size 4x3mm^2
	$Y_{1,4.33,8}$	No crystals

cooling rates lower than or equal to 2 °C/h, both kinds of crystals, plate-like and block-like, can be simultaneously obtained in the same crucible from all the compositions, provided that the proper heating procedure is followed.

Photographs of as-grown crystals (without any polishing or cleaving) obtained from two compositions, one rich in flux ($Y_{1,6,13}$) and the other with less flux ($Y_{1,4.33,8}$), are shown in Fig. 4.2 through Fig. 4.7. The photographs were prepared by photographer Mr. Tom Tatnall of HIG. The distance between the two marks is 1 mm. Both plate-like and block-like crystals are produced simultaneously in the same crucible for these two compositions. The thermal histories and the results are summarized in Table 4.I. Fig. 4.2 shows a plate-like crystal of size 6.1x4.8x0.05 mm^3 grown from the composition $Y_{1,4.33,8}$ which is generally considered favorable for the growth of block crystals [8]. The other side of the same crystal is shown in Fig. 4.3. It can be clearly seen that the crystal is free from any flux material and both sides are equally clean. Block crystals of sizes 1.5x1.2x0.56 mm^3, 1.2x1.3x0.76 mm^3, 1.3x1.17x0.55 mm^3, and 1.3x0.7x0.25 mm^3 obtained from the same crucible are shown in Fig. 4.4. Usually smaller blocks have more regular shapes than the bigger blocks. Fig. 4.5 shows plate-like crystals (of sizes 5x2.7x0.03 mm^3, 4x3x0.02 mm^3, and 3.9x3x0.15 mm^3) grown from the composition $Y_{1,6,13}$. Block crystals obtained from the same batch is shown in Fig. 4.6. The size of the biggest crystal shown in this picture is 1.62x1.21x0.75 mm^3. Fig. 4.7 shows a large thick plate-like crystal of size 7.3x7x0.14 mm^3 grown from the composition $Y_{1,6,13}$. The surface of this crystal is not optically flat and growth patterns are visible in contrast to the clean crystals shown in Fig. 4.5.

Fig. 4.8 shows the temperature dependence of the normalized resistance in the a-b plane of several as-grown crystals without any oxygen annealing. The corresponding

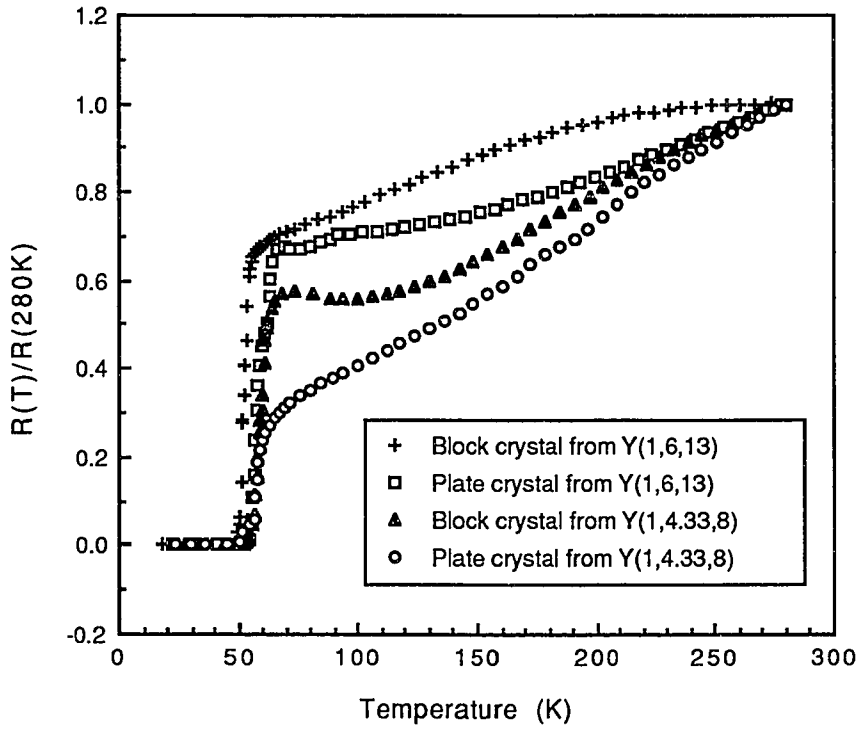

Fig. 4.8 : The normalized electrical resistance R(T)/R(280K) measured in the a-b plane plotted as a function of temperature for both kinds of crystals: plates and blocks, as grown from two different starting stoichiometric compositions $Y_{1,6,13}$ and $Y_{1,4.33,8}$ on alumina crucibles in air.

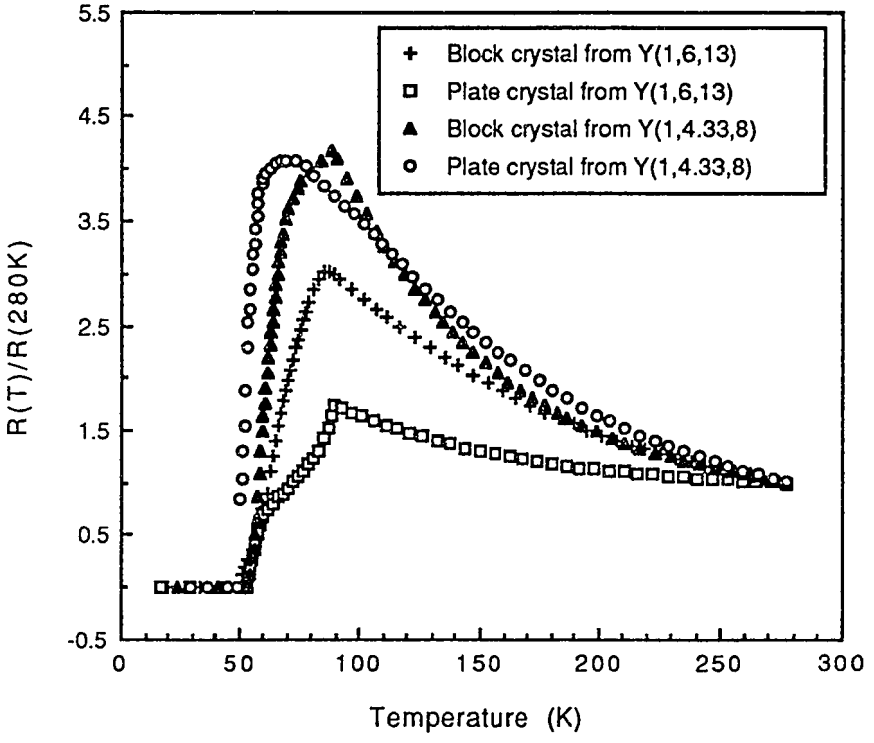

Fig. 4.9 : The normalized c-axis electrical resistance R(T)/R(280K) as a function of temperature for the respective crystals of Fig. 4.8. The as grown block crystals and plate crystals show similar resistive behavior. The result also show that crystals grown from two different starting stoichiometric compositions $Y_{1,6,13}$ and $Y_{1,4.33,8}$ exhibit similar $T_{c,onset}$ and $T_{c,zero}$.

Table 4.2 : Value of resistivity for as-grown crystals with no oxygen annealing at temperature of 280K.

DESCRIPTION	ρ_{ab} (mΩ.cm)	ρ_c (mΩ.cm)
1. Block crystal from $Y_{1,6,13}$	4.0	92.6
2. Plate crystal from $Y_{1,6,13}$	2.6	208.4
3. Block crystal from $Y_{1,4.33,8}$	3.3	74.7
4. Plate crystal from $Y_{1,4.33,8}$	1.4	119.5

resistance along the c-axis is plotted in Fig. 4.9. Numerical values of the a-b plane and c-axis resistivities are given in Table 4.2. As can be seen from the graphs, all crystals grown in air are superconducting near 50 K. As-grown crystals with higher T_c (>80 K) have been obtained by others [12,13] with a cooling rate of 12 °C/h from the highest heating temperature until 500 °C. In our experiments, the crystals were cooled at a much higher cooling rate of 50 °C/h from 900 °C to 500 °C resulting in lower T_c for our as-grown crystals. The low value of Tc,zero is not a problem, it just indicates that the oxygen content of the crystal is low. The oxygen incorporated in the crystal depends on cooling rate : lower cooling rates causes higher oxygen incorporation. The oxygen content of a crystal can be easily increased by annealing the crystal in flowing oxygen.

4.3.3 Geometrical factors

In general two kinds of crystals can be grown, i.e., plate-like crystals and block-like crystals [14]. It has been reported that plate-like crystals tend to grow close to a crucible's walls whereas block-like crystals grow in the crucible basal plane [15]. Use of the above information was made to find the proper geometrical shapes of crucibles and the arrangement of starting powders to optimize the growth process. It is found that large, clean plate-like crystals of sizes up to 5x5x0.07 mm^3 can be easily grown if loose powder is kept at one end of the crucible (boat or tray) while leaving the other end clean (or, alternatively, by keeping the powder in the middle of the crucible to form a "mountain" and leaving both ends clean). This arrangement of powder in a crucible is shown in fig 4.10. Large crystals in such arrangements, free standing and free from the flux, are formed near the clean ends of the crucible, with some small crystals near the region where the powders were originally placed. These large crystals can be easily removed with tweezers. It is found that pressing the powder in the form of a pellet

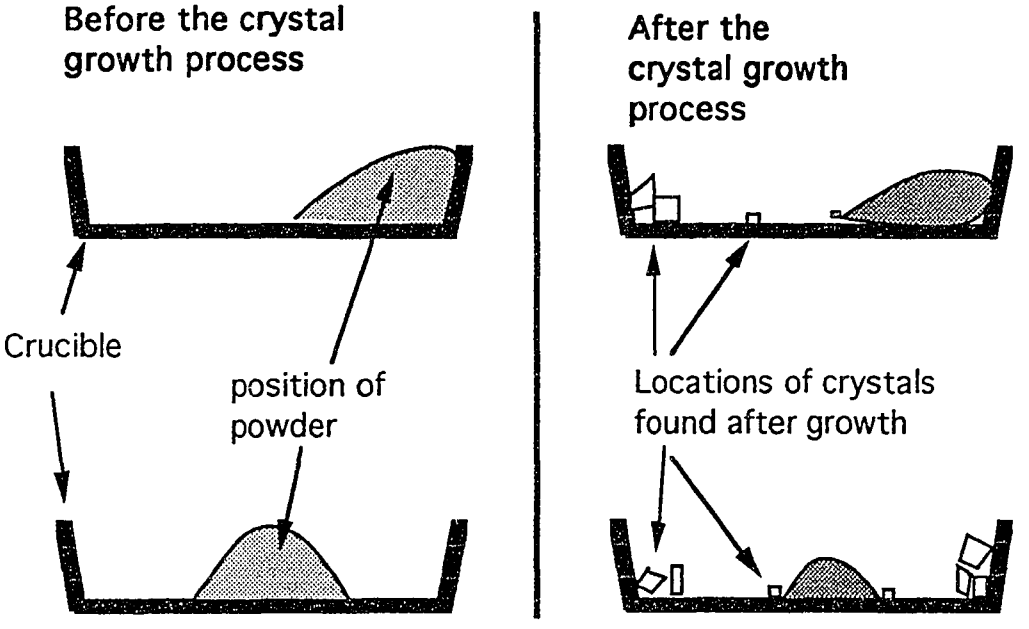

Fig. 4.10 : Large free standing crystals which are also completely free from the flux are obtained if the starting powder is placed on one end of the crucible instead of covering the whole crucible with the material. Figure shows the positions of starting powder in the crucible before the crystal growth process and the locations of large size crystals obtained after the growth process.

before heating results in smaller crystals which are difficult to remove. Crystals in such cases can only be removed mechanically by crushing the crucible.

Furthermore, putting the crucible on an inclined base with an inclination of 10° to 20°, with powder located at the higher end, improves the growth of plate-like crystals. The inclination of the crucible helps the flux in flowing to the lower part of the crucible where crystal growth takes place. No detailed experiments were performed to determine the best angle of inclination, which will depend on the viscosity of the flux and hence will depend on the starting stoichiometry and temperature of heating. Crystals up to 6x4 mm^2 in sizes can be easily grown by this technique. A similar technique of inclined crucible has been used by others [16] to separate flux from the crystals. As far as block crystals are concerned, the opposite is true. A uniformly distributed powder in a horizontally placed crucible yields better results than the inclined crucibles for the growth of block-like crystals.

4.3.4 The choice of crucibles

All the crystals that have been discussed so far were grown in alumina crucibles (boats and trays). Fig. 4.11 shows the normalized resistance of an oxygen annealed crystal (size 1.35x1.35x0.17 mm^3) as a function of temperature. The crystal was annealed at 400 °C in flowing oxygen for 6 days. The resistivity in the ab plane is 1.8 mΩcm and in the c-axis direction is 13.7 mΩcm at 280 K. $T_{c,onset}$ (the temperature at which superconducting transition starts) is 90.4 K and $T_{c,zero}$ (highest temperature at which resistance is zero) is 78 K. This behavior may be explained by the aluminum contamination resulting from the crucible material [17]. Crystals contaminated by aluminum are found to have $T_{c,zero}$ below 87 K. The amount of contamination depends on various factors such as the heating temperature, area of

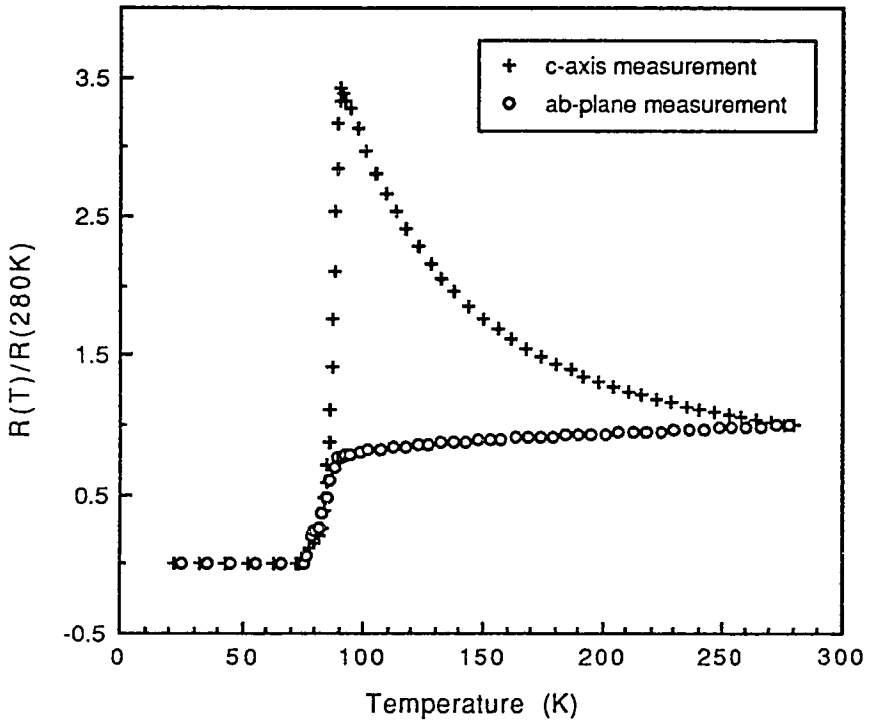

Fig. 4.11 : The normalized resistance vs temperature plot for an oxygen annealed crystal. The crystal was grown on an alumina crucible. The resistance plotted for two directions, ab-plane and c-axis, shows the anisotropic behavior.

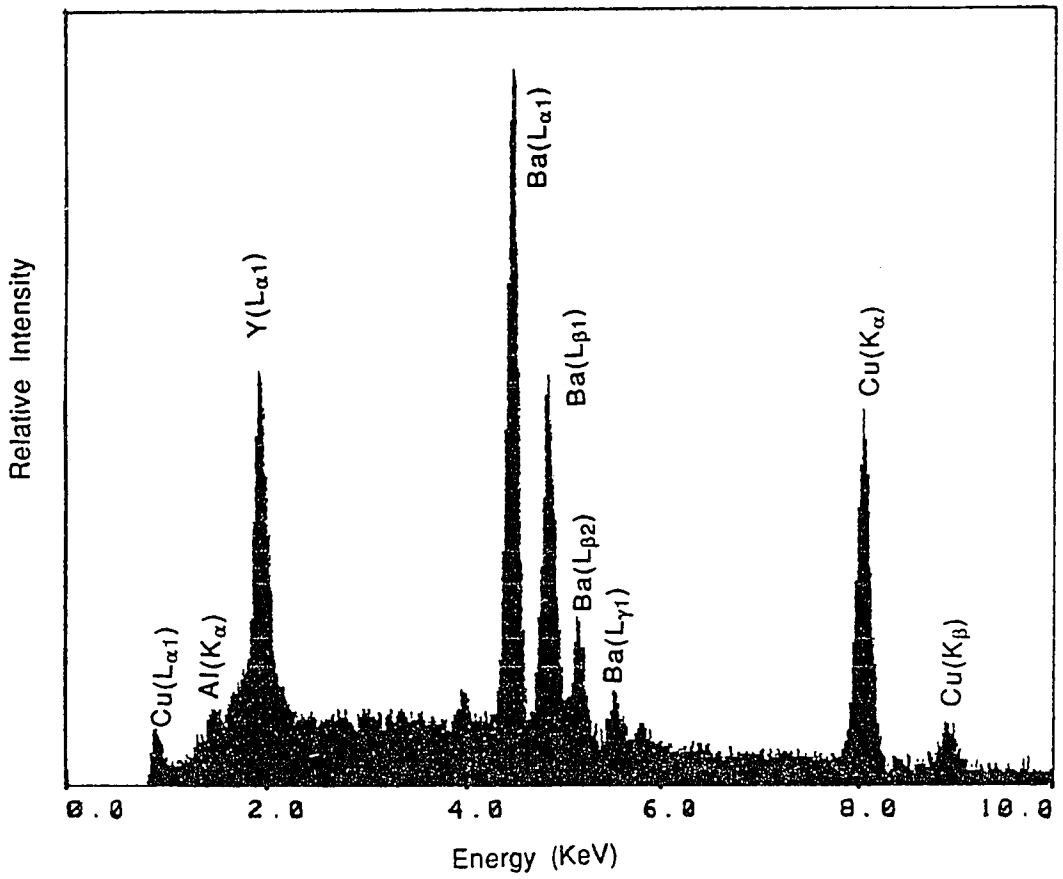

Fig. 4.12 : Energy dispersive spectrum of a $Y_1Ba_2Cu_3O_x$ single crystal. The spectrum was taken with the help of a scanning electron microscope. The heights of the peaks represent the relative intensity of characteristic X-rays emitted by the crystal. All major peaks are identified to belong to Y, Ba, and Cu. The main contaiminations were found to be due to Al(3.25 at.wt.%) and Si(1.46 at.wt.%).

contact, and the porosity of the crucible [17,18]. The higher the porosity, the higher the contamination. Elemental analysis of crystals grown on alumina was carried out with the help of scanning electron microscope. The technical help of Mr. Donald McGee and use of SEM at Analytical Electron Microscope Laboratory, SOEST, UH is gratefully acknowledged here. A total of 4 crystals were analyzed. Energy dispersive spectrum of a $Y_1Ba_2Cu_3O_x$ crystal is shown in fig. 4.12. The heights of the peaks represent the relative intensity of characteristic X-ray spectral lines. All major peaks were identified with Y, Ba, and Cu. The main contaminations were found to be due to aluminum (3.25 at.wt.%) and silicon (1.46 at.wt.%). The source of aluminum contamination is the alumina crucible used for crystal growth. The plausible source of silicon contamination is the quartz tube used in oxygen annealing setup. In order to avoid aluminum contamination, the crystal growth process was also studied in gold crucibles. The details are given in section 4.4.

Crucibles of different sizes and shapes were tested to study the possible effect on the size of crystal obtained, as reported by others [19]. The results from our experiments were inconsistent.

4.3.5 Effect of the highest heating temperature

In order to investigate how the heating temperature affects the quality of crystals, several samples of stoichiometric composition $Y_{1,4,10}$ were heated at various temperatures ranging from 970 °C to 1100 °C. The heating procedure and the results are summarized in Table 4.3. It was found that good quality crystals with no flux attached are obtained when the heating temperature was kept below 1025 °C. Heating at higher temperatures generate crystals that are clean only on one side while the other side is usually attached with flux. Also crystals are formed inside bubbles and they are

Table 4.3 : Effect of highest heating temperature on crystal growth

Composition : $Y_{1,4,10}$ (made from $Y_1Ba_2Cu_3O_x$, $BaCuO_2$, CuO)

Heating procedure : All samples were heated to temperature shown as "temperature" for time (in hours) shown in the brackets. Samples were then cooled with a cooling rate of 6°C/h (favorable for plate-like crystals) to the lower temperature of 820°C. From this temperature samples were cooled to room temperature with cooling rate of 50°C/h.

Temperature	Results
a) 1100°C (12h)	Formation of bubbles. Crystals were formed in the cavities of the bubbles. Crystals were clean only on one side.
b) 1050°C (5h)	Dull looking crystals of size 4x2 mm^2 were obtained.
c) 1025°C (5h)	Crystals of size bigger than 4x3 mm^2 were obtained. Crystals were clean and shiny on both sides.
d) 1020°C (5h)	6x4 mm^2, 5x5 mm^2 crystals obtained, clean on both sides.
e) 1000°C (5h)	Clean crystals of size 5x5 mm^2
f) 970°C (48h)	Clean crystals of size 4x3 mm^2

difficult to remove, with a higher probability of breaking while separating them from the crucible. The most suitable heating temperature was found to be 1010 °C at which clean and free standing crystals can consistently be grown. Temperatures as low as 970 °C can be used in the crystal growth [15] provided that the starting composition is rich in flux. Compositions with less flux do not melt at this low temperature [8]. No crystals could be obtained when the compositions $Y_{1,4.33,8}$ and $Y_{1,3.25,5.75}$ were heated at 970 °C.

4.3.6 Effect of the cooling rate

The effect of the cooling rate on the crystal thickness has been previously investigated by others [8]. In general, the thickness of crystals increases for slower rates of cooling. Our experiments indicate that for plate-like crystals there is an optimum cooling rate close to 2 °C/h for which the thickness of the plate crystal is maximum. Crystals from two different stoichiometric compositions $Y_{1,4,10}$ and $Y_{1,6,13}$ were made with the cooling rate ranging from 0.5 °C/h to 6 °C/h. The samples were heated to 1025 °C for 2 hours in air and then cooled to 820 °C without stopping at intermediate temperatures. From 820 °C they were cooled to room temperature at the higher cooling rate of 100 °C/h. Thicknesses of the crystals, which were bigger than 2x2 mm^2 , were measured using a travelling microscope with uncertainties of 0.01 mm. The result is plotted in Fig. 4.13. It is important to notice that the above result is true only for plate-like crystals produced from the heating procedure described above. Thickness of a crystal can be increased by introducing a heating step at plateau temperature (discussed in the next paragraph). In general, at lower cooling rates thicker block-like crystals can easily be grown. Thickness of block crystals increases as the cooling rate is lowered and no optimum has been observed so far. Our results on

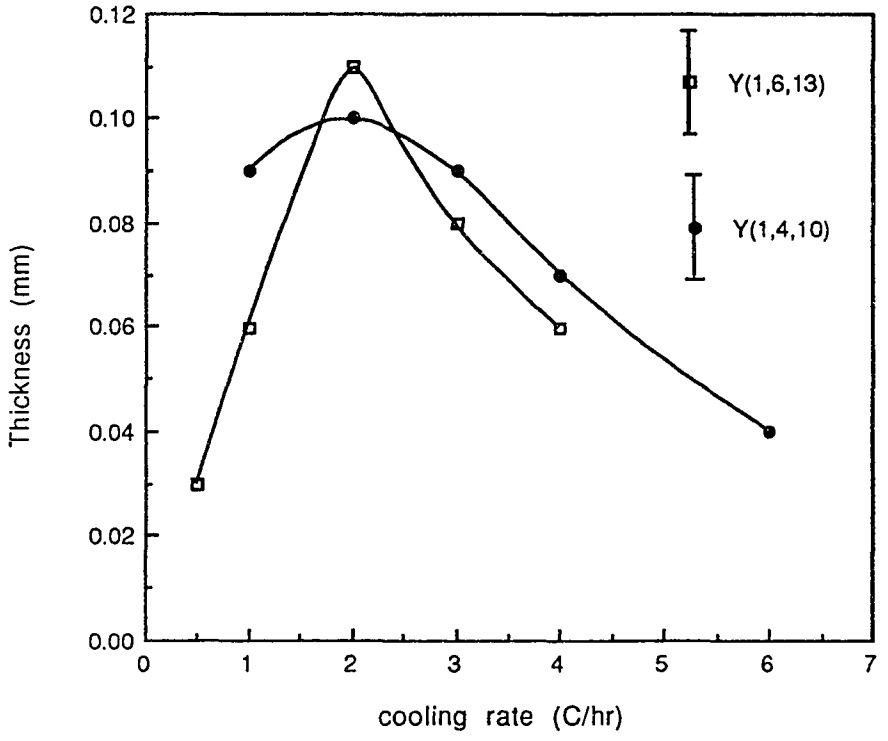

Fig. 4.13 : The thickness of plate-like crystals which are bigger than 2x2mm^2 (grown with no intemediate heating at plateau temperatures) plotted as a function of cooling rate. Crystals grown from two stoichiometric compositions $Y_{1,6,13}$ and $Y_{1,4,10}$ show optimum values of thickness at a cooling rate of 2°C/hr.

the thicknesses of block crystals are consistent with the literature. Block crystals with thicknesses up to 1 mm have been grown in the past with a cooling rate of 0.5 °C/h [12].

4.3.7 Effect of the plateau temperature

It was found that the growth of plate-like crystals may be improved by introducing an extra heating step at an intermediate temperature of 989 °C while cooling down from the highest heating temperature. To test the effect of the plateau temperature, samples were first heated to the highest temperature of 1010 °C and then cooled to different plateau temperatures. The samples were held at these plateau temperatures for 48 hours and finally they were cooled to the room temperature. Six plateau temperatures were tested and these are 1000 °C, 995 °C, 989 °C, 985 °C, 980 °C, and 970 °C, respectively. It was found that soaking at 1000 °C or 995 °C for a long time did not change the crystal growth, whereas soaking at other temperatures generated more crystals that were large and clean. The results are a direct consequence of the melting temperature of $Y_1Ba_2Cu_3O_x$, which is equal to 990 °C. Best results were obtained at the plateau temperature of 989 °C. From this batch, large plate-like crystals with a thickness of 0.15 mm were obtained. Staying at 980 °C and below did not produce thick crystals. The thickness of these plate-like crystals ranged from 0.02 to 0.04 mm.

4.3.8 Re-baking for better yield

It was found that using a crucible which had already gone through crystal growth, for the second time generated better yield and slightly larger crystals than the first growth process. The procedure was composed of the following steps: (i) removing all the large crystals; (ii) adding new raw materials on top of the previous melt; and (iii) going through the thermal treatment. The yield from such crucibles was sometimes twice as large as that obtained from new crucibles.

4.4 Discussion

To overcome the aluminum contamination problem, crystal growth properties were also studied using gold crucibles. Gold foils of thickness 0.1 mm were folded in the shape of boats and trays and were laid inside alumina crucibles. Crucibles made from gold foil are very economical compare to gold crucibles available from various chemical companies : the average cost of a gold foil crucible is about $50 in comparison with that of the gold crucibles of similar volume (40x10x6 mm^3) which cost over $1000 due to the extra weight of material and cost of processing involved. Using gold as the crucible material [15,20,21] restricts the range of the starting stoichiometry and the heating temperature for crystal growth. Gold foils melt completely at a heating temperature of 1000 °C, suggesting that a reaction takes place between the gold and the starting materials. Gold drops were seen along with the crystals grown on supporting alumina crucibles in a such melted batch. Heating temperatures of 970 °C and 980 °C are found to be safe for the gold foil crucibles. However, at such temperatures, crystals can be grown only from the flux-rich compositions. It was found that only very few small crystals could be grown from the starting stoichiometry $Y_{1,4,10}$, whereas many large crystals of sizes 4x3 mm^2 were easily grown from the composition $Y_{1,9,23}$. The heating process for the above batch is the following. First heat the starting materials to 980 °C for 24 hours. Then cool to 870 °C with a cooling rate of 3 °C/h and to 400 °C with 50 °C/h. Finally the crystals are cooled to room temperature with a cooling rate of 200 °C/h.

Elemental analysis was performed on two crystals using a scanning electron microscope. Amounts of gold introduced to the crystals were found to be 0.16 at.wt.% and 0.42 at.wt.%. X-ray diffraction analysis was performed on one of the single

crystals, grown on a gold foil crucible, by Mr. Philip Patalano. The use of an x-ray diffractometer at the U.H. Chemistry Department is gratefully acknowledged. The crystal structure was found to be orthorhombic with lattice parameters a=3.849±0.002 Å, b=3.862±0.002 Å, c=11.720±0.006 Å, α=89.99°±0.04°, β=90.00°±0.04°, γ=90.02°±0.04°. The lattice parameters are consistent with the reported values [22]. The crystal was found to be twinned. Twinning is commonly observed in these crystals.

The results discussed previously in the section on "geometrical factors", also apply to crystals grown in gold crucibles. Plate-like crystals are formed near the clean ends of the crucible and inclination of the crucible is helpful in the growth of such crystals.

Fig. 4.14 shows the temperature dependence of the normalized resistance, in the a-b plane and along the c-axis, of a crystal grown in air on gold foil from the composition $Y_{1,9,23}$ without any oxygen annealing. The resistivities at 280 K are 1.2 mΩcm in the a-b plane and 32.1 mΩcm along the c-axis, respectively. Fig. 4.15 shows the temperature dependence of normalized resistance of a crystal annealed at 450 °C in oxygen for 7 days. The resistivities at 280 K are 0.5 mΩcm in the a-b plane and 3.1 mΩcm along the c-axis, respectively. After oxygen annealing $T_{c,onset}$ is increased from 85 K to 93.6 K and $T_{c,zero}$ is increased from 67 K to 89 K. The resistivity is also reduced after oxygen annealing.

It is well known that $Y_1Ba_2Cu_3O_x$ melts incongruently [10] and therefore the flux growth method (also known as high-temperature solution growth method) is necessary for the preparation of these single crystals. The crystal growth process is essentially governed by supersaturation, heating temperature, crystal size, and fluid dynamics

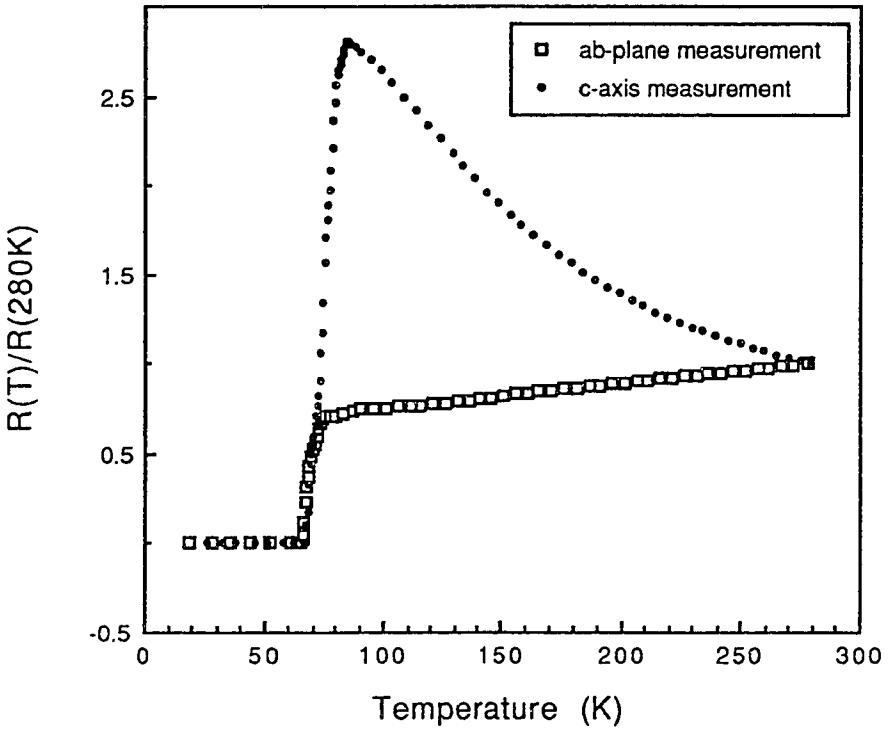

Fig. 4.14 : The normalized resistance vs temperature for an as-grown crystal without any oxygen annealing. The crystal was grown on gold foil in air from the composition $Y_{1,9,23}$.

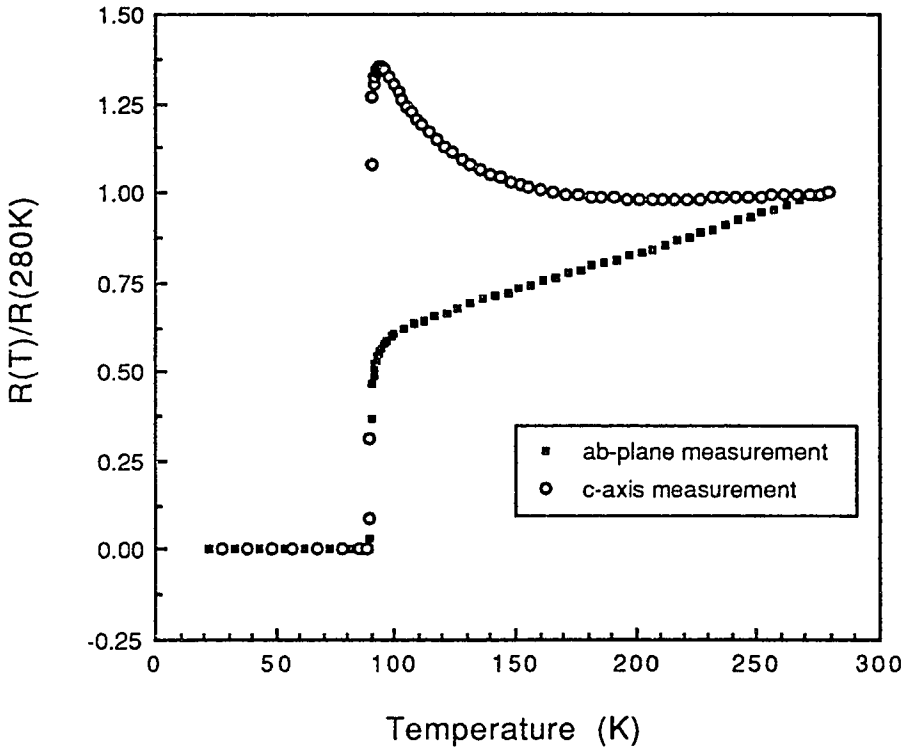

Fig. 4.15 : The normalized resistance vs temperature for an oxygen annealed crystal, grown on gold foil from the composition $Y_{1,9,23}$. Oxygen annealing was carried out at 450°C for 7 days.

[23]. In the growth of $Y_1Ba_2Cu_3O_x$ single crystals supersaturation is achieved by slow cooling, a commonly used method. Other alternatives include solvent reduction (partial removal of flux) and temperature gradient transport. The use of a plateau temperature as discussed in section 4.3 effectively plays the role of solvent reduction. The amount of flux is mainly reduced through absorption by porous crucible walls into the supporting ceramic block and partly by evaporation. It is found that for crystal growth on gold foil, the existence of a small temperature gradient (< 1 °C/cm) is crucial, whereas such a temperature gradient is not so critical for crystal growth in alumina crucibles. This behavior seems to be correlated with the fluid dynamics of the melting material since the melt flows easily in gold crucibles but is more viscous in alumina crucibles.

4.5 Conclusion

In summary, extensive studies on the growth of $Y_1Ba_2Cu_3O_x$ single crystals were performed using the flux method. Many growth factors related to materials, the environment, and the thermal treatment have been investigated. Experiments show that $Y_1Ba_2Cu_3O_x$ single crystals can be grown from starting materials with a wide range of stoichiometries. It is found that large free standing plate-like crystals can be easily grown by using an inclined crucible technique. The highest heating temperature of 1010 °C is found to be most suitable for growth of crystals free from any flux material. The use of an extra plateau temperature of 989 °C is found to be beneficial for crystal growth. It is also found that for growth of plate-like crystals there is an optimum cooling rate of 2 °C/h which yields crystals of maximum thickness while for block-like crystals this optimum cooling rate may possibly be lower than 0.5 °C/h.

References:

[1] H.Takei et al., Jpn. J. Appl. Phys 26 (1987) L1425.

[2] S. Bosi et al., J. of Materials Science Letters 8 (1989) 497.

[3] A. Drake et al., Submitted to E-MRS meeting ,strasbourg (1990) preprint.

[4] D. L. Kaiser et al., Appl. Phys. Lett. 51 [13] (1987) 1040.

[5] T. K. Worthington et al., Physica C 153-155 (1988) 32.

[6] X. D. Chen et al., Rev. Sci. Instrum. 58 (9) sept. (1987) 1565.

[7] R. P. Vasquez et al., Appl. Phys. Lett. 53 (1988) 2692.

[8] S. Shamoto et al., Solid State Commun. 66 no. 11(1988) 1151.

[9] I. V. Vodolazskaya et al., Physica C 162-164 (1989) 1213.

[10] L. F. Schneemeyer et al., Nature 328 Aug.(1987) 601.

[11] W. Sadowski et al., Physica C 162-164 (1989) 897.

[12] J. Kowaleski et al., Physica C153-155 (1988) 429.

[13] J. S. Abell et al., Physica C 162-164 (1989) 909.

[14] Hiroyuki Takeya et al., Physica C 153-155 (1988) 413.

[15] T. R. Dinger , High Temp. Supercond. Compounds: Processing and related properties, ed. S. H. Whang, Publication of The Minerals, Metals & Materials Society, Pennsylvania(1989) 23.

[16] Y. Wang et al., Jour. of Crystal Growth 106 (1990) 487.

[17] J. Wojcik , Proceedings of the European Conference of High Tc -Thin films and Single Crystal, Ed. W. Gorzkowski, world scientific, New Jersey (1989) 311.

[18] J. Kowalewski , Proceedings of the European Conference of High Tc -Thin films and Single Crystal, Ed. W. Gorzkowski, world scientific, New Jersey (1989) 3.

[19] F. Licci et al., Physica C 153-155 (1988) 431.

[20] H. Savary et al., Physica C 153-155 (1988) 419.

[21] A. Tressaud et al., Journal of less-common metals 151 (1989) 237.

[22] C. P. Poole, Jr., T. Datta, H. A. Farach in "Copper Oxide Superconductors", A Wiley-Interscience Publication, NY, (1988), page 93.

[23] M. Ohara and R. C. Reid, in "Modeling crystal growth rates from solution", Printice-Hall, Inc. Englewood Cliffs, N.J., (1973).

CHAPTER 5

EXPERIMENTAL SETUP

This chapter consists of four sections. In section 5.1, the setup for resistivity measurement is discussed. Section 5.2 describes the experimental setup for ac susceptibility. Measurement of 1/f noise using a cross correlation method is described in section 5.3. The error involved in the above experiments and their analysis is given in section 5.4.

5.1 Resistivity measurement

Resistance of a sample is measured by simple circuits based on Ohm's law. Simplest of all methods is "use of an ohmmeter" which is a two-probe method. In a two-probe method, current is passed through the sample using two probes and voltage is measured across the sample using the same probes. The resistance is then obtained by the ratio of voltage and current. The value of resistance obtained in this fashion is the sum of both the sample and contact resistances. In most cases the contact resistance is several orders of magnitude smaller than the sample resistance; the measured resistance is very close to the sample resistance. In the case of copper oxide superconductors, however, the normal state resistivity is of the order of 10^{-3} Ωcm and the contact resistance is of the order of few ohms. Therefore a two probe method is not practical in the case of copper oxide superconductors. Resistance in these cases, where sample resistance is comparable to or lower than the contact resistance, is measured using a four-probe method.

In a four-probe method [1], the outer two probes are used for passing the

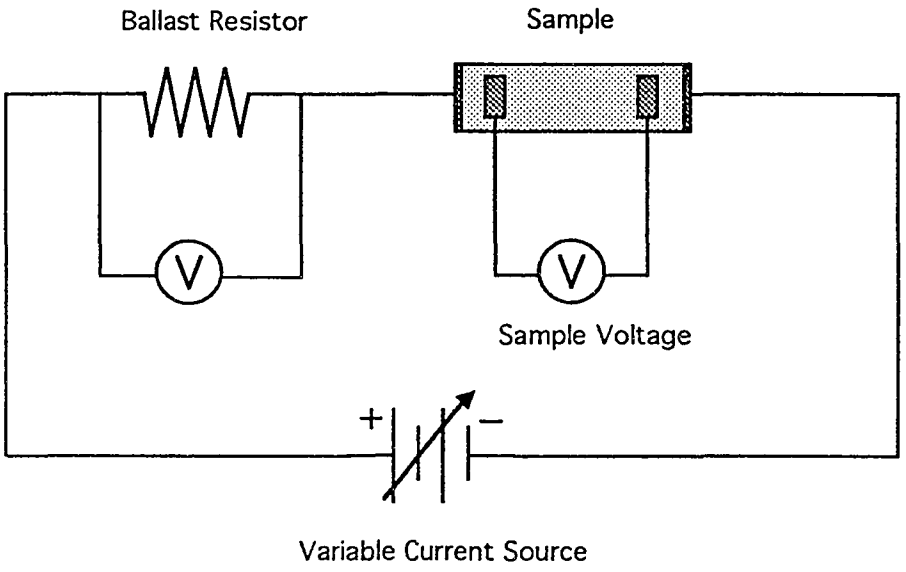

Fig. 5.1 : Four probe method for resistivity measurement.

current and inner two probes are used for measuring the voltage, as shown in the Fig. 5.1. This arrangement highly reduces the contributions from the contact resistance. However, it is still important to have low resistive ohmic contacts. A highly resistive contact can give rise to heating effects, which may heat up the sample by a few degrees. In the case of bulk samples low resistance contacts are easily obtained by pressing indium wafers onto the sample. Silver epoxy or paint may also be used for making contacts, but care must be taken to avoid excessive diffusion into the pores of the sample. At present, indium contacts on a single crystal of $Y_1Ba_2Cu_3O_x$ cannot be used because of the small size of the crystals and the large force required to adhere the indium wafers to a sample. A direct application of silver paste on the crystal was found to give a highly resistive contact. Contacts on small single crystals are made by depositing gold or silver pads on the crystals and then connecting gold or silver wires to these pads using silver paste. This process is discussed in chapter 4.

The experiment is carried out by passing a small dc current through the sample from a constant current source. The current must be smaller than the critical current of the sample. Also it should be small enough to cause no heating of the sample and large enough so that the measured voltage is much higher than the sensitivity of the voltmeter. In our experiments, a nanovoltmeter was used. A current of 1 mA is found to be appropriate for the resistance measurement of most copper-oxide superconductors. The constancy of the current is maintained by connecting a large ballast resistor in series with the sample. The resistance of the ballast resistor is chosen to be several orders of magnitude higher than the sample resistance. A high value of total resistance of the circuit maintains the dc current level even when the sample resistance is changing in the transition region.

The ballast resistor is also used to monitor the current through the sample. If

somehow the sample becomes insulating, then the voltage would also drop to zero, but the current would follow and one could immediately tell the difference between a superconductor and an insulator. A crack in the sample can cause the sample voltage to go to zero while still showing a constant current reading. Such a crack is shown below:

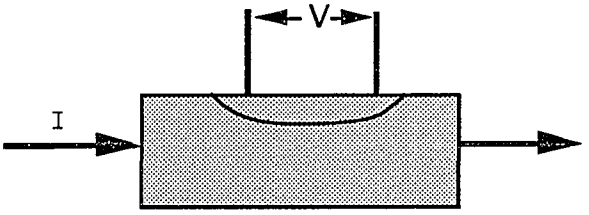

This type of situation is easily identified since the sample will show zero resistance most of the time, independent of the temperature of the sample. The situation can be further made clearer by using various combinations of current and voltage leads by permuting the leads. Existence of cracks or highly resistive contacts are easily checked by monitoring the room temperature resistance of the sample with the help of a multimeter, while permuting the leads.

Contacts with different values of contact resistance can cause a temperature gradient in the sample due to nonuniform heating effects. This can produce a thermal e.m.f. in the sample. In order to eliminate the voltage contribution from the thermal e.m.f. effects, the applied current should be switched back and forth and the voltage across the sample should be averaged over two readings corresponding to two directions of the current.

Effects of thermal fluctuations are also reduced by carefully designing the cryostat. It is important to surround both the sample and the thermal sensor in an isothermal enclosure. An enclosure made of copper is found to be satisfactory for above purpose. In an ideal case, a sample should be kept on top of the thermal sensor and measurement be carried out slowly so that the sample and the sensor have enough time to

reach thermal equilibrium. In our experiments, samples were cooled to a low temperature of either 77 K or 20 K and slowly warmed up to the room-temperature in a period of 5 to 7 hours. Bulk samples of high Tc superconductors are easily measured by cooling them with liquid nitrogen. Use of liquid nitrogen was avoided in the measurements involving single crystal samples. A "liquid nitrogen dip" usually produces a thermal shock which is big enough to produce cracks in the crystal. Also, use of liquid nitrogen introduces a small amount of water moisture into the sample, which greatly affects the properties of the sample. Resistances of single crystals were measured by cooling them in vacuum using a cryogenic closed cycle helium refrigerator; hence avoiding both the thermal shock and water vapors.

5.2 Susceptibility measurement

There are two classical ways to define superconductivity, one involving the property of zero resistance and the other based on perfect diamagnetism. In an ideal homogeneous superconductor both measurements should provide the same transition temperature. For the resistivity measurement, it is important that the superconducting grains are well connected with each other, forming a complete conduction path for the current. Such a condition is not required for the susceptibility measurement. Hence the susceptibility measurements have an advantage over the resistivity measurement in searching for new superconductors. A susceptibility measurement can detect the existence of small scattered superconducting phases which may be invisible in the resistivity measurement of the sample [2].

A mutual inductance method was used to detect the qualitative behavior of susceptibility of copper oxide superconductors. Fig. 5.2 shows the circuit used in this

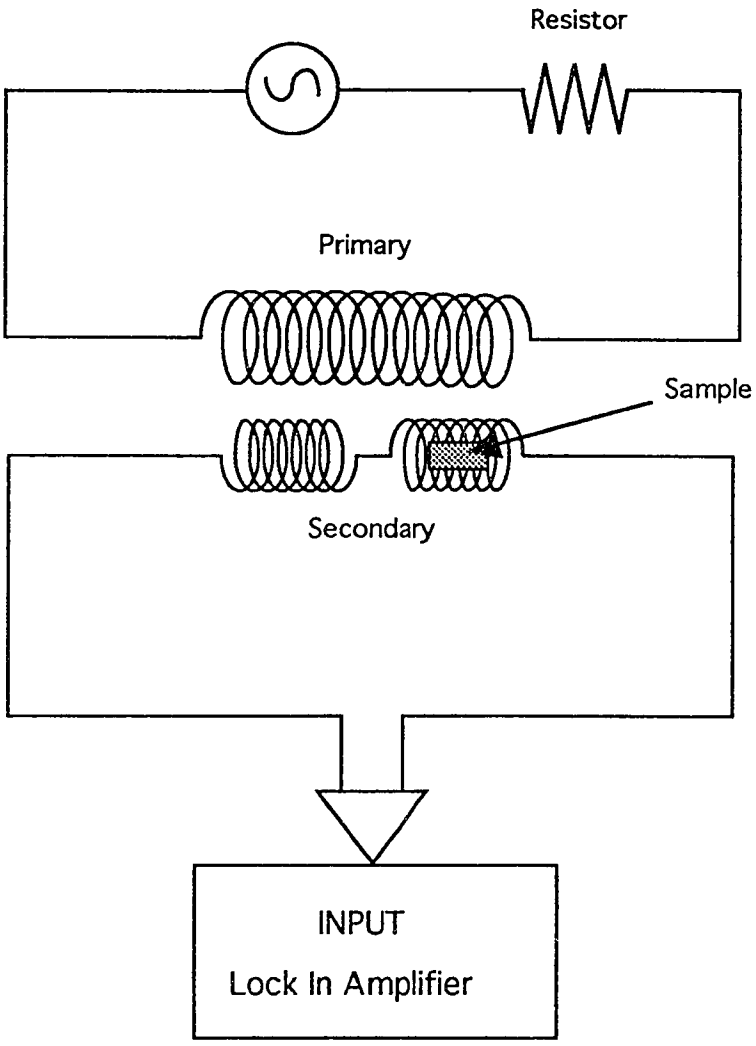

Fig 5.2 : Circuit diagram for susceptibility measurement.

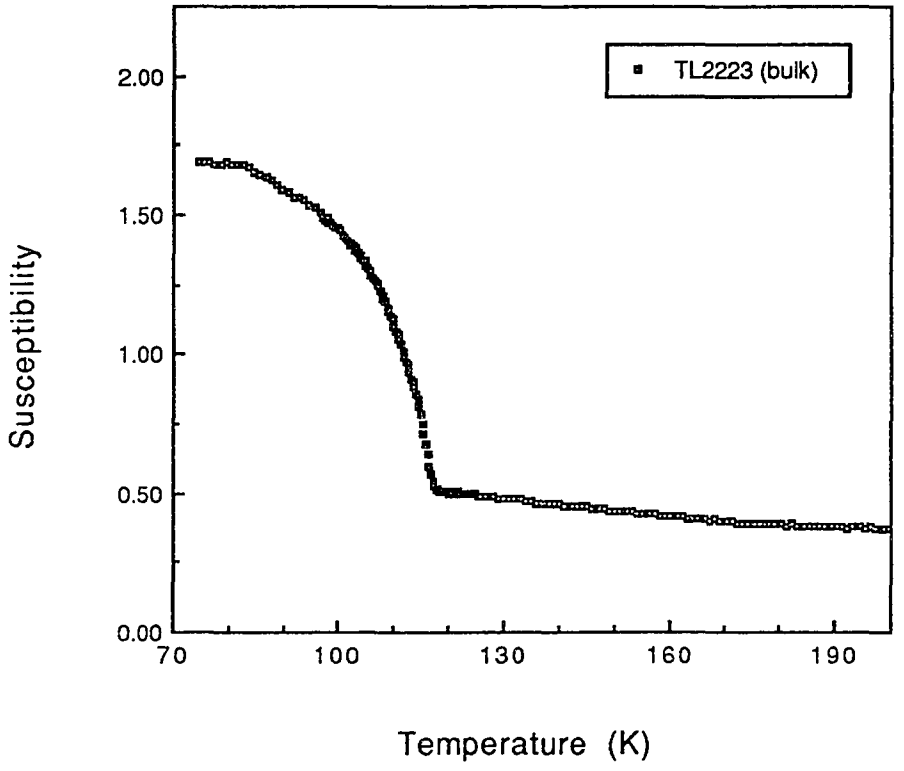

Fig. 5.3 : ac susceptibility in arbitrary units as a function of temperature for a $Tl_2Ba_2Ca_2Cu_3O_{10}$ bulk sample. The sample shows clear diamagnetic signal at 118K. The value of T_c = 118K is in close agreement with $T_{c,zero}$ = 119K, measured by the four probe resistivity method.

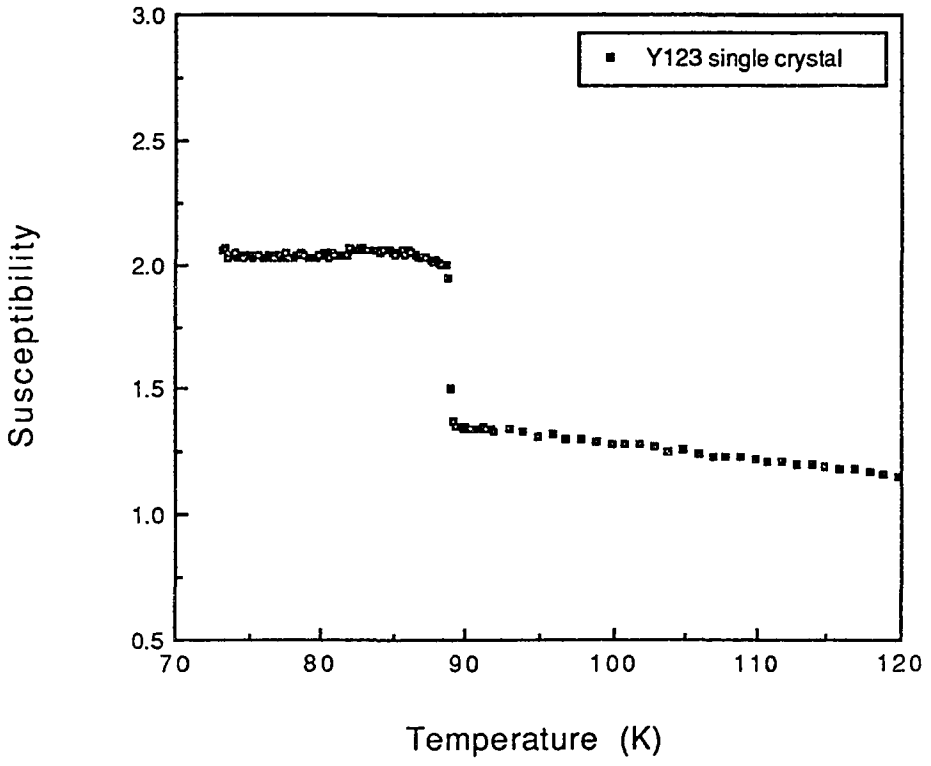

Fig. 5.4 : Susceptibility in arbitrary units as a function of temperature for a $Y_1Ba_2Cu_3O_x$ single crystal. The crystal was grown on gold foil and annealed in oxygen for 7 days at 450°C. The small signal to background ratio is a direct consequence of tiny mass of the crystal (0.0023g). However, a clear transition is indicated at T_c of 89K. The $T_{c,zero}$ of this crystal was found to be 89.5K by the four-probe method.

method. An ac signal is passed through the primary circuit, which consists of a primary coil and a ballast resistor. The signal induces an e.m.f. in the secondary coils. The secondary circuit consists of two identical secondary coils which are connected in opposite directions. In an ideal situation the induced current produced by one coil is cancelled by the induced current produced in the opposite direction by the other coil. However, it is very rare to build two identical coils, hence there is always a small induced current flowing through the secondary circuit giving a background signal. The sample to be measured is placed in one of the coils. When the sample is in the normal state, the magnetic field produced by the coil extends throughout the sample. As the sample becomes superconducting, the magnetic fields are expelled from the interior by superconducting shielding currents that flows in opposition to the applied field. This change in the field changes the inductance of the sample coil, producing an imbalance in the induced currents due to two secondary coils. The resulting signal shows up as a very significant change in the out of phase component of the voltage across the coils (relative to the phase of the current measured across the resistor in series with the primary coil). A lock-in-amplifier is used both as the source of ac signal in the primary and as the detector, monitoring the out of phase component in the secondary circuit.

Fig. 5.3 shows the susceptibility (arbitrary units) vs temperature plot for a $Tl_2Ba_2Ca_2Cu_3O_{10}$ bulk sample. The T_c of the sample is 118 K. T_c is defined as the temperature at which the diamagnetic signal starts showing up. This value of T_c is the same as $T_{c,zero}$ measured from the resistivity measurements [2]. The $T_{c,zero}$, measured by resistivity experiment for this sample, was found to be 119 K. Fig 5.4 shows the result of susceptibility measurement on a single crystal of $Y_1Ba_2Cu_3O_{7-\delta}$. The small signal to background ratio is a direct consequence of the tiny mass of the crystal

(0.0023 g). However, a clear transition is indicated by the plot. The T_c of the crystal is equal to 89 K which is close to $T_{c,zero}$ of the crystal (89.5 K).

5.3 1/f noise measurement

Electrical noise power was measured by a DC four-probe cross-correlation method [3]. Fig. 5.5 shows the circuit diagram for this method. A DC current was passed through the sample which was connected in series with a large ballast resistor. The value of the ballast resistor was at least 1000 times larger than the sample resistance. The voltage across the sample was DC filtered through a large capacitor (1.0 F). The signal was then split into two parallel branches, providing identical sources for the cross correlation measurement. In each branch, the signal was amplified by feeding into a transformer and then into a preamplifier. For each branch, a PAR model 1900 low noise transformer was used. The 10 : 1000 transformer turns ratio was used in most measurements producing a voltage amplification by a factor of 100. The amplified signal was then passed to a PAR model 113 low noise preamplifier, ac coupled with low and high frequency roll-offs set at 0.03 Hz and 1 kHz respectively, at maximum gain of 10k. Finally the cross-correlation spectrum was measured by an HP3562A dynamic signal analyzer, which detected signals from the two preamplifiers.

The noise power spectrum was measured from 0.1 Hz to 100 Hz with a frequency increment of 0.125 Hz. Inside the analyzer, the analog voltage signal was first converted into digital form by sampling the signal every 3.91 μs. A total of 2048 digital samples are then used to fill one "time record". The "time record" is defined as the amount of time domain data required to perform one fast fourier transform (FFT). The time domain signal is then converted into frequency domain by a FFT processor. The

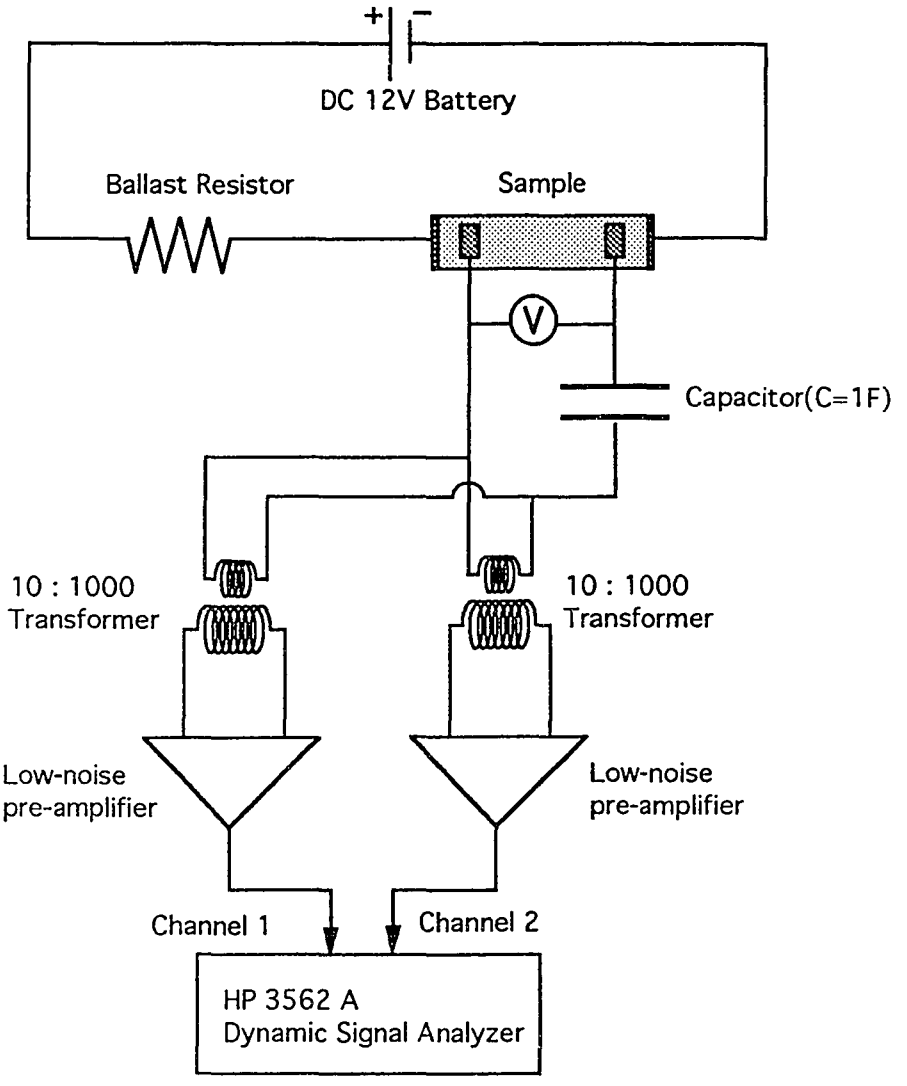

Fig 5.5 : DC four-probe cross-correlation method for measurement of noise spectral density.

frequency dependent cross correlation spectrum is calculated by multiplying the FFT of signal in one branch (F_x) by the complex conjugate of the FFT of the signal in the other branch (F_y^*); and then averaging the product. The noise spectral density of the voltage fluctuation is then given by :

$$S_v = \langle F_x F_y^* \rangle \frac{T}{A}$$

where T is the length of each time record (T=8 s) and A is the total power amplification factor of the transformers and preamplifiers. The cross correlation technique effectively reduces the noise background generated by the preamplifiers since the two noise sources from the preamplifier circuits are not correlated and only the noise signal from the sample is preserved in the averaging process.

It is important to keep the temperature of the sample constant during the measurement of noise. This requirement is crucial for the noise measurement in the superconducting transition region of the sample, where a small change in the sample temperature causes a large change in the sample resistance. A temperature control unit was constructed by mounting the sample and the thermal sensor to a copper block. The copper block was thermally linked to the cold head of the cryogenic refrigerator. The whole assembly was kept in a vacuum to provide good thermal insulation from room temperature. A copper enclosure surrounding the sample cell (copper block) was included to help exclude the background noise. The enclosure was designed so that it could be filled with liquid nitrogen. The copper enclosure maintained at the temperature of liquid nitrogen was found to be useful in stabilizing the sample temperature by providing a constant low temperature surrounding. The sample temperature was adjusted by a battery driven DC heater which was mounted on the outside of the copper block to produce a uniform heating of the block. The electronics, except for the signal

analyzer, were kept inside a mu-metal box and batteries were used to supply power for the components inside the box.

For a noise measurement, the temperature of the sample was first stabilized. Sample voltage and temperature were read and then the voltmeter and the thermometer were disconnected from the circuit. After the noise measurement, sample temperature and voltage were again measured and data corresponding only to stable sample temperatures were retained. The fluctuations in the sample temperature for measurements near the superconducting transition region were kept below 0.05 K. In the normal state, where the sample voltage is a slowly varying function of temperature, the sample temperature was maintained within an accuracy of 0.2 K.

The ballast resistor used in the circuit maintained an approximately constant load on the battery as the sample resistance changed. A large ballast resistance also reduces the relative contribution of contact noise to the total noise measured. Mantese [4] demonstrates why this is the case by evaluating the contributions of the current contacts, with resistance r_i, to the noise, in addition to the sample resistance R_s and ballast resistance R_b. For a noise free current source and ballast resistor, the excess noise (the total noise minus the thermal noise) is given by

$$S_{v,excess} \approx I^2 \left[S_{R_s} + 2S_{r_i} \left(\frac{R_s}{R_b} \right)^2 \right]$$

where S_{R_s} and S_{r_i} are the noises due to the sample and the current contacts respectively. A ballast resistance at least 1000 times the sample resistance reduces the contribution of the current contact noise to the total noise by a factor of 10^6. However, good contacts are necessary to avoid self heating of the sample. To check the contact noise contribution to the measured noise power spectrum, both the ballast resistance and the driving e.m.f. were increased by a factor of 2 so that the voltage across the sample remained constant

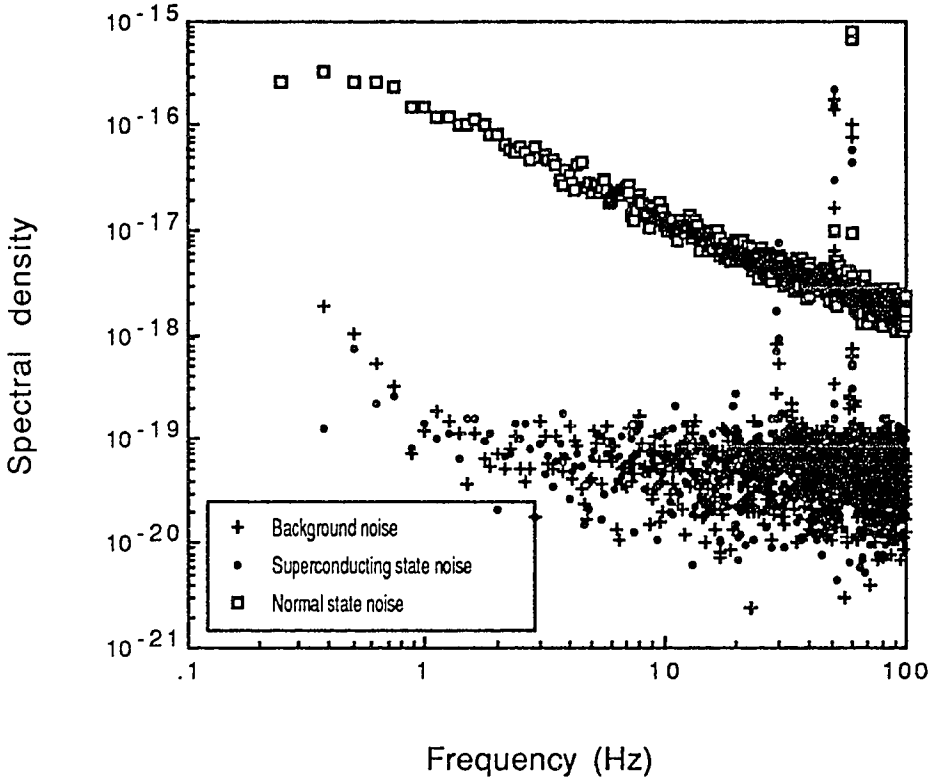

Fig. 5.6 : The noise spectral density $S_v(f)$, in the units of (V^2/Hz), of a single crystal of $Y_1Ba_2Cu_3O_x$ vs frequency measured in the normal state (T=170K) and in the superconducting state (T= 77.6K). The crystal completes its superconducting transition at 88K. The noise in the normal state shows clear 1/f behavior. The noise in the superconducting state is same as the background noise.

but the ratio of ballast resistance to sample resistance was doubled. No change in the slope and the magnitude of the noise power spectrum was observed, indicating that the contribution from the contact noise was negligible [5]. The noise spectrum was also checked for a V^2 dependence. This was done by measuring noise spectra at different values of the driving current. All noise spectra had V^2 dependence. This result assured that there was no large self-heating in the sample during the measurement which, if present, would have given a noise power magnitude with a dependence other than V^2.

The total noise spectrum measured is the sum of thermal noise, amplifier noise and "excess noise" from the sample. The thermal noise and the amplifier noise are both frequency independent in the frequency range studied. The excess noise which is 1/f in shape was extracted from the total noise by subtracting the background noise. The background noise, which was essentially the amplifier noise and the thermal noise, was determined by measuring the noise power spectrum in the absence of driving current. Fig. 5.6 shows a typical example of the spectral density $S_V(f)$, in the units of (V^2/Hz), of noise measured on a single crystal of $Y_1Ba_2Cu_3O_{7-\delta}$. The noise measurement for this crystal was performed along the c-axis of the crystal. The crystal completes its superconducting transition at 88 K. It can be seen that the noise spectra in the normal state (T=170 K) has a characteristic 1/f behavior whereas the noise measured in the superconducting state (T=77.6 K) is same as the background noise. In the normal state, 1/f noise is much larger in magnitude than the background noise and is easily measurable even in a very small crystals. The size of this crystal is only $0.8 \times 0.56 \times 0.17$ mm^3.

5.4 Error analysis

A four-probe method was used for both the measurement of noise and resistivity. The advantage of using a large ballast resistor in a four-probe method is discussed in the previous section. Here, in this paragraph, it will be shown that the relative error in the measurement of resistance using a four-probe method is much less than a two-probe method. Fig. 5.7 shows the schematic diagram for both a two-probe method and a four-probe method for resistivity measurement. For simplicity, all contact resistances are assumed to have the same value, denoted by r_c. R_s is the sample resistance and R_v is the resistance of the voltmeter. It should be noted here that R_s in a four-probe method represents the portion of total sample resistance between the voltage leads. Under the assumption that the total current i_T is constant, it can be easily shown that the relative error in a two-probe method is given by :

$$\frac{\Delta R}{R} = \frac{R_{measured} - R_{actual}}{R_{actual}} = \left[\frac{(R_v+R_s)(R_s+2r_c)}{R_s(R_v+R_s+2r_c)} - 1\right]$$

Under the assumption $R_v >> R_s$ and $R_v >> r_c$, which is normally the case, the above expression approximates to

$$\frac{\Delta R}{R} \approx \frac{2r_c}{R_s}$$

For a four-probe method, these expressions are :

$$\frac{\Delta R}{R} = \left[\frac{(R_v+R_s)(R_v+2r_c)}{R_v(R_v+R_s+2r_c)} - 1\right]$$

and under the assumption $R_v >> R_s$ and $R_v >> r_c$, the above expression approximates to

$$\frac{\Delta R}{R} \approx \frac{2r_c}{R_v}$$

Since R_v is much larger than R_s, the relative error in a four-probe method is extremely

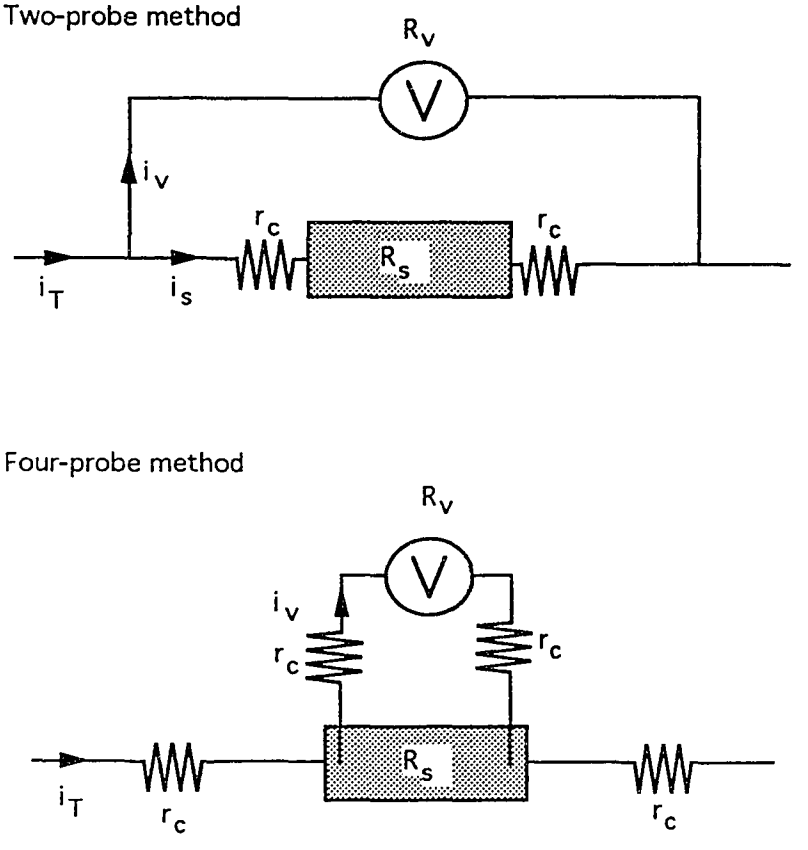

Fig. 5.7 : Schematic diagram for two-probe and four-probe methods.

small compare to that of a two probe method. The typical values of R_v, R_s, and r_c in our experiments are of the order of 10^9 Ω, 0.1 Ω, and 1 Ω respectively.

One of the main problems in the noise and resistivity measurement is the determination of sample temperature. Because of practical reasons, it is not always possible to keep the sample on top of the thermal sensor. Also, since a large current was used in measuring the noise, a local heating of the sample takes place. The amount of heat produced depends on the values of driving current, sample resistance, and the contact resistance. Since these values differ from sample to sample, the error in the measurement of sample temperature will vary with samples. It may be possible to estimate the change in the sample temperature by calculating the amount of heat produced by the sample and amount of heat transferred from the sample to the surrounding. For such a calculation one would need the exact values of sample resistance, contact resistance, specific heat of the sample and the surrounding materials and other factors such as coefficients of heat conduction. Such a calculation will not be simple. However, there is a simple way of estimating sample temperature by simply measuring the sample resistance as a function of temperature for various values of driving current. This method is discussed below.

The resistance of a single crystal of $Y_1Ba_2Cu_3O_{7-\delta}$ was measured as a function of temperature for different values of driving current. The result of this measurement is shown in Fig 5.8. It can be seen that $T_{c,zero}$ of the crystal decreases as the value of driving current was increased. By extrapolating the graph between the $T_{c,zero}$ and driving current, it was found that a current of 164 mA would make the sample nonsuperconducting at 77 K (temperature measured by the sensor). This value of current corresponds to a critical current density of 82 A/cm^2 (the cross section area of

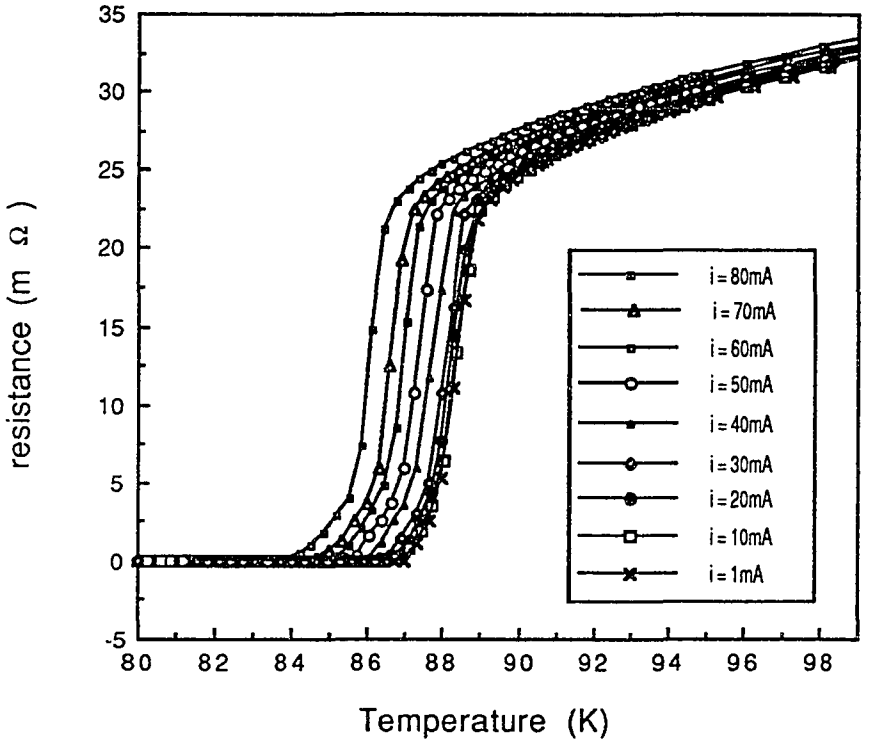

Fig. 5.8 : Resistance as a function of temperature for a single crystal of $Y_1Ba_2Cu_3O_x$ shown for different values of driving current. The shift in the normal state resistance with the increase in the driving current is related to the local heating of the crystal due to large current flowing through the sample which causes the sample temperature to be higher than the thermal sensor temperature. The graph is then used to find the systematic error in the measurement of sample temperature.

the crystal was $2x10^{-3}$ cm^2); whereas the critical current density of a single crystal of $Y_1Ba_2Cu_3O_{7-\delta}$ is of the order of 10^5 A/cm^2. This observation suggests that there is a local heating of the sample, causing the sample to be at a higher temperature than the surrounding. By assuming that the rate of heat produced and lost by the sample is constant, one would expect the difference between the temperatures of the sample and that of the surrounding to be a constant. In other words, it is assumed that local heating of the sample is giving a systematic error in the measurement of temperature of the sample. Such an error can be graphically determined if one knows the values of sample resistance as a function of the exact sample temperature. This data can be obtained by passing a very small current though the sample, so that negligible heating of the sample takes place. A current of 1mA was found suitable to serve the above purpose. The rise in the sample temperature was then graphically measured as a difference in the values of measured temperatures, corresponding to same value of resistance, for i=1 mA and i= x mA (where x = 10,20,...,80). This was done here by drawing a horizontal line at R = 32 Ω in the R-T plot of Fig 5.8 and measuring the difference in the values of measured temperatures. The rise in the temperature of the sample due to different values of driving current, obtained from the above method, is plotted in Fig 5.9. The data suggests that the effect of the local heating is negligible if the driving current is lower than 10 mA. The plot also shows the expected quadratic behavior due to the Joule heating of the sample (heat produce $\propto i^2$). Data from Fig 5.9 were then used to determine the correct sample temperature. The resistance data shown in Fig 5.8 was then replotted in Fig 5.10 as a function of corrected temperature. The plot indicates that the existence of a systematic error was indeed the case, in the absence of which one would not expect the same trace to be followed by the nine RT plots. The broadening of RT

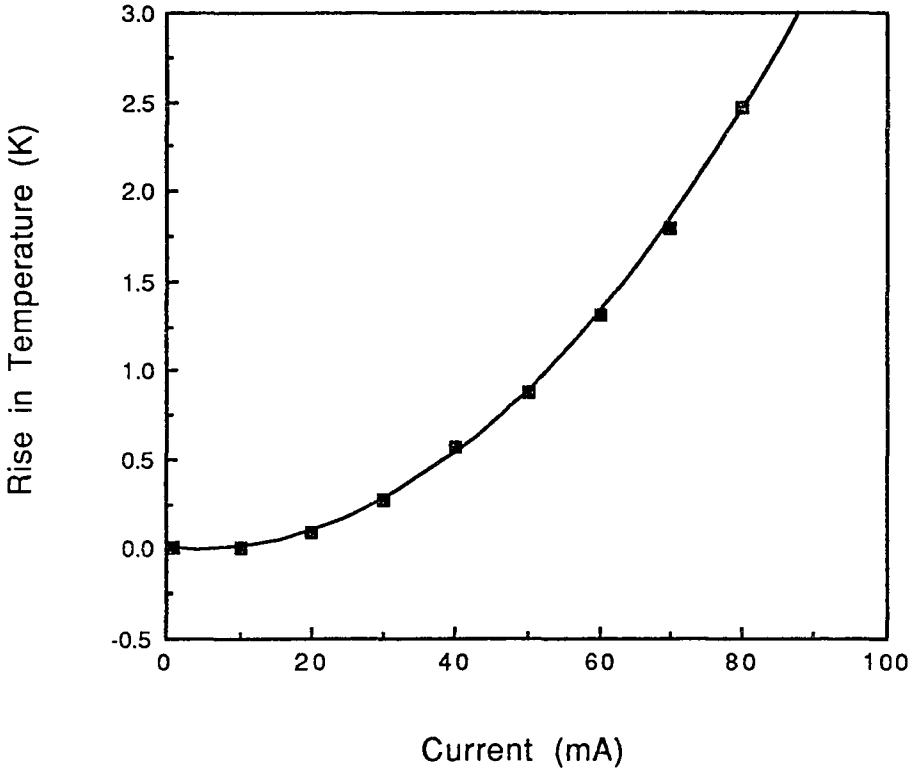

Fig. 5.9 : The difference between the sample temperature and thermal sensor is shown as a function of driving current through the crystal. The data is calculated from Fig. 5.8. The plot suggests that the effect of local heating of the crystal is negligible if the driving current is lower than 10mA. The quadratic behavior of the plot is in agreement with the Joule heating of the crystal.

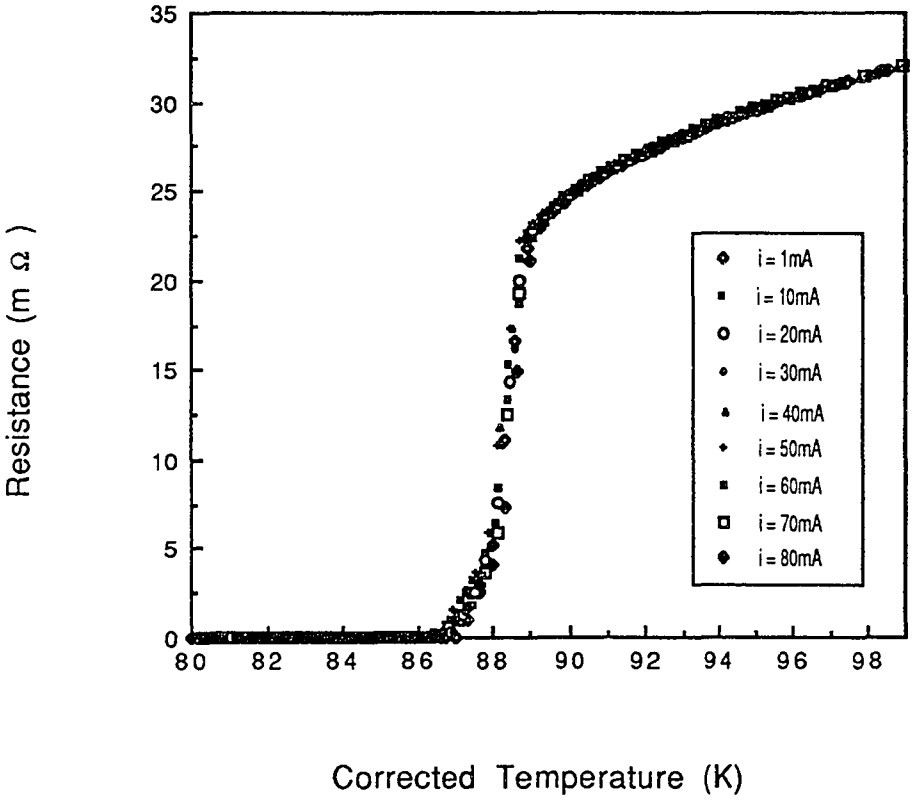

Fig. 5.10 : The resistance vs temperature data shown in Fig. 5.8 is replotted here as a function of corrected temperature. The amount of corrections made in the temperature is shown in Fig. 5.9. All nine RT plots are shown to follow the same trace, hence confirming the correctness of the method used in estimating the systematic error in the measurement of sample temperature due to local heating effect.

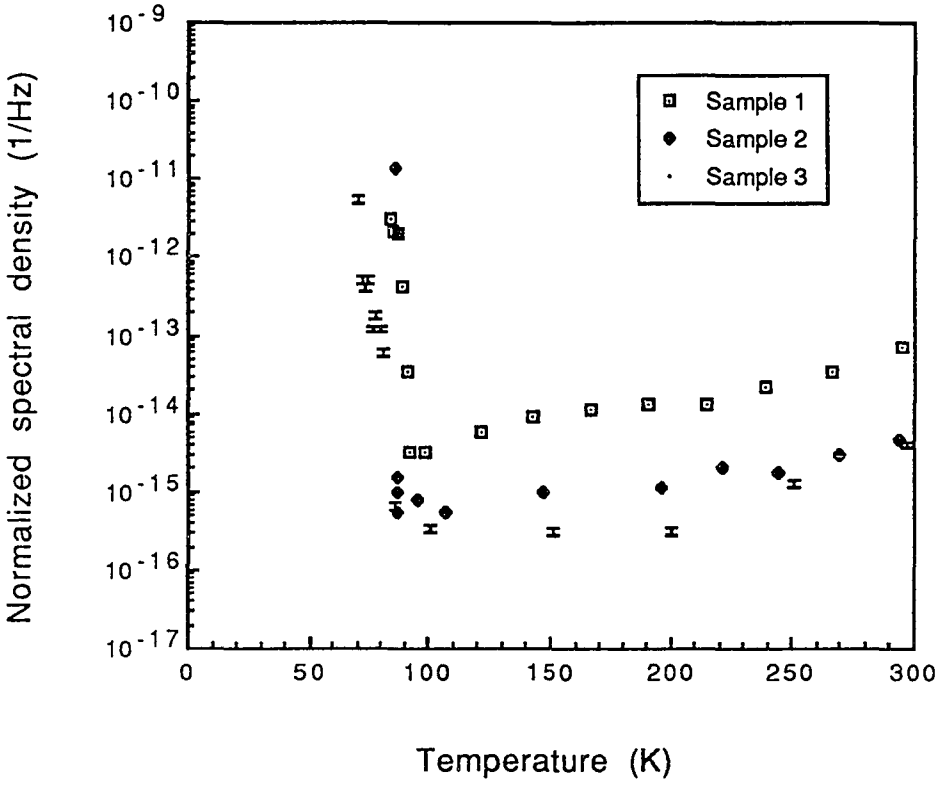

Fig. 5.11 : The normalized noise spectral density vs temperature for a single crystal of $Y_1Ba_2Cu_3O_x$. The error bars are shown for sample 3. All error bars represent 10% error. The different lengths of error bars are results of logarithemic scale used. The source of error is the unstability in the sample temperature during the noise measurement which in turn gives the fluctuations in the sample voltage.

plots near the tail of the transition region is a result of shift in $T_{c,zero}$ due to various values of driving current. The method described above uses the sample to act as a thermal sensor to determine its own temperature from its characteristic RT data.

The main error in the reported values of noise levels in this document is due to the normalization process. The normalization was done by dividing the spectral noise density by the square of the sample voltage. During the measurements, because of fluctuations in the sample temperature, there were fluctuations in the sample voltage. Typical values of sample voltage fluctuation during the noise measurements were of the order of 5% in the superconducting transition region and 0.2% in the normal state region of the sample. These fluctuations will produce an error of 10% in the reported values of normalized noise density in the transition region and of 0.4% in the normal state region. Data shown in Fig 6.11 is replotted here, in Fig 5.11, with error bars with heights corresponding to 10% of the values of normalized noise density. Error bars are shown for sample 3 only, whose plot symbol is changed to a "point" to show that the sizes of the error bars are approximately same as that of the plot symbols used for other samples. The different lengths of the error bars (all corresponding to 10% error) are results of the logarithmic scale used. Error bars were avoided in the rest of the figures, which otherwise would make the plot symbols indistinguishable from each other. Fluctuations in the sample temperature during the noise measurements were of the order of 0.05 K in the transition region and 0.2 K in the normal state.

References:

[1] X. D. Chen et al., Rev. Sci. Instrum. 58 (9) sept. (1987) 1565.

[2] Charles P. Poole, Jr. et al. in "Copper Oxide Superconductors" a Wiley-Interscience Publication (1988) p24.

[3] B. K. Jones and J.D. Francis, J. Phys. D 8, 1172 (1975)

[4] J. V. Mantese, Ph.D. thesis, Cornell Univ. (1986)

[5] C. Leeman, M.J. Skove, and E.P. Stillwell, Solid State Commun. 35, 97 (1980)

CHAPTER 6

EXPERIMENTAL RESULTS

This chapter is organized in three parts : 1/f noise in bulk samples of $Tl_2Ba_2Ca_{n-1}Cu_nO_{4+2n}$ (n=2 and 3), 1/f noise in thin films of $Tl_2Ba_2Ca_1Cu_2O_8$, and 1/f noise in $Y_1Ba_2Cu_3O_x$ single crystals. In the first part, section 6.1, measurements of the 1/f noise and resistivity in bulk samples of $Tl_2Ba_2Ca_{n-1}Cu_nO_{4+2n}$ (n=2 and 3) are presented. One of the purposes of this study was to confirm the previously reported results [1,2] on $R_1Ba_2Cu_3O_x$ (R=Y,Er) bulk samples. It was found that the magnitude of 1/f noise power in these materials is relatively large in the normal state, compared to that of conventional materials, and the noise is enhanced by many orders of magnitude in the superconducting transition region. No 1/f noise could be detected in the superconducting state. The TlBaCaCuO superconductors are different from YBaCuO superconductors in the sense that they have higher superconducting transition temperatures and their crystal structure is tetragonal instead of orthorhombic [3], hence twinning effects are not present in this class of superconductors. In this part, a possible correlation between 1/f noise and behavior of the resistivity is investigated.

In the second part, section 6.2, measurements of 1/f noise in thin films of $Tl_2Ba_2Ca_1Cu_2O_8$ are reported. This part of the study gives potentially important results that could be useful for the fabrication of electronic devices consisting of thin films. It is also interesting to compare the 1/f noise power and its temperature dependence with that of bulk samples, since thin films are limited in size in one direction and are more or less two-dimensional systems. One important difference between thin films and bulk

samples is that thin films are usually prepared in a very clean environment. Hence the sample quality is much higher than that of bulk or single crystals which normally contain contaminations coming from crucible and the atmosphere. The influence of highly c-axis oriented grain structure on 1/f noise was also investigated.

In the third part, section 6.3, measurements on single crystals of $Y_1Ba_2Cu_3O_x$ are reported. This study is more fundamental in the sense that composite effects are absent in single crystals. Measurements on single crystals also show the effect of a reduced number of grain boundaries on 1/f noise behavior. These results can provide useful information about the source of 1/f noise. The main focus of this study was on the anisotropic nature of 1/f noise since we succeeded in making noise measurements in two different crystallographic directions which have different resistivities at the same temperature [4].

From the results of this study the following fundamental questions can be answered:

1) Is 1/f noise an intrinsic property of Cu-oxide superconductors?

2) Is there a correlation between resistivity and 1/f noise? If so, are they produced by the same source(s)?

3) Is enhanced noise in the superconducting transition region a characteristic of these materials?

4) Is a high level of 1/f noise always observed in these materials in the normal state?

5) Is there a correlation between the superconducting quality of sample (like higher superconducting transition temperature) and 1/f noise? Will a better superconductor be noise free?

6) Does noise depend on the direction of current in a crystal which shows anisotropic resistive behavior?

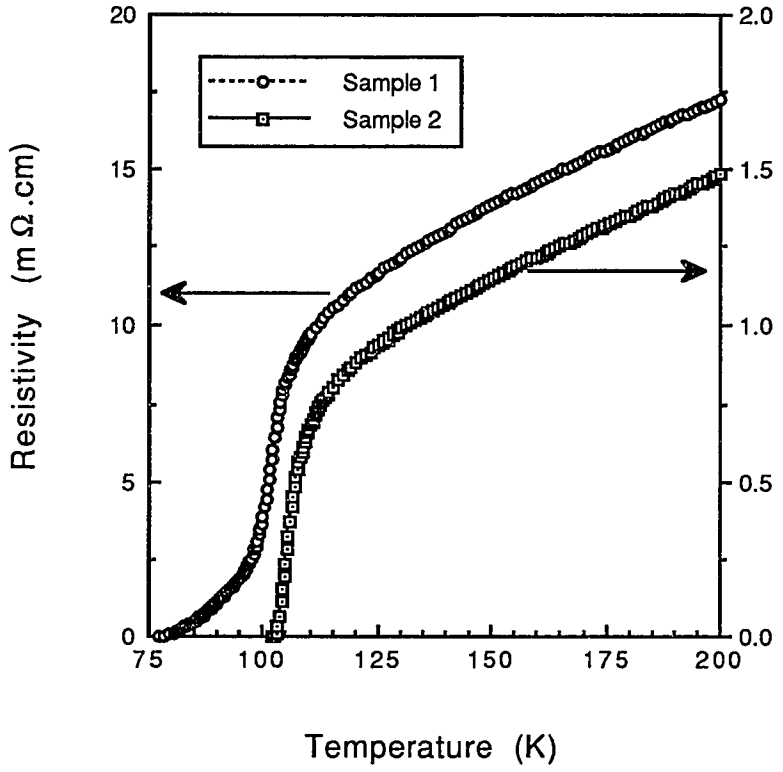

Fig. 6.1 : The electrical resistivity as a function of temperature for bulk samples of $Tl_2Ba_2Ca_1Cu_2O_8$. The magnitude of probing current was 100mA. Sample 1 was prepared by sintering it at 900°C for 10 minutes in one step. Sample 2 was prepared in two steps by sintering it at 900°C for 20 minutes and sintering it a second time at 900°C for 2 hours.

7) Does 1/f noise depend on sample preparative conditions?

8) Will there be less noise in the single crystal compared to that of bulk sample of similar size?

9) Is it possible to use these copper-oxide superconductors for practical applications which require low noise level?

6.1 1/f noise in bulk samples of $Tl_2Ba_2Ca_{n-1}Cu_nO_{4+2n}$

1/f noise and resistivity measurements were performed on bulk samples of thallium based superconductors with two different stoichiometries: $Tl_2Ba_2Ca_1Cu_2O_8$ and $Tl_2Ba_2Ca_2Cu_3O_{10}$. The experimental results obtained on these bulk samples are discussed in section 6.1.1 and section 6.1.2 respectively.

6.1.1 1/f noise in bulk samples of $Tl_2Ba_2Ca_1Cu_2O_8$

Two different kinds of samples (with stoichiometry $Tl_2Ba_2Ca_1Cu_2O_8$) were prepared by the solid state reaction method. Sample 1 was prepared by sintering at 900 °C for 10 min. in one step. Sample 2 was prepared in two steps by sintering at 900 °C for 20 min. and then sintering a second time at 900 °C for 2 hours after regrinding and pressing the powder into pellet. This second sintering yields samples with better grain connections. Crystal structures of these samples, determined by x-ray powder diffraction measurements, were found to be tetragonal. Lattice constants for sample 1 were found to be 3.8503±0.0039 Å for a-axis and 29.2101±0.1671 Å for c-axis. For sample 2 these values are 3.8506±0.0058 Å and 29.3861±0.2157 Å respectively. These values are in agreement with the literature [5,6,7].

The electrical resistivity as a function of temperature for both samples is shown in Fig.6.1. The magnitude of the probing current was 100 mA. The reason for using

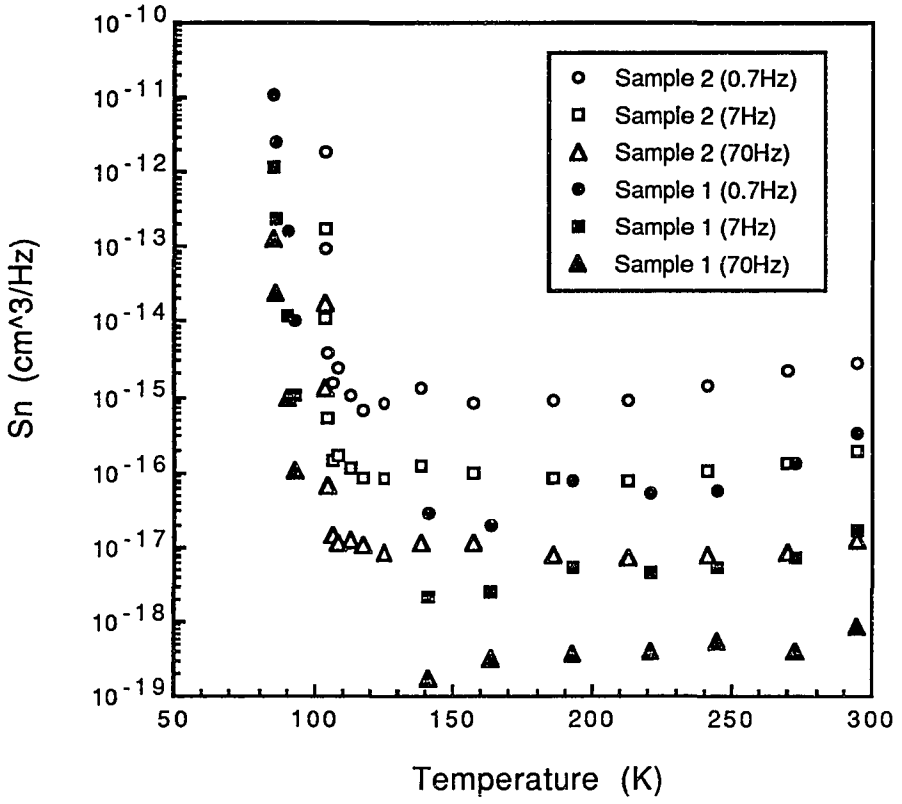

Fig. 6.2 : The normalized noise spectral density Sn (normalized by dividing by the voltage squared and multiplying by the volume of the sample) for bulk samples of $Tl_2Ba_2Ca_1Cu_2O_8$ plotted as a function of temperature. Both samples show enhanced noise in the superconducting transition regions.

such a large current (compared to the 1mA current normally used for resistivity measurements) was that comparably large currents were used (from 100 mA to 260 mA) in the 1/f noise measurements and it was desirable to have comparable parameters for the resistivity and 1/f noise measurements. The sample size was typically 3x1x8 mm^3. It can be seen from the graph that the resistivity of sample 1 is larger than that of sample 2 by an order of magnitude. Also, sample 1 has a lower superconducting transition temperature ($T_{c,zero}$) of 80 K compared to 103 K of sample 2. Furthermore there was a large shift in superconducting transition temperature T_c from 100 K to 80 K for sample 1 when the probing current in resistivity measurements changed from 1 mA to 100 mA. For sample 2 this shift in T_c was 1 K. These observations suggest that in sample 1 there exist "weak link" structures, possibly between individual grains. The existence of these "weak link" structures was not surprising because of the short heat treatment received by this sample. Sample 2, on the other hand, had an additional heat treatment so presumably the grains are better connected. So as far as the superconducting properties are concerned sample 2 is superior to sample 1.

The noise power for all our samples was measured from 0.1 Hz to 100 Hz by a DC four-probe cross-correlation method [8]. The noise power as a function of frequency, "1/f noise spectra", was fit to the equation $S_V(f) = Af^{-\alpha}$, in order to obtain the 1/f noise exponent α from the slope. For the whole normal state temperature range, $\alpha(T)=1.08\pm0.10$, falling well into the accepted 1/f noise range. The normalized spectral density S_n (normalized by dividing by the voltage squared and multiplying by the volume of the sample) [9] for sample 1 and 2 is given in Fig.6.2 as a function of temperature for three different frequencies. The following observations

can be made from Fig.6.2:

1) The 1/f noise power decreases with decreasing temperature in the temperature range 200 K to 300 K. The temperature dependence is relatively weak.

2) There seems to exist a turning point near 180 K. In sample 1 the noise density is slightly higher around this temperature and in sample 2 there is a change of slope of the curve and its temperature dependence is changed.

3) The noise of sample 2 (which is better sample than 1 in the sense that it has better superconducting properties) in the normal state is higher than sample 1 at least by one order of magnitude.

4) The noise power in the superconducting transition region is enhanced by several orders of magnitude, for both samples. This enhancement of noise power in the transition region has been previously observed in $R_1Ba_2Cu_3O_{7-\delta}$ (R = Y or Er) systems and in BiSrCaCuO system [1,2]. The enhancement in the noise power is at least five orders of magnitude for sample 1 and three orders of magnitude for sample 2.

5) In the superconducting region ($T < T_{c,zero}$) no 1/f noise could be detected. Noise measured at these temperatures were the same as the background noise.

The existence of "weak link" structures in sample 1 seems to be a possible reason for the enhanced noise power intensity because of its composite nature. In sample 2 which went through further heat treatment such enhancement is reduced from five orders of magnitude to 3 orders of magnitude. On the other hand, however, such an argument is difficult to use in order to explain the behavior of the noise power intensity in the normal state ($T_c < T < 300$ K) because in this temperature region the noise power intensity of sample 2 is about one order of magnitude higher than that of sample 1. This observation suggests that 1/f noise in the normal state and in the superconducting

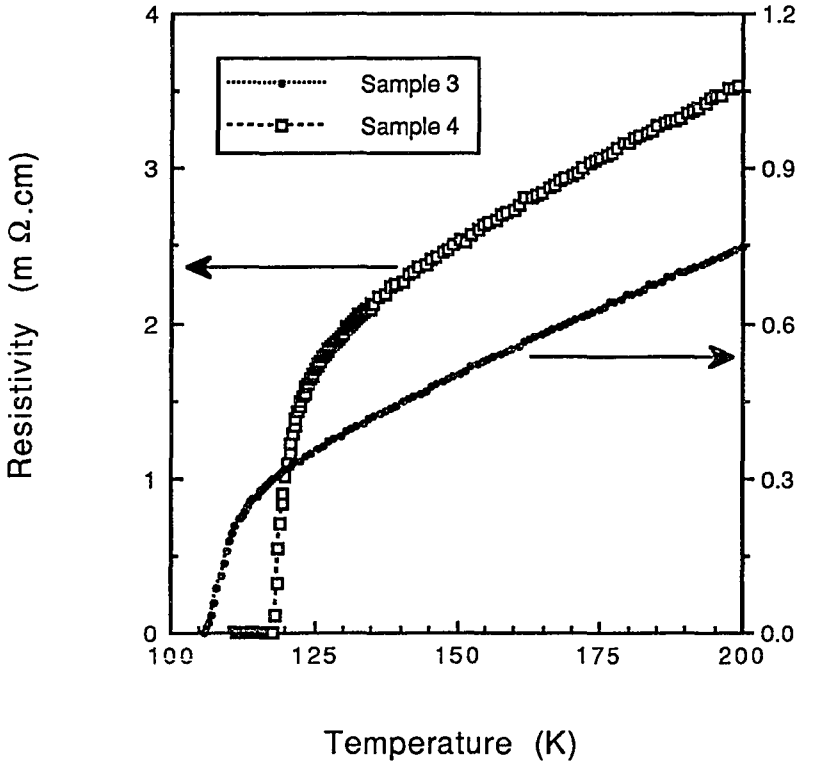

Fig. 6.3 : The electrical resistivity as a function of temperature for bulk samples of $Tl_2Ba_2Ca_2Cu_3O_{10}$. The magnitude of the probing current was 100mA. Both samples went through two stages of sintering. In the first step both samples were sintered at 900°C for 10 minutes and in the second step sample 3 was sintered at 880°C for 2 hours while sample 4 was sintered at 900°C for 4 hours.

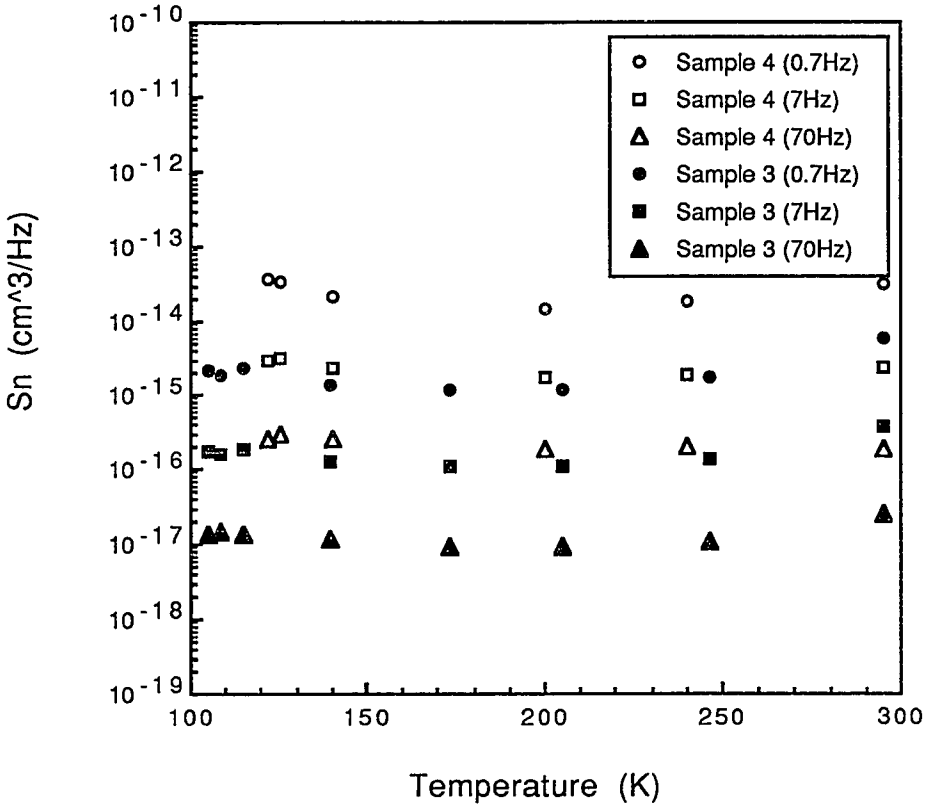

Fig. 6.4 : The normalized noise spectral density Sn (normalized by dividing by the voltage squared and multiplying by the volume of the sample) for bulk samples of $Tl_2Ba_2Ca_2Cu_3O_{10}$ plotted as a function of temperature. No enhanced noise is observed in the superconducting transition regions. This observation of absence of enhanced noise in the transition region has never been observed before in bulk samples of superconducting materials.

transition region comes from two different origins.

6.1.2 1/f noise in bulk samples of $Tl_2Ba_2Ca_2Cu_3O_{10}$

Two samples (sample 3 and 4) of composition Tl_{2223} were prepared by solid state reaction. Both samples went through two stages of sintering, in the first step both samples were sintered at 900 °C for 10 min and in the second step sample 3 was sintered at 880 °C for 2 hours where as sample 4 was sintered at 900°C for 4 hours. For sample 3, a=3.8539±0.0026 Å and c=36.7805±0.2078 Å while for sample 4, a=3.8419±0.0028 Å and c=35.3876±0.1608 Å. The value of constant c for sample 3 is larger than the commonly reported values of 35.66 Å to 36.26 Å [5,6,7]. This is possibly due to depletion of Tl, a result of evaporation of Tl from the sample and migration to other sites during the heating process [10]. Structural imperfections of this type lead to a reduced superconducting transition temperature. The electrical resistivity as a function of temperature for both samples is given in Fig.6.3. The magnitude of the probing current was 100 mA.

The superconducting transition temperature ($T_{c,zero}$) is 106 K for sample 3 and 119 K for sample 4. On the other hand, the resistivity of sample 3 is much smaller than that of sample 4. This result suggests that sample 3 does not have "weak link" structures between grains but possesses instead defects on a microscopic scale, as indirectly shown by the X-ray measurement results.

Normalized spectral density S_n (normalized with respect to voltage squared and volume of the sample) for sample 3 and 4 is given in Fig.6.4 with respect to temperature for three different frequencies. The following observations can be made from Fig.6.4:

1) The 1/f noise power decreases with decreasing temperature in the temperature range

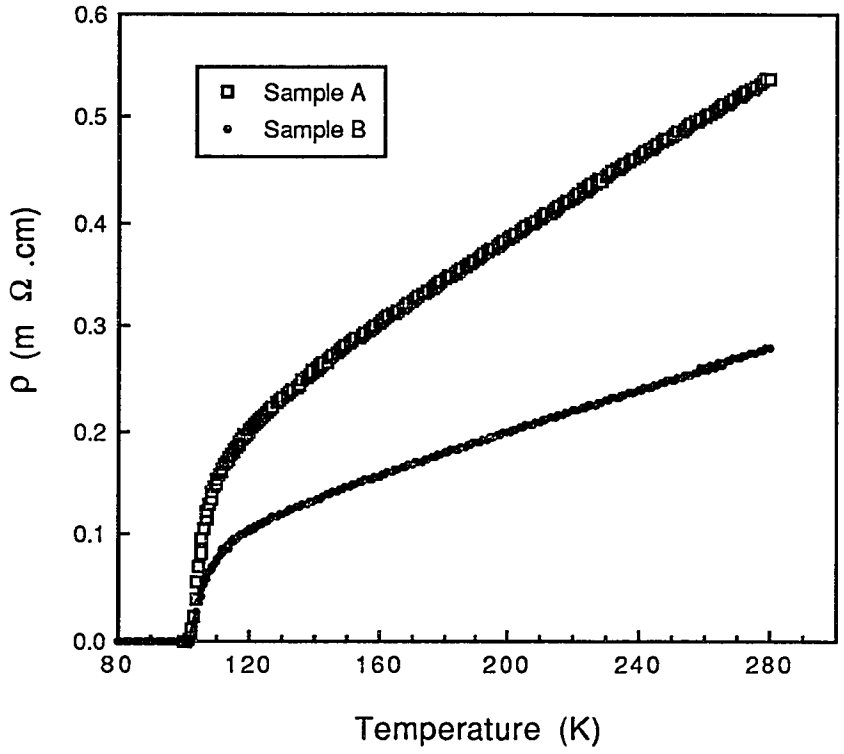

Fig. 6.5 : The electrical resistivity measured on thin films of $Tl_2Ba_2Ca_1Cu_2O_8$ as a function of temperature. The superconducting transition is completed at 101K. Both samples are of good quality as indicated by superconducting transition with no tail and linear resistivity behavior in the normal state.

200 K to 300 K. The temperature dependence is relatively weak.

2) The noise density of sample 4 (which is a better superconducting sample than sample 3) is higher by at least one order of magnitude than that of sample 3.

3) No 1/f noise was detected in the superconducting state.

4) In the superconducting transition region, there is no enhanced noise power intensity. In this region measurements were carried out very close to T_c. To best of our knowledge, this is the first observation of the absence of enhanced 1/f noise power intensity of copper oxide superconductors in the superconducting transition region.

It can be seen from Fig.6.2 and Fig.6.4 that the noise densities for all the four samples in the normal state are comparable to each other, indicating a common source of noise in all samples at these temperatures ($T>>T_{c,onset}$). The absence of enhanced noise in sample 3 and 4 supports the idea that 1/f noise in the normal state and in the superconducting transition region comes from two different origins.

Another important observation which can be made from Fig.6.2 and Fig.6.4 is that there is a lack of correlation between normal state resistivity and normal state 1/f noise spectral density. Sample 1, which has higher resistivity than sample 2 , has a lower noise, whereas sample 4 which has higher resistivity than sample 3 has a higher noise. On the other hand data indicates that samples with better superconducting properties in this class of superconductors exhibit higher 1/f noise densities in the normal state.

6.2 1/f noise in $Tl_2Ba_2Ca_1Cu_2O_8$ thin films

1/f noise measurement was done on $Tl_2Ba_2Ca_1Cu_2O_8$ thin films. These samples were supplied by Albert H. Cardona of Superconductor Technologies, Inc. California.

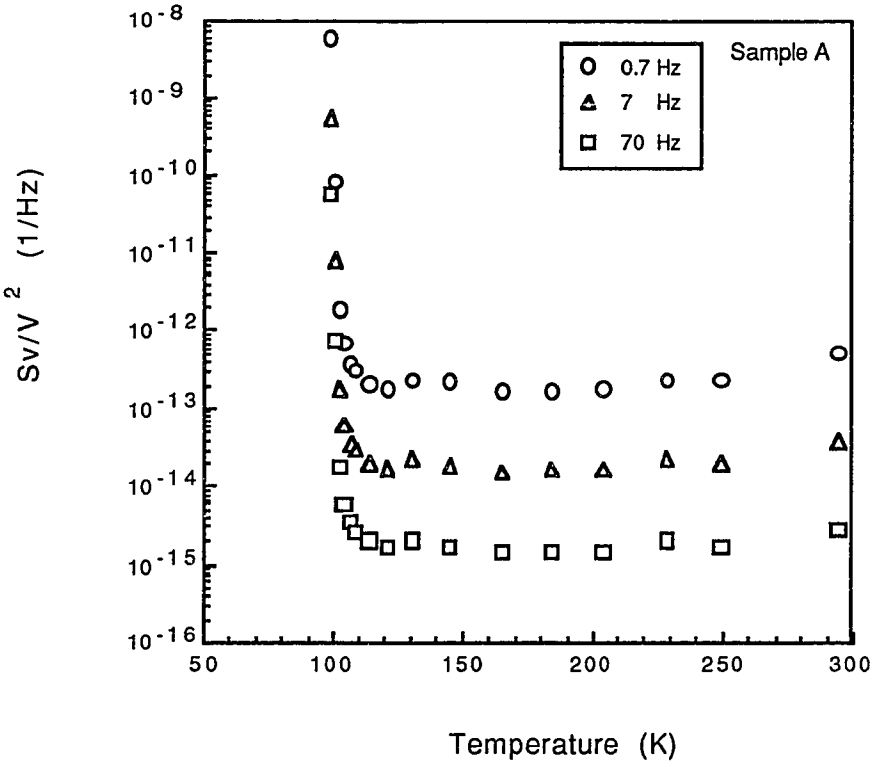

Fig. 6.6 : Normalized 1/f noise spectral density S_V/V^2 vs sample temperature for thin film sample A. Noise spectral density is shown for three frequencies : 0.7Hz, 7Hz,70Hz. In the superconducting transition region noise density is enhanced by 5 orders of magnitude for this sample.

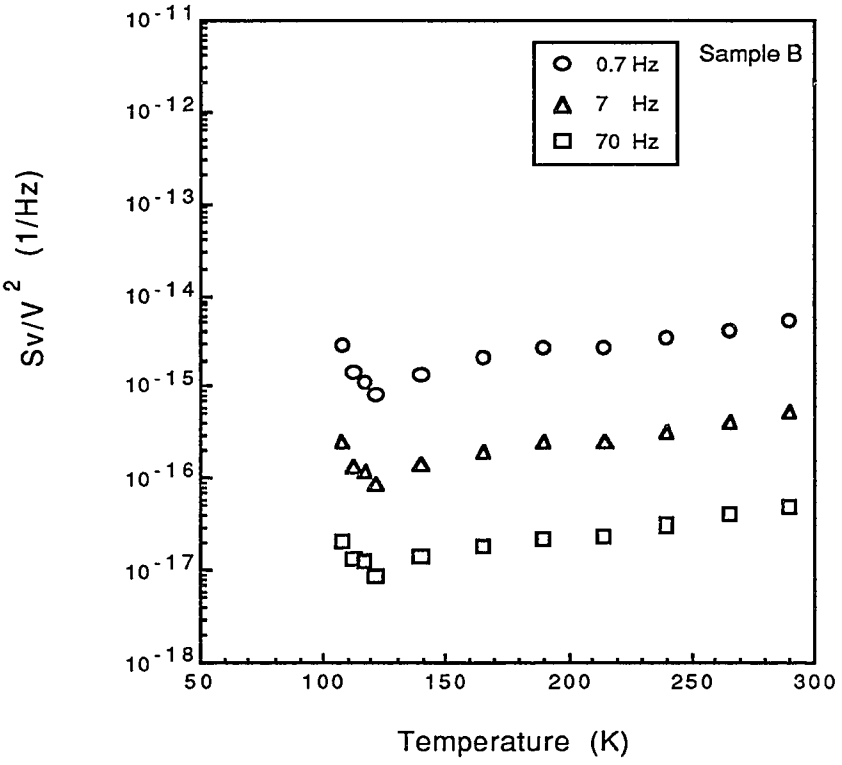

Fig. 6.7 : Normalized 1/f noise spectral density S_v/V^2 vs sample temperature for thin film sample B. In the superconducting transition region noise density is enhanced by less than 1 order of magnitude for this sample. Grains of sample B are more c-axis alighned than that of sample A. Plot shows that the enhanced noise in the transition region is not intrinsic property of these materials.

Since two batches of thin films were received 6 months apart from each other, the preparation conditions for two sets of films are not expected to be exactly the same. Hence study of these two different sets of films will give information about the effect of microstructure of samples on 1/f noise.

The electrical resistivity as a function of temperature is given in Fig.6.5 for sample A (which is from the first set of the films) and for sample B (which is from the second set of the films). The resistivity is seen to decrease linearly with decreasing temperature until the superconducting transition region is approached. Both samples are of good quality as indicated by the lack of a superconducting transition tail and linear resistivity behavior in the normal state. The superconducting transition temperature is 101 K for both samples. The difference in the value of resistivity is consistent with the fact that the two samples were not prepared under identical conditions. Possible contributions to resistivity can be from individual grains and from grain boundaries. Since both samples have a similar chemical structure and resistivity is a microscopic quantity, the difference in resistivity indicates different grain-boundaries in two samples. The lower value of resistivity of sample B indicates a better grain to grain contact compared to that in sample A.

In Fig.6.6 the normalized spectral density $S_V(f)/V^2$ of the 1/f noise obtained on sample A as a function of temperature is shown. Fig.6.7 shows the normalized spectral density $S_V(f)/V^2$ of the 1/f noise obtained on sample B as a function of temperature. The noise spectra of both samples can be fitted to $S_V(f) = Af^{-\alpha}$, with the noise exponent $\alpha(T)=1.10\pm0.15$ for the measured temperature range. At each temperature the noise spectrum was measured from 0.1 Hz to 100 Hz with a frequency increment of 0.125 Hz.

Films analyzed by x-ray diffraction patterns show almost exclusively the

$Tl_2Ba_2Ca_1Cu_2O_8$ phase, with dc critical current densities of J_c (77 K)=0.5x10^6 to 1x10^6 A/cm^2. Microstructural analysis show mostly c-axis normal epitaxy, with occasional a-axis normal plates. X-ray diffraction rocking curve data from the (00$\underline{10}$) peak show that the full width at half-maximum (FWHM) is 0.75° for sample A and 0.40° for sample B. Since the width of these curves indicates the degree of epitaxy (a smaller FWHM means better c-axis grain alignment), data indicates that sample B has better c-axis alignment than sample A.

The first observation which can be easily made from Fig.6.6 and Fig.6.7 is that the magnitude of the normalized spectral density, S_v/V^2, in the normal state ($T >> T_c$) for sample A is 100 times higher than sample B. A simple way of quantitatively analyzing the data is to use Hooge' empirical formula [11] $S_v = \gamma V^2/N_c f$. In this equation N_c is the total number of charge carriers in the sample which is proportional to the sample volume. N_c can be calculated as the product of carrier density [12] (2x10^{21} cm^{-3}) and the sample volume (1.0x10^{-9} cm^3 for sample A and 2.9x10^{-7} cm^3 for sample B). γ is in the range of 10^{-1} to 10^{-5} for most metals [11]. The difference between the magnitude of S_v/V^2 of samples A and B in the normal state can be explained by the difference in volume of these two samples. Since the volume of sample A is about 100 times smaller than that of sample B and S_v/V^2 is inversely proportional to the sample volume, the magnitude of S_v/V^2 of these two samples is of the same order of magnitude.

In the superconducting transition region the enhancement of S_v/V^2 is 5 order of magnitude for sample A. This same enhancement is only to less than 1 order of magnitude in sample B, however. Since sample B has better c-axis alignment than

sample A, the enhancement of 1/f noise in the superconducting transition region may be substantially suppressed in highly c-axis oriented films. In the 1/f noise measurement of these highly c-axis oriented films, the current is passed in the plane of the film which is normal to c-axis and the noise was measured from the same plane. This plane will correspond to the ab-plane of a single crystal. Therefore no enhancement of 1/f noise is expected in the ab-plane of a single crystals, in the superconducting transition region.

From the data one can see that the magnitude of S_V/V^2 of thin film samples in the normal state is much lower than that previously observed in thin films of other copper oxide materials [13]. Some samples have an S_V/V^2 that is as small as those found in conventional metals. This observation strongly suggests that the noisy behavior previously observed in many copper oxide superconductors is not an intrinsic property of these materials.

Other observations consistent with the results of noise measurement on bulk samples (discussed in section 6.1) are: (i) in the temperature range of 200 K to 300 K the noise decreases with the decrease in temperature. (ii) The existence of a turning point in the temperature dependence is observed in sample A near 180 K. The slope of the curve is changed around this temperature for sample A. For sample B the noise is a little higher near this temperature.

Two important facts are discovered from the above experimental work. First, it is possible to have a superconducting thin film sample with a very low 1/f noise (comparable to that of metals) and secondly, it is also possible to make samples without enhanced noise in the superconducting transition region. Both of these facts are reported for the first time. These are important results for the fabrication of bolometers and

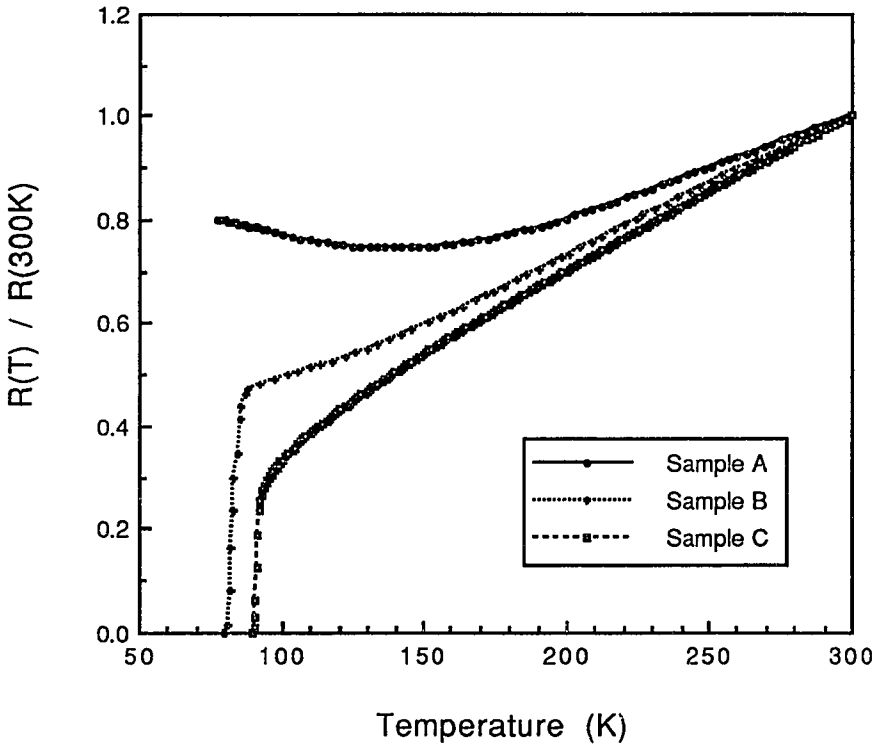

Fig. 6.8 : Normalized resistance as a function of temperature is shown for single crystals of $Y_1Ba_2Cu_3O_x$. The measurements were done in the ab-planes of the crystals. The crystals were prepared to keep their electrical properties very different from each others.

other optical and electronic devices which will work near the superconducting transition temperature.

6.3 1/f noise in $Y_1Ba_2Cu_3O_{7-\delta}$ single crystals

1/f noise measurements were done on eight different single crystals of $Y_1Ba_2Cu_3O_{7-\delta}$. Fig.6.8 shows the normalized resistance (normalized at 300K) of three single crystals of $Y_1Ba_2Cu_3O_{7-\delta}$ as a function of temperature. The resistance measurement was done in the ab-plane for these samples. These three crystals were chosen because of their different resistance and superconducting behaviors. A study of 1/f noise measurement on these samples will give information about the possible correlation of 1/f noise with resistivity or superconductivity. Sample A and B were grown on alumina crucibles in an air atmosphere. Details of crystal growth are given in the chapter 4. Sample B was annealed in oxygen for 7 days at 500 °C to increase its oxygen content whereas sample A did not go through this oxygen annealing process. Both sample A and B have aluminum contamination coming from the alumina crucible [14,15]. A good quality sample (sample C) was grown on a gold [16,17] instead of alumina crucible to overcome this problem.

The resistance of sample A is seen to decrease initially with decreasing temperature and below 170 K start to increase. The change of the resistance behavior is known to be a result of large oxygen deficiency. There is no superconducting transition observed above 77 K, due to the insufficient oxygen content in this sample. The result is consistent with the fact that sample A did not go through any oxygen annealing process. The resistance of sample B decreases with decreasing temperature at all temperatures. Below 130 K there is an observable change of the slope of the resistance, suggesting a

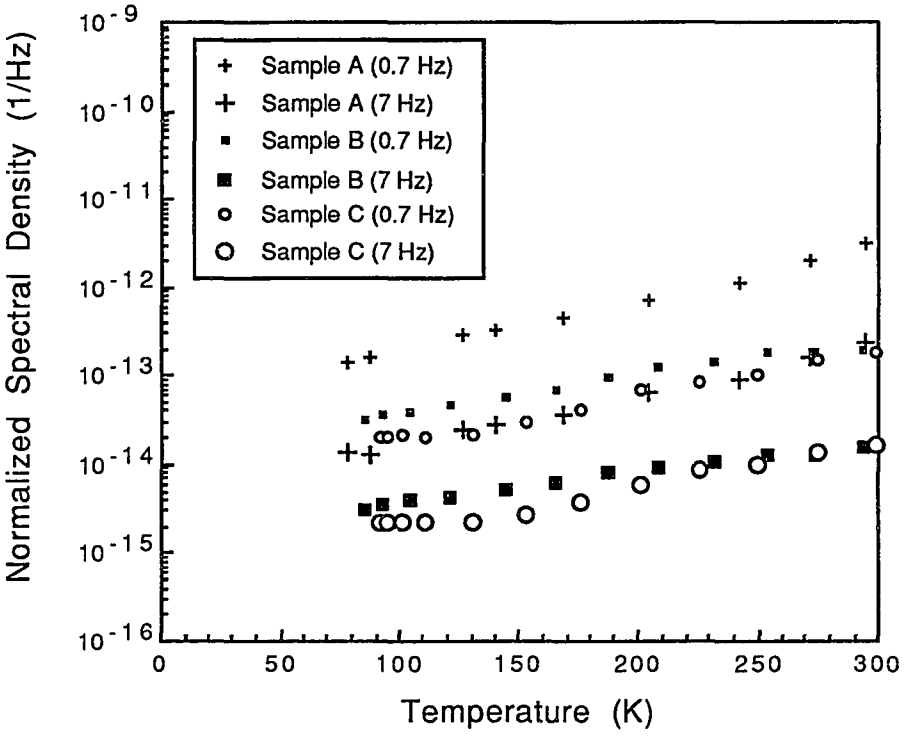

Fig. 6.9 : Normalized 1/f noise spectral density S_V/V^2 vs sample temperature for single crystals of $Y_1Ba_2Cu_3O_x$ in the ab-planes of the crystals. The corresponding resistance vs temperature plot is shown in Fig. 6.8. In the superconducting transition region no enhanced noise is observed. Measurements of 1/f noise on single crystals are the first reported.

small oxygen deficiency in this sample. The superconducting transition starts at 86 K and zero resistance is achieved at T_c = 80 K. The observed width (6 K) of the superconducting transition region is due to the small oxygen deficiency, consistent with the resistance behavior. The lower value of 80 K of $T_{c,zero}$ is consistent with the aluminum contamination of the sample. Crystals contaminated with aluminum usually show superconductivity below 86 K. The resistance of sample C decreases linearly with decreasing temperature until the superconducting transition temperature. There is no change of slope of the resistance in the normal state indicating no oxygen deficiency in this sample. Sample C has a $T_{c,zero}$ of 90 K and the width of the superconducting transition region is within 2 K. One can conclude that sample C has better superconducting and resistive behaviors than sample B and sample B is better than sample A.

The noise spectrum (S_V) was measured in the ab-plane of the above crystals by using the same configuration as that of the resistance measurement. The noise spectra of all the three samples can be fitted to $S_V(f) = Af^{-\alpha}$, with the noise exponent $\alpha(T)$ = 1.06±0.10 for the measured temperature range. Fig.6.9 shows the normalized spectral density $S_V(f)/V^2$ of the 1/f noise at selected frequencies as a function of sample temperature. At each temperature the noise spectrum was measured from 0.1 Hz to 100 Hz with a frequency increment of 0.125 Hz. All noise spectra have characteristic 1/f behavior.

The following observations can be made from the above graph:

1) There seems to be no correlation between the resistance behavior of the sample and the 1/f noise behavior. All samples show a decrease in noise with a decrease in temperature, in spite of their very different resistance behaviors, as shown in Fig.6.8.

The lack of correlation between the temperature dependence of S_v/V^2 and the resistivity suggests that the major contributions to the 1/f noise and the resistivity have different origins.

2) Samples with different superconducting behaviors show a similar 1/f noise temperature dependence. Hence the phenomenon of 1/f noise and superconductivity may have different origins.

3) In sample B and C no enhanced 1/f noise was observed in the superconducting transition region. Measurements were carried out very close to T_c in the transition region until the superconducting state where no 1/f noise could be detected.

4) The magnitude of the 1/f noise spectral density of $Y_1Ba_2Cu_3O_{7-\delta}$ single crystals is much larger than that of conventional materials. Consider the following empirical formula [11] : $S_v = \gamma V^2/N_c f$ where N_c is the total number of charge carriers in the sample and γ is in the range of10^{-1} to 10^{-5} for most metals. N_c can be calculated from the charge carrier density n_c ($2x10^{21}$ cm^{-3}) [12] and sample volume. Finally the value of γ can be calculated using the experimental data for the normalized spectral density for 7 Hz at 300 K. The result of the calculation is given below. The values of γ in single crystal samples are at least 4 orders of magnitude larger than that found in most metals.

Sample	S_v/v^2 (1/Hz)	Volume (cm^3)	γ
A	$2.5x10^{-13}$	$1x10^{-5}$	$3.5x10^{4}$
B	$1.6x10^{-14}$	$3x10^{-5}$	$6.7x10^{3}$
C	$1.8x10^{-14}$	$7.8x10^{-5}$	$1.9x10^{4}$

Sample C, which has better superconducting properties than sample B, has a high

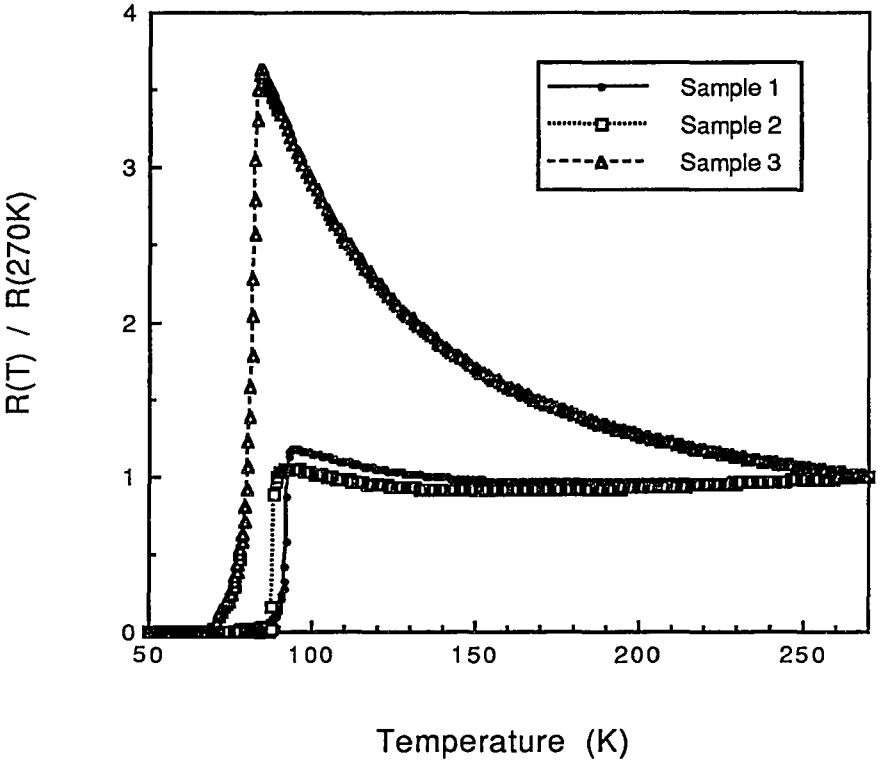

Fig. 6.10 : Normalized resistance as a function of temperature is shown for three single crystals of $Y_1Ba_2Cu_3O_x$. The measurements were done along the c-axes of these crystals. The probing current was 1mA.

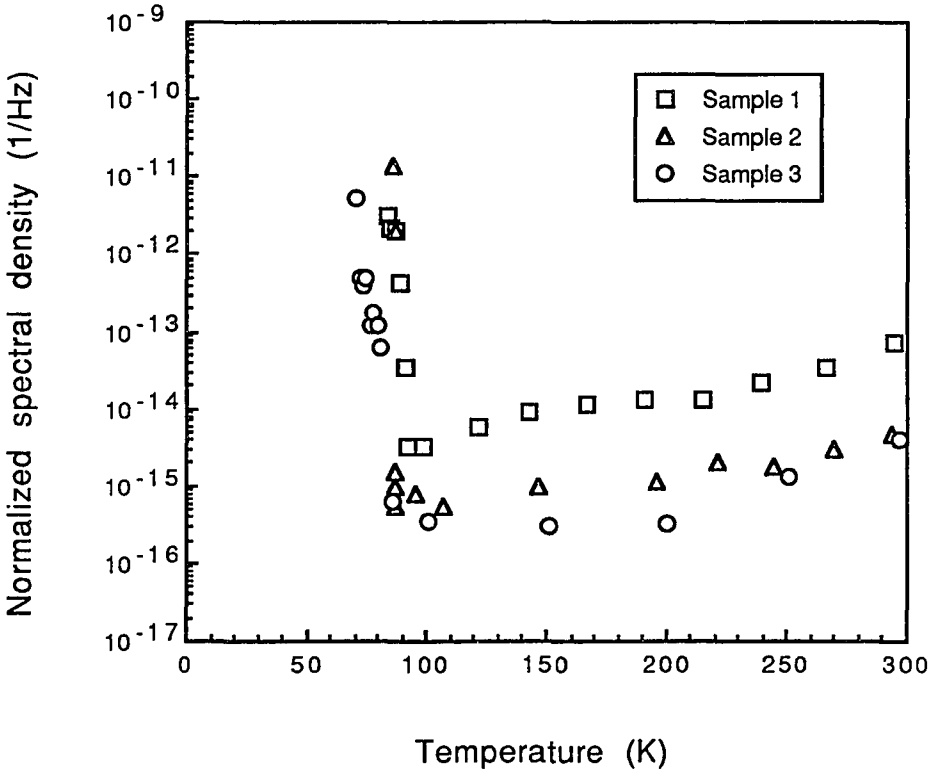

Fig. 6.11 : Normalized 1/f noise spectral density S_V/V^2 vs sample temperature for single crystals of $Y_1Ba_2Cu_3O_x$ along the c-axes of the crystals. The corresponding resistance vs temperature plot is shown in Fig. 6.10. In the superconducting transition region enhancement of noise density was observed for all the samples when the probing current was along the c-axis of the crystal. Observed anisotropic behavior of 1/f noise is the first reported.

noise density, whereas sample B, which is better than sample A, has a lower noise density. This observation rules out any possible correlation between the superconducting properties and 1/f noise behavior.

1/f noise measurement were also made on single crystals along the c-axis. The ab-plane and c-axis noise measurements were done on different crystals for the reason that the noise density is proportional to square of sample voltage and inversely proportional to sample volume. In order to have enough noise to be easily detected one would require a long thin plate crystal for the measurement of ab-plane noise and a small thick block crystal for the measurement of c-axis noise. Fig.6.10 shows the temperature dependence of resistance of three single crystals along their c-axes. The resistance is normalized at 270 K.

Sample 1 and 2 have similar c-axis resistance behavior in the normal state. In the superconducting transition region sample 1 has a tail which extends below 80K. Sample 2 has no such tail and the transition is sharp. The existence of a tail indicates the lower oxygen content of sample 1 compared to sample 2. Both of these single crystals were grown on gold foil crucibles. Sample 3 was grown on an alumina crucible, hence has a much lower $T_{c,zero}$ of 70 K. The resistance of sample 3 shows dominating semiconducting behavior and it has no metallic behavior. The resistance of this sample increases with decrease in temperature in the normal state. This observation is consistent with the literature [4]. On the other hand samples 1 and 2 exhibit slight metallic behaviors near room temperature, indicated by the positive temperature coefficient of resistivity. Several explanations have been proposed for this variation : 1) small misalignment of leads [18]; 2) oxygen deficient interior of the sample [19]; 3) electrical shorting by the ab-component of resistivity due to crystal imperfections [19]. Since crystals grown on gold foil have better quality as far as crystal perfection

and oxygen content are concerned, explanation 1 seems to be more correct than explanation 2 and 3.

Fig.6.11 shows the normalized spectral density $S_V(f)/V^2$ of the 1/f noise at selected frequencies as a function of sample temperature measured along the c-axis for all three samples. At each temperature the noise spectrum was measured from 0.1 Hz to 100 Hz with a frequency increment of 0.125 Hz. All noise spectra have characteristic 1/f behavior. The following observation are made from Fig.6.11 :

1) In the normal state, the temperature dependence of the 1/f noise in the c-axis direction is similar to that of the ab-plane. In both cases the noise density decreases with a decrease in the temperature.

2) In the superconducting region there is an enhancement of the 1/f noise. This enhancement is by three orders of magnitude within a 5 K temperature change for sample 1, five orders of magnitude within 1K for sample 2, and four orders of magnitude within 15.5 K for sample 3.

3) The magnitude of the 1/f noise spectral density of $Y_1Ba_2Cu_3O_{7-\delta}$ single crystals in the c-axis direction is much larger than that of conventional materials. The value of γ is calculated using the experimental data for the normalized spectral density for 7 Hz at 300 K and using the empirical formula [11] : $S_V = \gamma V^2/N_c f$ where N_c is the total number of charge carriers in the sample. N_c was calculated from the charge carrier density n_c ($2x10^{21}$ cm^{-3}) [12] and sample volume. The results are given below.

Sample	S_V/v^2 (1/Hz)	Volume (cm^3)	γ
1	$8x10^{-14}$	$1.2x10^{-4}$	$1.34x10^5$
2	$5x10^{-15}$	$7.62x10^{-5}$	$5.3x10^3$
3	$4x10^{-15}$	$1x10^{-4}$	$5.6x10^3$

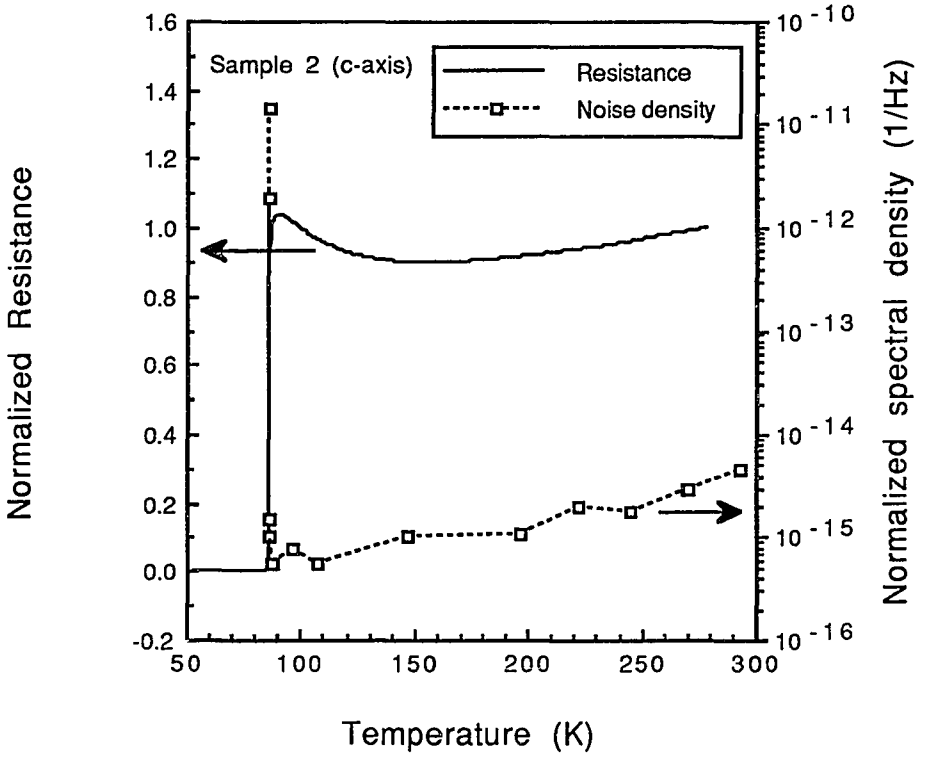

Fig. 6.12 : Normalized resistance and normalized noise spectral density is plotted as a function of temperature for single crystal (sample 2) of $Y_1Ba_2Cu_3O_x$. It can be seen that the enhancement of noise is observed only in the superconducting transition region. The measurements are along the c-axis of the crystal.

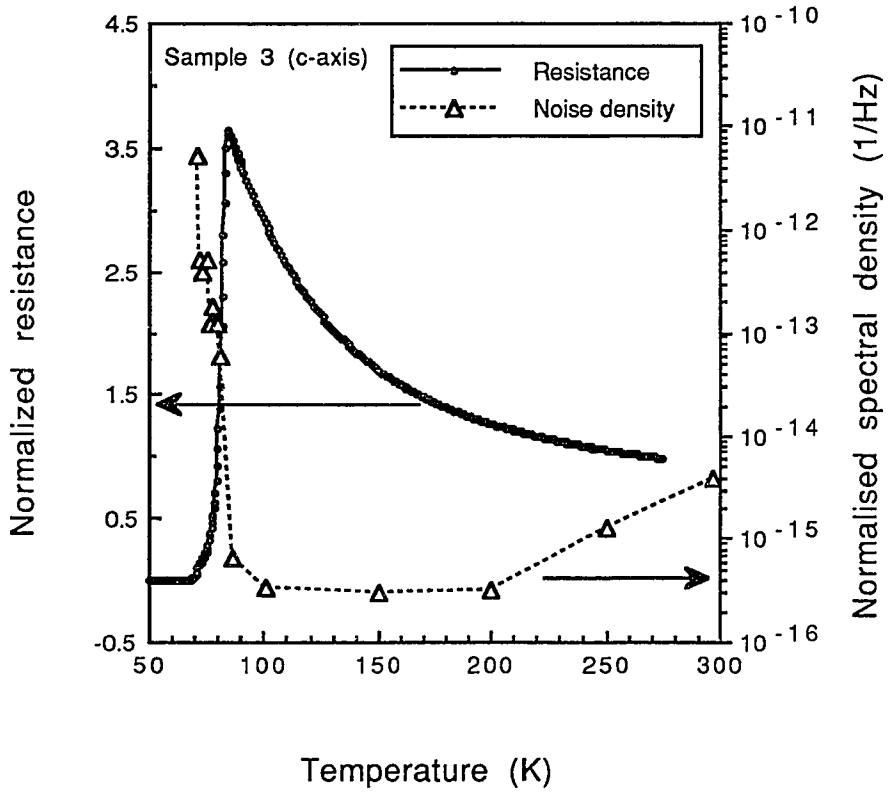

Fig. 6.13 : Normalized resistance and normalized noise spectral density is plotted as a function of temperature for single crystal (sample 3) of $Y_1Ba_2Cu_3O_x$. It can be seen that the enhancement of noise starts from the temperature corresponding to $T_{c,onset}$. 1/f noise keeps on increasing with the decrease in the temperature in this region. It has its maximum value near $T_{c,zero}$. The measurements are along the c-axis of the crystal.

Comparing the results of 1/f noise measurements in the ab-plane and in the c-axis direction, it is found that :

1) In the superconducting transition region no enhanced noise is observed in the ab-planes, whereas noise is found to be enhanced by several orders of magnitude in the c-axis direction.

2) In the normal state, the noise is of the same order of magnitude along both the ab-plane and c-axis of single crystals.

3) In the normal state, the temperature dependence of the noise is similar along both the ab-plane and c-axis directions despite of very different resistivity behavior. This behavior is usually metallic along the ab-plane and semiconducting along the c-axis.

4) Noise in single crystals of $Y_1Ba_2Cu_3O_x$ is much larger than that found in conventional materials.

In Fig.6.12 and Fig.6.13 , resistive behavior and noise in the c-axis direction is plotted as a function of temperature for samples 2 and 3. Sample 2 has a much sharper transition than sample 3. It can be seen that the enhancement of 1/f noise starts from the temperature corresponding to $T_{c,onset}$. 1/f noise keeps increasing with the decrease in temperature within this region. It reaches its maximum value near $T_{c,zero}$ and in the superconducting state ($T< T_{c,zero}$) no 1/f noise could be detected. From Fig.6.12 and Fig.6.13 it is found that the increase in the 1/f noise in the superconducting transition region of sample 2 is much sharper than that of sample 3. This enhancement of noise is five orders of magnitude per degree kelvin for sample 2 and 0.258 orders of magnitude per degree kelvin for sample 3. The superconducting transition width for sample 2 is 1.5K and for sample 3 is 14K.

Finally, it is of interest to compare the noise densities in the bulk sample, thin

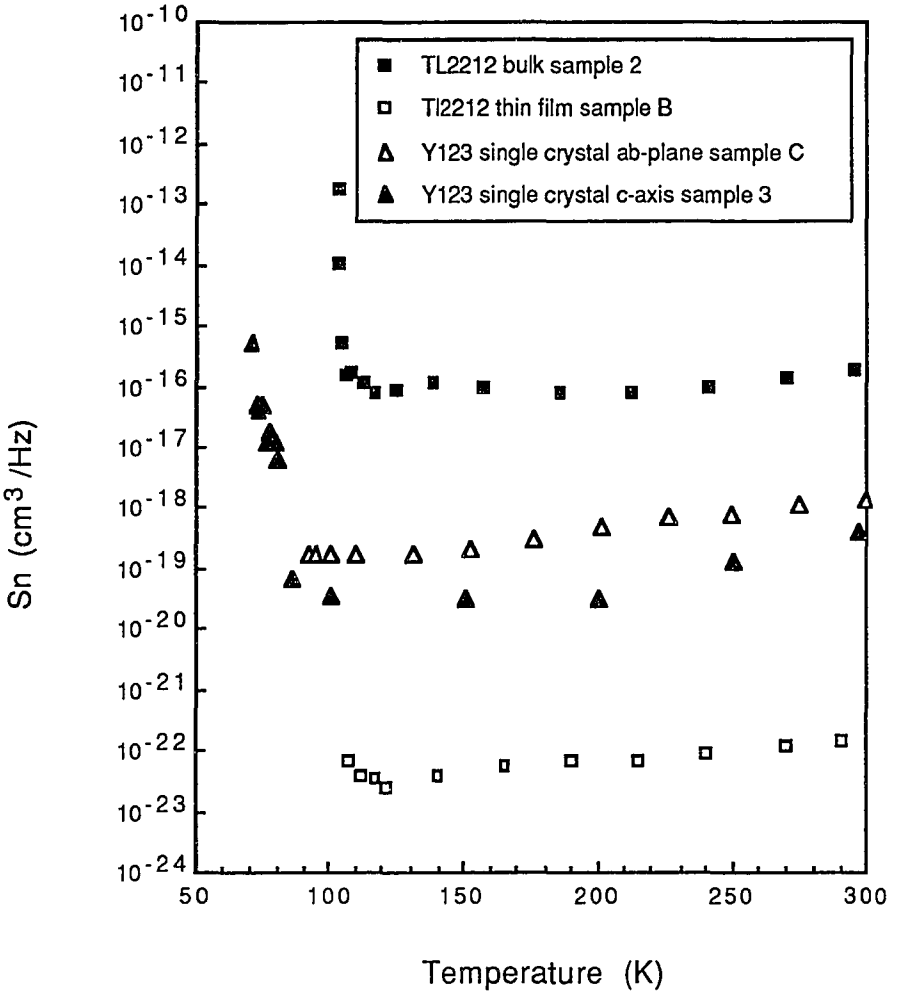

Fig. 6.14 : The normalized noise spectral density Sn (normalized by dividing by the voltage square and multiplying by the volume of the sample) for bulk and thin film samples of $Tl_2Ba_2Ca_1Cu_2O_8$, and single crystals of $Y_1Ba_2Cu_3O_x$ plotted as a function of temperature. A very low level of noise observed in the thin film sample is reported for the very first time.

films, and single crystals. Since 1/f noise spectral density is inversely proportional to the volume of the sample, one would have to consider the effect of different volumes of above samples. In Fig.6.14 normalized noise density versus temperature is given for the Tl_{2212} bulk sample, Tl_{2212} thin film sample, and single crystals of Y_{123} in both ab-plane and c-axis direction. The noise spectral density is further normalized by multiplying the already normalized noise (normalized by dividing by the square of the sample voltage) by sample volume. This normalized spectral density is denoted here by Sn with units cm^3/Hz. From Fig.6.14 it can be seen that the noise for the bulk sample is much higher than in the thin film sample and single crystal samples. In doing such a comparison it must be kept in mind that Y_{123} and Tl_{2212} belong to two different classes of superconductors, hence noise densities of Y_{123} single crystals may be very different than that of Tl_{2212} single crystals. Comparison of bulk and thin film samples of Tl_{2212} is possible and it can be seen from Fig.6.14 that noise density of bulk sample is six orders of magnitude higher than that of the thin film sample. This observation strongly supports the idea that 1/f noise is not an intrinsic property of these materials. A very low noise found in the thin film sample may be due to the very high quality of the sample with no impurity phase. A much higher noise density found in the single crystal sample of Y_{123} was surprising. It is also important to note that noise in two directions (ab-plane and c-axis) are of the same orders of magnitude. The highest noise observed in the case of bulk materials may be due to the larger number of grain boundaries in the bulk compared to the number found in a thin film or single crystal sample.

References:

1) J. A. Testa, Y. Song, X. D. Chen, J. Golben, S. I. Lee, B. R. Patton, and J. R. Gaines, Phys. Rev. B 38, 2922 (1988)

2) A. Maeda, Y. Nakayama, S. Takebayashi, and K. Uchinokura, Physica C 160, 443 (1989)

3) "Copper oxide superconductors" by Charles P. Poole Jr., Timir Datta, H. A. Karach, Wiley-Interscience Publication, 1988, page 105.

4) Yasuhiro Iye, Tsuyoshi Tamegai, Toshiro Sakakibara, Tsuneaki Goto, Noboru Miura, Hiroyuki Takeya and Humihiko Takai, Physica C 153-155 (1988) page 26.

5) R. Beyers, S. S. P. Parkin, V. Y. Lee, A. I. Nazzal, R. Savoy, G. Gorman, T. C. Huang, and S. La Placa, Appl. Phys. Lett. 53, 432 (1988)

6) C. C. Torardi, M. A. Subramanian, J. C. Calabrese, J. Gopalakrishnan, K. J. Morrisssey, T. R. Askew, R. B. Flippen, U. Chowdhry, and A. W. Sleight, Science, 240, 631 (1988)

7) D. E. Cox, C. C. Torardi, M. A. Subramanian, J. Gopalakrishnan and A. W. Sleight, Phys. Rev. B 38, 6624 (1988)

8) B. K. Jones and J. D. Francis, J. Phys. D 8, 1172 (1975)

9) P. Dutta and P. M. Horn, Rev. Mod. Phys. 53, 497 (1981);
M. B. Weissman, ibid, 60, 537 (1988)

10) I. K. Gopalakrishnan, P. V. P. S. S. Sastry, H. Rajagopal, A. Sequeira, J. V. Yakhmi, and R. M. Iyer, Physica C 159, 811 (1989)

11) F. N. Hooge, T. G. M. Kleinpenning, and L. K. J. Vandamme, Rep. Prog. Phys. 44 , 479 (1981)

12) J. Clayhold, N. P. Ong, P. H. Hor, and C. W. Chu, Phys. Rev. B 38, 7016 (1988); P. Mandal, A. Poddar, A. N. Das, B. Ghosh, and P. Choudhury, Phys. Rev. B 40, 730 (1989)

13) R. D. Black, L. G. Turner, A. mogro-Campero, T. C. Mcgee, A. L. Robinson, Appl. Phys. lett. 55(21) Nov.1989, page 2233

14) J. Wojcik, Proceedings of the European Conference of High Tc -Thin films and Single Crystal, Ed. W. Gorzkowski, world scientific, New Jersey (1989) 311.

15) J. Kowalewski, Proceedings of the European Conference of High Tc -Thin films and Single Crystal, Ed. W. Gorzkowski, world scientific, New Jersey (1989) 3.

16) T. R. Dinger, High Temp. Supercond. Compounds: Processing and related properties, ed. S. H. Whang, Publication of The Minerals, Metals & Materials Society, Pennsylvania(1989) 23.

17) A. Tressaud et al., Journal of less-common metals 151 (1989) 237.

18) P. W. Anderson and Z. Zou, Phys. Rev. Lett. 60, 132 (1988)

19) Iye, "Mechanisms of High Temperature Superconductivity", eds. H. Kamimura and A. Oshiyama, (Springer-Verlag, New York,1989)

CHAPTER 7

DISCUSSION

This chapter contains six sections. In section 7.1, it is shown that the results from the three sections of chapter 6 (Experimental Results) are consistent with each other. Answers to the questions given in the beginning of the chapter 6 are briefly given before starting the discussion of various models.

In section 7.2, Hooge's empirical law and the Voss-Clarke thermal fluctuation model are compared with the experimental data and it is shown that these models are inadequate to explain the noise level observed in Cu-oxide materials.

In section 7.3, a model based on metal-insulator-metal (MIM) junctions by Yi Song is shown to have success in explaining the noise level and its temperature dependence in the normal state of these materials. Results from Mantese's model of metal-insulator composites are used to support the MIM model. Then it is postulated that the possible source of 1/f noise in the normal state is the existence of various structural defects while the source of enhanced 1/f noise in the superconducting transition region is different than that in the normal state.

In section 7.4, the 1/f noise in the superconducting state is discussed. The question of whether the 1/f noise disappears in the superconducting state or the measuring tools fail is addressed. Assuming it is the limitation of the electrical methods for detecting the noise in the superconducting state, the behavior and enhancement of 1/f noise in the superconducting state, measured by several other groups by using magnetic measurements, is related to our measurements in the normal state.

In section 7.5, it is shown that the thermally activated motion of vortices is a

plausible source of enhanced 1/f noise in the transition region. The temperature dependence of the 1/f noise spectra in the transition region is related to that of the distribution of thermal activation energies for vortex motion, as predicted by the magnetic flux model by Ferrari. It is also shown that the correlation between the 1/f noise in the transition region and the distribution of activation energies is better than the previously observed correlation between 1/f noise and that predicted by the thermal fluctuation model of Voss and Clarke. The observed anisotropy of 1/f noise is explained in terms of the difference in the values of activation energies for flux motion along two crystallographic directions: ab plane and c-axis. Other phenomena such as vortices pinning and flux lattice melting are also discussed as possible explanations for the behavior of 1/f noise in the transition region.

Finally the conclusions drawn from this discussion are given briefly in section 7.6.

7.1 Self consistency of experimental results

It is shown below that the results obtained from this study of 1/f noise on bulk samples, thin films, and single crystals of high T_c-superconductors are consistent with each other. Also, since single crystals are the basic building blocks of materials, the results obtained on bulk samples and thin films should be understandable in terms of the single crystal data.

7.1.1 Noise in thin films

It is found from this study that 1/f noise in the ab-plane of a single crystal is not enhanced in the superconducting transition region, whereas an enhancement of the noise is always observed when the measurements are done in the c-axis direction. This

behavior explains the absence of enhanced noise in the superconducting transition region of thin films with highly c-axis oriented grain structure. In these films the grains are aligned so that the c-axes of the grains are perpendicular to the substrate. Measurement of the 1/f noise was carried out by passing the current in the plane of the film and the voltage was measured in the same plane. This plane will be parallel to the ab-planes of the grains which are oriented along the c-axis. Hence the results of 1/f noise measurements from these thin film samples should be similar to those from the ab-plane of single crystals. The temperature dependence of 1/f noise of thin film sample B, whose grains are more c-axis oriented than sample A, is similar to that of ab-plane of single crystals.

7.1.2 Noise in bulk samples

A bulk sample can be treated as a collection of randomly oriented single crystals, connected to each other by grain boundaries. So the noise measured on a bulk sample will be superposition of noise from following three factors :

(i) ab-planes of the grains

(ii) c-axes of the grains

(iii) grain-boundaries.

In the normal state, the noise is of the same order of magnitude along both the ab-plane and the c-axis. Also, in the normal state, the temperature dependence of the noise is similar in both directions. Hence in the normal state, contributions to the overall noise of a bulk sample from the first two factors cannot be distinguished. However, in the superconducting transition region because of observed anisotropic behavior of 1/f noise it is possible to make such distinction. The enhancement of noise in the superconducting transition region observed in a bulk sample is due to the existence of grains which have their c-axes parallel to the direction of current. The

relative magnitude of the enhanced noise in the transition region is directly proportional to the number of grains which have their c-axes oriented along the direction of the current.

Results of 1/f noise measurements on four bulk samples of $Tl_2Ba_2Ca_{n-1}Cu_nO_{4+2n}$ (n=2 and 3) are given in chapter 6. Sample 1 and 2 had the stoichiometry $Tl_2Ba_2Ca_1Cu_2O_8$ and sample 3 and 4 were of stoichiometry $Tl_2Ba_2Ca_2Cu_3O_{10}$. Sample 1 was prepared by sintering at 900°C for 10 min. in one step. Sample 2 was prepared in two steps by sintering at 900°C for 20 min. and then sintering it a second time at 900°C for 2 hours after regrinding and pressing the powder into a pellet. Samples 3 and 4 went through two stages of sintering, in the first step both samples were sintered at 900°C for 10 min and in the second step sample 3 was sintered at 880°C for 2 hours whereas sample 4 was sintered at 900°C for 4 hours.

A longer sintering process usually yields bulk samples containing large oriented grains and a reduced number of grain boundaries. Sample 1 was sintered only once whereas others were sintered twice. Sample 1 is therefore expected to have grains which are smaller and more randomly oriented than samples 2, 3, and 4 and, in addition, more grain boundaries. Accordingly, the noise in sample 1 is enhanced more in the superconducting transition region than that of samples 2, 3 and 4.

The noise of a bulk sample in the normal state is affected by the number of grain boundaries and by the noise from individual grains. Longer sintering, apart from giving samples with fewer grain-boundaries, also gives point defects in the crystal structure, in this class of superconductor. These defects are usually generated by depletion of thallium atoms due to their highly volatile nature. Since sample 2 was sintered longer than sample 1 and sample 4 was sintered longer than sample 3, one would expect a

greater number of point defects - like vacancies, interstitial sites - and fewer grain-boundaries in samples 2 and 4 compared to those in samples 1 and 3 respectively. In the normal state, samples 2 and 4 show higher noise than samples 1 and 3 respectively, in spite of their better superconducting properties. This would indicate that the noise of the individual grains of samples 2 and 4 is higher than that of samples 1 and 3 respectively. Accordingly, the noise density of an individual grain is proportional to the number of point defects in the grain. The relationship between 1/f noise and the number of point defects in a sample is further discussed in section 7.3. The relationship between the number of point defects and the superconducting properties of this class of superconductor is still under investigation [1].

7.1.3 Conclusions based on the experimental results

From the experimental results of this study, answers to the questions, which are given in the beginning of experimental results chapter, are clear and are briefly given below:

1) 1/f noise is not an intrinsic property of Cu-oxide superconductors.

2) No correlation between the resistivity behavior and 1/f noise was observed. This indicates that the source of 1/f noise is different than that of resistivity.

3) Enhanced noise, in the superconducting transition region, is observed for bulk sames, unoriented thin films, and even single crystals but only if the measurements are carried out in the c-axis direction of crystals.

4) A high noise power is not always observed in these materials.

5) In the TlBaCaCuO superconductor it was found that a superconductor with high $T_{c,zero}$ usually has a high noise density. This correlation between the value of $T_{c,zero}$ and noise density was not observed in the Y_{123} system.

6) The noise was found to depend on crystal anisotropy. However the anisotropic nature of noise is not related to the anisotropic nature of resistivity.

7) 1/f noise does depend on the sample preparative conditions.

8) A single crystal has a lower noise level than the bulk sample of similar size in the normal state.

9) It is possible to use these materials for practical applications such as a bolometer, etc. With proper sample preparation techniques it is possible to make devices with very low noise levels in the normal state and no enhanced noise in the superconducting transition region.

However there are still many important questions which come to mind when one analyzes the results. These questions are:

1) What are the sources of 1/f noise in these Cu-oxide superconductors ?

2) Why does a single crystal, which has metallic resistivity behavior in the ab-plane, have much higher 1/f noise than conventional materials ?

3) Why is the 1/f noise in the ab-plane and c-axis direction of the same order of magnitude in the normal state of these materials, in spite of very different resistivity behavior? In the ab-plane, the resistivity is "metallic" while along the c-axis it is more like a semi-conductor.

4) Why is there an anisotropic nature to the 1/f noise behavior ? What is the source of enhanced noise along the c-axis in the superconducting transition region ?

5) Why do thin film samples have very low noise levels compared to bulk samples of the same material ?

7.2 Comparison of the data with models

In order to answer the questions discussed in previous section, it will be helpful to compare the experimental results with existing models of 1/f noise.

7.2.1 Comparison with Hooge's empirical formula

Hooge's empirical formula [2]

$$S_v(f) = \frac{\gamma V^2}{N f}$$

was found to be valid in the sense that 1/f noise found in these class of materials is a bulk effect [3] and hence inversely proportional to the total number of charge carriers (N). Also the 1/f noise has a V^2 dependence for all samples. The major problem with the Hooge's formula is that the value of γ is not a universal constant as Hooge predicted. The value of N can be calculated from the product of sample volume and carrier density. The carrier density was calculated from the experimental values of Hall coefficient, measured by others [4,5,33,34]. The average value of the carrier density was taken to be 2×10^{21} cm^{-3} in this calculation. The value of γ can then be calculated from the experimental data on S_V/V^2 at say 7Hz. The calculated value of γ is given below for some samples :

Sample	Volume (cm^3)	S_V/V^2 (1/Hz)	γ
Tl_{2212} bulk #1	0.024	8.3×10^{-16}	2.8×10^5
Tl_{2223} bulk #4	0.024	1.25×10^{-13}	4.2×10^7
Tl_{2212} film #A	1×10^{-9}	4×10^{-14}	0.56
Tl_{2212} film #B	2.9×10^{-7}	5.2×10^{-16}	2.11
Y_{123} crystal #A(ab)	1×10^{-5}	2.5×10^{-13}	3.5×10^4
Y_{123} crystal #3(c)	1×10^{-4}	4×10^{-15}	5.6×10^3

It can be seen that numerical value of γ varies from a number of order unity (0.56) to a large number of order 10^5 (2.8×10^5) for the Tl_{2212} superconductor instead having a universal value.

7.2.2 Comparison with thermal fluctuation model

Previous studies [6] of 1/f noise on Y_{123} bulk material showed a correlation between 1/f noise and the temperature derivative of the resistivity. The Voss and Clarke thermal fluctuation model [7] was then thought to be a suitable predictive model. This model predicts the following equation for the 1/f noise power spectral density

$$\frac{S_v(f)}{V^2} = \frac{\beta^2 T^2 k}{C_v \left[3+2 \ln \left(\frac{\ell}{w}\right) \right] f}$$

Where $\beta = \frac{1}{R}\frac{dR}{dT}$ is the temperature coefficient of resistivity, k is the Boltzmann constant, C_v is specific heat capacity, ℓ is the length of the sample, w is the width of the sample, T is temperature and f is frequency.

The model considers the thermal fluctuations to be the source of 1/f noise. These thermal fluctuations in turn give rise to resistance fluctuations through the temperature coefficient of resistance. The inadequacy of the theory lies in the fact that no enhanced noise was experimentally detected in the superconducting transition region of single crystal in the ab-plane. The absence of this enhanced noise cannot be explained by the Voss-Clark temperature fluctuation model, which predicts an enhancement of the noise due to a large change in value of β in the transition region, regardless of the direction of the applied current. This model fails to predict the qualitative features of the data.

To further show the inadequacy of the temperature fluctuation model, one can

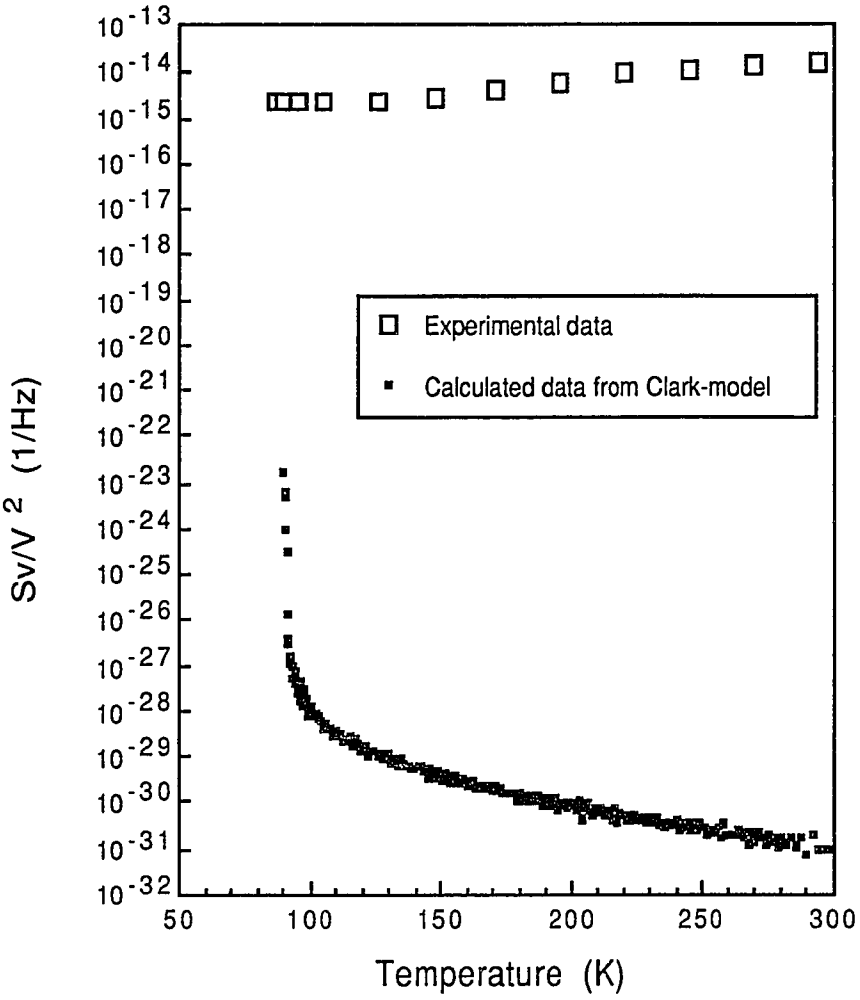

Fig. 7.1 : Normalized noise density calculated from Voss-Clarke thermal fluctuation model as a function of temperature for a single crystal of $Y_1Ba_2Cu_3O_x$ in the ab-plane. The experimental data, obtained by this study, is also shown for comparison. It can be seen that the thermal fluctuation model fails to predict the qualitative or quantitative features of the data.

calculate the noise power using the above equation. The value of β was calculated from the ab-plane resistivity data of single crystal. The specific heat was obtained from the polynomial fits $C_v = 0.009\ T + 37x10^{-5}\ T^3 + 1.3x10^{-6}\ T^5$ to the experimental data obtained from the specific heat measurements on single crystals of Y_{123} [8]. Fig.7.1 shows the result of the above calculation along with the experimental 1/f noise measurement on a single crystal in the ab-plane direction. It can be seen that the predicted noise level is 15 orders of magnitude lower than the experimental values. Also, theory predicts a different temperature dependence of noise in the normal state and enhancement of noise in the transition region. Therefore the Voss-Clarke model fails to predict either the qualitative or quantitative features of the data.

7.3 1/f noise in the normal state (tunneling mechanism)

Well away from the transition region, the sample have electrical resistances characteristic of "dirty metals". They also have corresponding large noise powers compared to metals. The behavior in this region is discussed below.

7.3.1 MIM junctions model

A model developed by Yi Song et al. [9,10] appears to be more promising in predicting 1/f noise that agrees with the experimental data. This model results from a direct application of Mcwhorter's potential fluctuation mechanism [11] to metal-insulator-metal (MIM) junctions. In the normal state, the copper oxide materials are composed of metal-insulator-metal regions. In the case of bulk samples, individual grains, considered as metallic regions, are separated by grain-boundaries considered to be insulating (or semiconducting) regions. In the case of single crystals, insulating regions are considered to be due to structural defects such as twin boundaries,

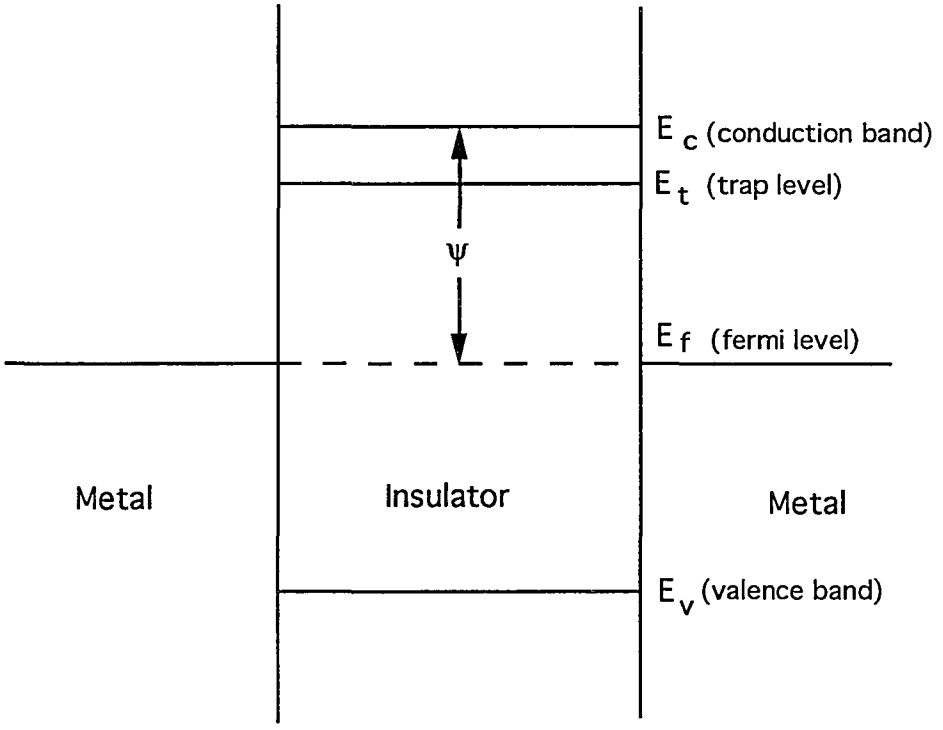

Fig. 7.2 : A schematic diagram of the metal-insulator-metal junction showing the simplified band structure.

dislocation lines, or oxygen deficient domains [12]. In general, a sample is assumed to consist of structurally perfect regions that are separated by defective regions. A schematic diagram of such a junction is shown in the Fig.7.2.

For conduction to occur, charge carriers have to overcome an energy barrier which is due to the difference in the energy-level of the bottom of the conduction band of the insulator and fermi level of the metal. When some charge carriers become trapped in the junctions, the height of the energy barrier is changed due to Coulomb interactions. Fluctuations in the number of trapped charge carriers lead to fluctuations in the barrier height, which in turn gives rise to fluctuations in conductance. The model considers the tunneling process to be the dominant conduction process [13] as opposed to a thermally activated hopping process, by assuming the thickness of the insulating region to be of the order of 10 Å. The choice of a 10 Å thick insulating layer is consistent with the thickness of the twin boundary layer [14] and the size of an oxygen vacancy ordered domain [15]. The model calculates the normalized 1/f noise spectral density of voltage fluctuations for the whole sample from the equation :

$$\frac{S_V(f)}{V^2} = \frac{\pi^5 m e^4}{h^2} \frac{s^4 \ell}{wt\varepsilon^2\psi} \left[1 - \frac{\pi kT}{2\psi} \frac{\cos(\pi kBT)}{\sin(\pi kBT)}\right]^2 \frac{N}{\Omega \ln(\frac{\tau_2}{\tau_1})} \frac{1}{f}$$

where m = electron mass, e = electron charge, h = Planck constant, k = Boltzmann constant, ψ = barrier height, s = spatial thickness of the insulating region, ε = dielectric constant of the insulating layer, $A = 4\pi s(2m)^{1/2}/h$, $B=2\pi s(2m/\psi)^{1/2}/h$, w and t = spatial lateral dimensions of the junction, ℓ = spatial longitudinal dimension of the metallic region, Ω = the sample volume, and N = number of trapped charge carriers in one junction (which is related to the trapped charge carrier density n by N = ntws), f is frequency and there are two cutoff frequencies $1/\tau_1$ and $1/\tau_2$ such that $1/\tau_2 << f << 1/\tau_1$.

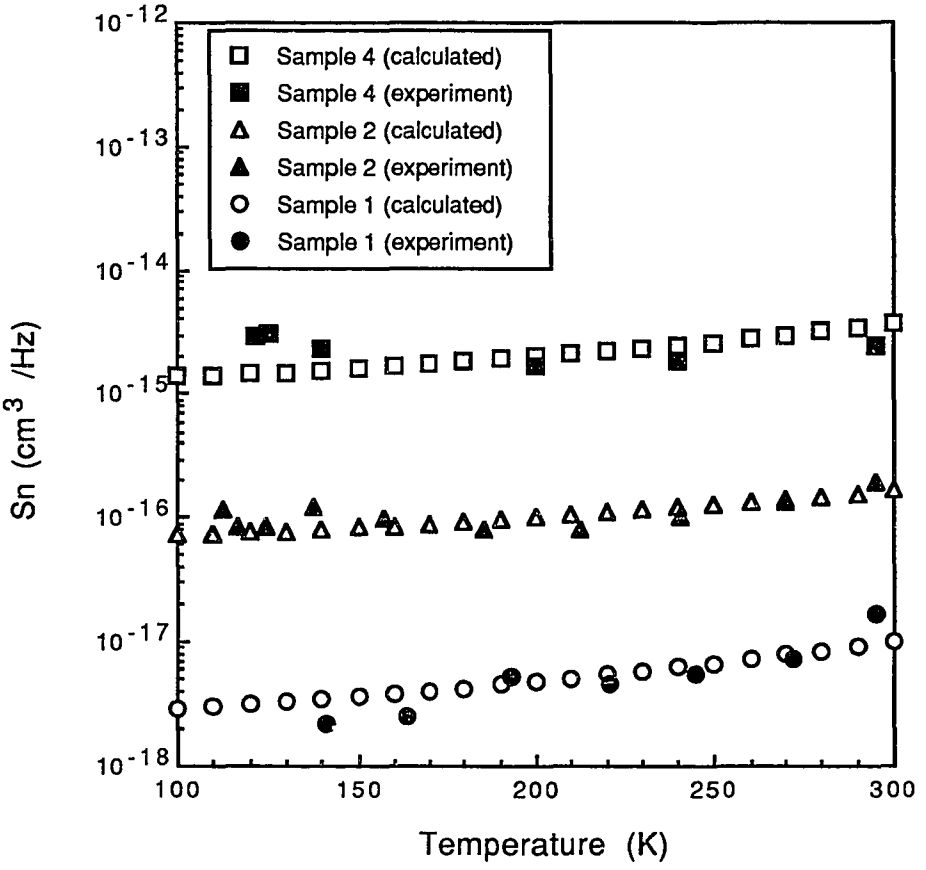

Fig. 7.3 : Normalized noise density calculated from MIM model as a function of temperature for bulk samples of TlBaCaCuO superconductors. The experimental data is also shown for comparison. The agreement between the theory and the experiment is good. The MIM model successfully predicts the right temperature dependence and spectral density of 1/f noise, in the normal state of a high T_c superconductor.

The calculation is insensitive to the actual numerical values of τ_1 and τ_2 because of the logarithm. The model takes $\ln(\tau_2/\tau_1) = 10$ to represent a broad range of characteristic time constants. The derivation of the above complicated equation is long and hence will not be included here. The details of the model can be found in Ref. 35. A brief discussion of the model can be found in Ref. 9.

7.3.2 Success of MIM junctions model

Using "n" as the only adjustable parameter, the model is able to calculate the 1/f noise spectral density of copper oxide superconductors in the normal state for both bulk samples [10] and single crystals [9]. Fig.7.3 shows the experimental data and calculated results of normalized 1/f noise spectral density for bulk samples of TlBaCaCuO superconductors. The values of the fitting parameters can be found in Ref. 10. The model succeeds in the following sense:

1) The model predicts that the 1/f noise is a bulk effect. 1/f noise is found to be a bulk effect in copper-oxide materials [3].

2) The model predicts the correct temperature dependence of 1/f noise in the normal state of these Cu-oxide materials. The small deviations from the experimental results, at low temperature, are ascribed to the simplifications used in the calculation, such as treating the barrier height as a temperature independent term.

3) The model also predicts the correct noise level in these materials. According to the model the noise is very sensitive to the thickness "s" of the tunneling barrier and model is capable of explaining the difference between the noisy sample and the quiet sample made by similar preparation techniques, in terms of thickness "s". Quiet samples would be those with a small value for "s".

The value of $n = 2 \times 10^{20}$ cm^{-3} used in the model for the number of trapped charge

carriers seems high considering that the total number of free charge carriers per unit volume is roughly equal to $2x10^{21}$ cm^{-3}. Assuming the trapped charge carriers in a single crystal of Y_{123} are due to oxygen deficiency, one can calculate the number of charge carriers in the trap region. Suppose there is one oxygen deficiency per 20 unit cells of size 4x4x12 $Å^3$ corresponding to the stoichiometry $Y_1Ba_2Cu_3O_{6.95}$. Then there is one defect region in the volume of $3.84x10^{-21}$ cm^3 and that will correspond to $2.6x10^{20}$ number of trapped charge carriers per cm^3. Even though this number looks reasonable, in the case of copper oxide superconductors one can argue that these oxygen deficient domains are randomly located rather than grouped together. On average, there is only 1 defective cell in 20 unit cells. Since these defective unit cells are not in touch with other defective cells, there is a clear metallic percolating path for the conduction process to take place and there is no need for conduction through tunnelling. Hence one could argue that the model based on MIM structure which requires tunneling as a conduction process is not applicable.

7.3.3 Mantese's two component model

The previous reasoning is not quite valid. The above picture of perfect cells with a few defective cells is similar to the previously noted behavior observed by Mantese [16] in metal-insulator-metal composites. In their two-component model, effective medium theory is used to examine the resistivity $\rho(x)$ and normalized 1/f noise density $s(x)$ of a model metal-insulator composite, with volume fraction x of metal. They considered two distinct conduction mechanisms: (i) metallic conduction and (ii) conduction due to charge tunneling through the insulating component. The results from the model are consistent with the experimental measurements [17] of both $\rho(x)$ and $s(x)$ on Pt-Al_2O_3 composite over the full range of x, including the metallic conduction

threshold at x_c. The model calculates the resistivity for a simple cubic lattice (coordination number z = 6) as a solution to the equation:

$$1 = \frac{3f}{2+\frac{\rho}{\rho_M}} + \frac{3(1-f)}{2+\frac{\rho}{\rho_T}}$$

where f = f(x) is the probability that two neighboring cells are connected by metallic resistors with resistivity ρ_M. The tunneling resistivity is taken to be of the usual form

$$\rho_T(x) = \rho_0 \exp[\chi t(x)]$$

which depends exponentially on the tunnel barrier thickness t(x). ρ_0 and χ are used as adjustable parameters (χ=0.5 Å^{-1} and ρ_0=8x10^{-5} Ωcm), in determining the resistivity. This model calculates the 1/f noise in the resistivity from the equation:

$$\frac{s}{(1+\gamma)} = f(x)\frac{(g_M^2 s_M + \gamma g^2 s)}{(g_M + \gamma g)^2} + [1-f(x)]\frac{(g_T^2 s_T + \gamma g^2 s)}{(g_T + \gamma g)^2}$$

where the conductances (g_i) are $g = \rho^{-1}$, $g_M = \rho_M^{-1}$, $g_T = \rho_T^{-1}$, and $\gamma = (z-2)/2$, where z is the coordination number and

$$s_M = \frac{S_{\rho_M}(x)}{\rho_M^2(x)}, \quad s_T = \frac{S_{\rho_T}(x)}{\rho_T^2(x)}$$

are normalized noise powers from the metallic conduction and tunneling conduction respectively. Clearly $s = s_M$ for x = 1.0 and $s = s_T$ for x = 0, since f(0) = 0 and f(1) = 1.

For $x >> x_c$, which is the case we are interested in and is similar to the above picture of oxygen deficient cells in a single crystal, it is found that the presence of a tunneling path has no effect on the value of conductivity. The calculated resistivity versus x plots were almost the same as the experimental data for both of the following

cases: (i) when tunneling was included as a possible conduction mechanism; and (ii) when tunneling was totally ruled out as a possible conduction mechanism. The unchanged value of the resulting resistivity for the above two cases can be explained by the argument that the current carried by the tunnel paths is quite small compared to that carried by the metallic paths. However the resultant noise for the $x>>x_c$ region deviates substantially from the experimental data if the tunneling is totally removed as a conduction mechanism. They concluded that it is the tunnel junctions which are responsible for the noise for all values of x (even for $x>>x_c$). Thus for $x \geq x_c$, the dominant sources of conduction and of noise in the composite arise from completely different mechanisms. This conclusion is consistent with our experimental results on copper-oxide materials in the sense that no correlation between the resistivity behavior and 1/f noise was observed.

7.3.4 Justification for the existence of MIM junctions

In the above paragraph, it is assumed that an oxygen deficient single crystal of $Y_1Ba_2Cu_3O_{7-\delta}$ has features that are similar to those of metal-insulator composites. The assumption is valid if one realizes that a particular unit cell of Y_{123} can only contain an integral number of oxygen atoms. Therefore a unit cell is metallic if there are 7 oxygen atoms in the cell or insulating if there are 6 oxygen atoms. If this is the case, then one would expect a percolation threshold for conduction to take place as the oxygen content of the sample is varied from 6 to 7. Several groups have measured the electrical resistivity of $Y_1Ba_2Cu_3O_x$ with varying oxygen content. It is found [36,37,38] that the normal state resistivity increases as the oxygen content of the sample is lowered. The increment in the value of resistivity is of the order unity when the oxygen content of the sample is lowered from 7 to 6.5. The resistivity increases by 3 orders of magnitude

when the oxygen content is lowered from 6.5 to 6.3. Samples with oxygen content of 6.3 and below are found to be highly insulating: the resistivity sharply increases with decreasing temperature. The oxygen content of 6.3 corresponds to 30% of the unit cells having 7 oxygen atoms and being "metallic". The percolation threshold is then observed when about one third of the unit cells are metallic, which is a reasonable number since for a 3D system, the EMA value is 1/D or 1/3. The existence of a percolating metallic path will be more obvious if the metallic region becomes superconducting. In this case, the resistance due to various tunneling and thermally activated hopping will be shunted by the superconducting percolating path. It is found [1,32,39,40] that the superconducting transition temperature ($T_{c,zero}$) sharply drops to zero, if the oxygen content is less than 6.36. This number suggests that if the oxygen content of the sample is lower than 6.36 then there is no superconducting percolating path. The above argument supports the existence of MIM junctions in the copper oxide superconductors.

7.3.5 The source of 1/f noise: point defects vs twin boundaries

The existence of a tunneling processes can also be due to the presence of insulating layers, which are usually the grain-boundaries in the bulk samples. The insulating layers can also exist in single crystals of Y_{123} due to twinning, dislocation lines and other surface and volume defects. The twin boundaries in Y_{123} will be parallel to the c-axis since twinning occurs due to mixing of the a and b axes. So if the source of 1/f noise is tunneling through twin boundaries then one would expect less noise in the c-axis direction since now the current is flowing parallel to the twin boundary and charge carriers do not have to cross it. Experimental data suggest that the noise level is of the same order of magnitude in both the ab-plane and in the c-axis direction in the normal state, hence the source of 1/f noise is more likely to be point defects than twin

boundaries. However further experiments can be done to make the above situation more clear.

In the first experiment one could study the noise level as a function of the oxygen content of single crystals of Y_{123}. In order to keep the number of other defects (foreign atoms, interstitial sites, twinning boundaries etc.) constant, one should study the noise level in a specific crystal as a function of oxygen content instead of comparing the noise levels of several different crystals with different oxygen content. In the second experiment one could measure the noise level of a twinned crystal and then "de-twin" the crystal by applying a uniaxial pressure [18]. The difference between the noise level of the twinned state and de-twinned state of the same crystal will give useful information about the effect of twin boundaries on 1/f noise. These experiments have not been done yet.

In the above experiments, one would expect the noise level to decrease with a decrease in the number of defects. We did observe a very low noise level in the thin film sample of Tl_{2212}. Since thin films are usually prepared under high vacuum, the quality of the sample is usually better than that of single crystals or bulk samples which normally face contamination problems due to the crucible and their surroundings. Also these thin films are free from twinning defects because twinning does not occur in this class of superconductor. Hence a very low level of noise observed in the thin film sample may be associated with a smaller number of defects in the sample.

The argument is supported by the recent experiment by Fleetwood [19] on metal-oxide semiconductor (MOS) transistors which shows that the magnitude of 1/f noise of unirradiated MOS transistors correlates strikingly with the radiation-induced hole-trapping efficiency of the oxide. They found that by decreasing the radiation

induced hole trapping efficiency of SiO_2, one can decrease the 1/f noise of the device proportionally. This decrease in noise suggests that the defects which cause 1/f noise in MOS transistors are linked closely to radiation-induced hole traps, the *E'* center (a trivalent Si center in SiO_2), or an oxygen vacancy. In p-MOS transistors, 1/f noise is attributed to the exchange of holes with hole traps. Similarly, for n-MOS transistors, the 1/f noise is attributed to electrons interacting with electron traps. This is the first time that the 1/f noise of MOS transistors has been linked to a point defect with known microstructure.

The nature of 1/f noise in the c-direction can be explained as a superposition of two noise levels, one due to normal state noise and the other due to a new noise in the transition region which is observed only in the c-direction and hence is anisotropic in nature.

7.4 1/f noise in the superconducting state : vortex motion

In the superconducting state, noise has been detected through magnetic measurements done by other groups. Their results have a bearing on our interpretation of noise in the transition region.

7.4.1 Limitations of experimental techniques for noise measurements

In the superconducting state we could not observe any 1/f noise. But, if the 1/f noise in the normal state is due to various defects and tunneling phenomena (MIM model), then when the sample becomes superconducting, the metallic regions would become superconducting and the insulating regions would remain the same. Then one

would have superconductor-insulator-superconductor junctions and noise would be expected to exist due to tunneling through the insulating regions. Since the measured noise in the superconducting state was the same as the background noise, it is possible that the background noise is higher than the 1/f noise in the superconducting state.

The reason why we could not observe 1/f noise in the superconducting state is that the 1/f noise is proportional to square of the sample voltage ($S_V \propto V^2$) and in the superconducting state the sample has a zero resistance. So it is impossible to measure the noise in the superconducting state through electrical measurements. However, since the superconducting sample will have a very strong diamagnetic signal, measurement of noise is possible through the magnetic measurements in the superconducting state. Since the magnetic signal is weak in the normal state, it is difficult to use the same magnetic techniques to measure 1/f noise in the normal state. In the above picture one assumes 1/f noise exists at all temperatures since the defects in the sample exist at all temperatures however each of the measurement techniques has a limited range.

Another possibility is that the noise decreases as the measuring signal decreases since noise is proportional to square of the signal and vanishes below $T_{c,zero}$. In the case of magnetic measurement, where noise is expected to be due to motion of vortices, the noise in the normal state will disappear with the disappearance of the very existence of the vortices. But, in the case of electrical 1/f noise measurements one cannot say that the charge carriers are going to disappear in the superconducting state. However since the charge carriers are now correlated with each other the noise could be reduced due to the correlated behavior. The correlation of charge carriers is supported by the fact that the entropy of the superconducting state is lower than the normal state. The correlated motion of charge carriers will reduce the number of carriers tunneling and hopping

because both of the charge carriers (which are located at different places) must tunnel simultaneously or break the pairing and tunnel individually. So the electrical noise in the superconducting state will be reduced (a lot), but it will not be zero since there is always a possibility of tunneling or some other thermally activated phenomenon. However, it would be difficult to detect weak 1/f noise signals since they would be masked by the background noise.

7.4.2 Magnetic 1/f noise vs electric 1/f noise

1/f noise has been studied by various groups in the superconducting state with the help of magnetic measurements [24-29]. It is found that the magnetic 1/f noise level increases with the temperature in the superconducting state. The noise level is enhanced by several order of magnitudes in the superconducting transition region. The maximum value of the noise is found at critical temperature T_c, defined as the temperature at which diamagnetic screening vanishes [25]. In the region $T>T_c$ the noise level decrease with the increase in the temperature until the signal is lost in the background noise. The critical temperature T_c defined above is same as critical temperature $T_{c,zero}$ defined as the temperature at which the electrical resistivity vanishes [30]. In our measurements of electric 1/f noise we also observed the maximum noise level at temperature close to $T_{c,zero}$. The region $T>T_c$ where the magnetic 1/f noise decreases sharply with temperature will correspond to the enhanced electric 1/f noise measured in the transition region : in both cases noise rises with decrease in the temperature. Away from the transition region both the electric 1/f noise and the magnetic 1/f noise have similar temperature dependence. In the normal state, the electric 1/f noise decreases with the temperature and in the superconducting state, the magnetic 1/f noise decreases with the temperature.

It is found [26] that the magnitude of the magnetic 1/f noise depends strongly on the microstructure of the thin film sample, and is lowest for a sample which is predominantly oriented with its c-axis perpendicular to the substrate. This observation is consistent with our measurements on highly oriented films, which showed very low noise levels.

7.4.3 Magnetic flux model

The source of magnetic 1/f noise is considered to be the motion of vortices[26]. It is found that the noise power is linearly proportional to the applied magnetic field, indicating that the vortices move incoherently. In the case of magnetic flux noise, a model calculation was done by Ferrari et.al. [24], based on the assumption that 1/f noise arises from the incoherent superposition of many thermally activated processes where vortices hop over temperature dependent barriers U(T). The characteristic time for this process is

$$\tau = \tau_0 \exp\{\frac{U(T)}{kT}\}$$

where τ_0^{-1} is a temperature independent attempt frequency, and k is the Boltzmann constant. Each hopping process yields a Lorentzian power spectrum and the spectral density of noise from many such processes is proportional to

$$\int \frac{\tau}{(1+\omega^2\tau^2)} D(U)\, dU$$

where D(U) is taken as a broad featureless distribution of activation energies, with D(U)dU being the number of processes with activation energies between U and U+dU. This model is a modified version of random fluctuation model of Dutta, Dimon and Horn, the major modification being the existence of temperature-dependent activation energies.

7.5 1/f noise in the transition region (anisotropic behavior)

Magnetic 1/f noise arises from thermally activated hopping of vortices. It is possible that the source of enhanced noise in the superconducting transition region, for both the electric and magnetic 1/f noise, is the thermally activated motion of vortices. Vortices formed in the transition region move transverse to the applied current because of the Lorentz force. The movement of the vortices induces an electric field which is transverse to the velocity of the vortices and hence will be parallel to the current direction. This induced electric field generates fluctuations in the voltage because of fluctuations in the velocities of the vortices.

It is shown by Palstra et al. [41] that in the superconducting transition region, the resistivity is dominated by thermally activated motion of flux. The thermally activated behavior is evident from the Arrhenius plot of resistance. Fig.7.4 shows such an Arrhenius plot for single crystal of $Y_1Ba_2Cu_3O_7$ (sample #2) where resistance is plotted on a log scale with respect to inverse of sample temperature. The values of the corresponding temperatures for 5 points are shown on the top axis for convenience. The resistance was measured along the c-axis. The straight line segments of the plot indicate that the dissipation mechanism is thermally activated. In the transition region, the dissipation mechanism has been related to the following two phenomena :

(i) Thermally activated motion of flux [41-46]

(ii) Flux lattice melting [47-49]

In the following paragraphs, the above two phenomena will be discussed in relation with 1/f noise.

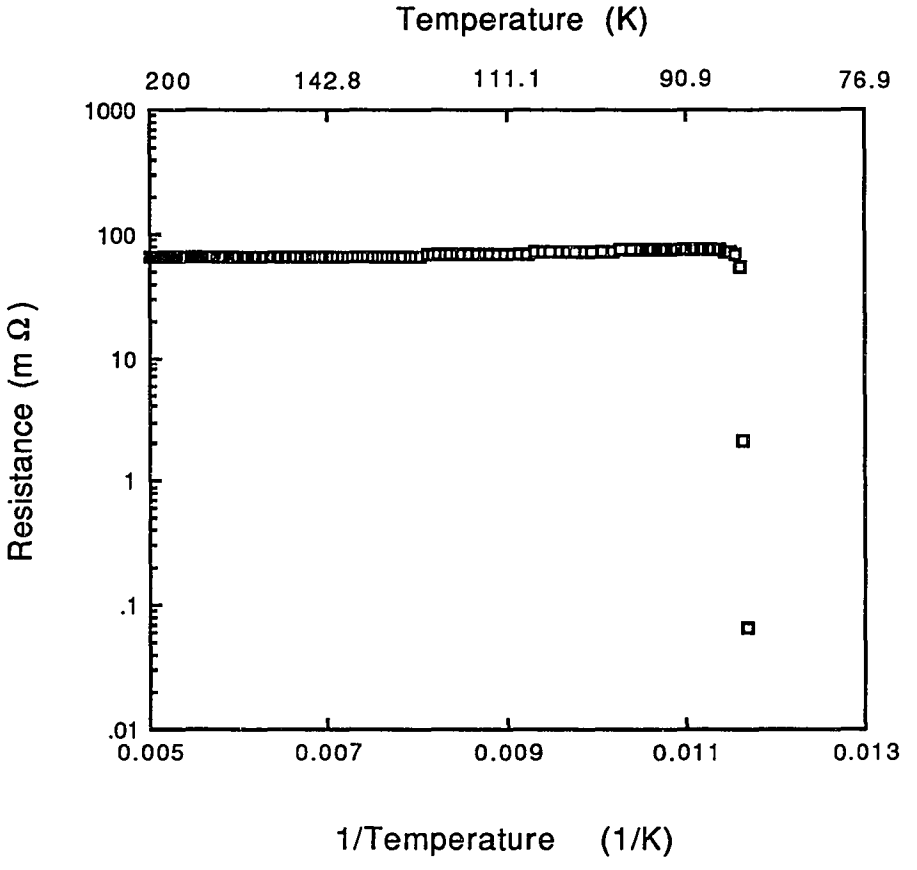

Fig. 7.4 : An Arrhenius plot for single crystal of $Y_1Ba_2Cu_3O_x$ (sample #2) where resistance is plotted on a log scale with respect to inverse of sample temperature. The values of corresponding temperatures for 5 points is shown on the top (non-linear scale) for convenience. The resistance was measured along the c-axis of the crystal. The straight line segments of the plot indicate that the dissipation mechanism is thermally activated.

7.5.1 Thermally activated flux motion and 1/f noise

In thermally activated flux motion, the resistance in the transition region is given by the equation [42,43]

$$R = R_o \exp(\frac{-U}{kT})$$

where U is the activation energy for flux hopping. At present, the temperature dependence of U is a controversial issue. This controversy has resulted in two approaches : one based on the temperature dependent activation energy [43] and the other based on the distribution of various activation energies [45]. In either case two types of flux motion have been identified in the transition region : (i) flux flow, and (ii) flux creep. Flux creep occurs when the Lorentz force acting on the vortex is smaller than the pinning force. Flux flow occurs when the pinning force is smaller than the Lorentz force. Both type of flux motion cause dissipation in the conduction process. 1/f noise in the transition region could possibly be explained by the magnetic-flux model of Ferrari (discussed in the previous section) [24]. The enhancement of noise in the transition region would be a direct consequence of vortex formation and their resultant thermally activated motion. The enhancement of the noise would be observed only in the transition region since the vortices are expected to freeze by pinning in the superconducting state and be non-existent in the normal state.

7.5.2 Anisotropic 1/f noise: difference in activation energies

In order to explain the anisotropic behavior of 1/f noise (enhanced noise is observed only in the c-direction), one needs to consider the difference in the values of activation energies along both the ab-plane and the c-axis directions. Experimentally, it is found that activation energies are much larger when the applied magnetic field is parallel to the ab-plane than when the field is parallel to the c-axis [31]. This suggests

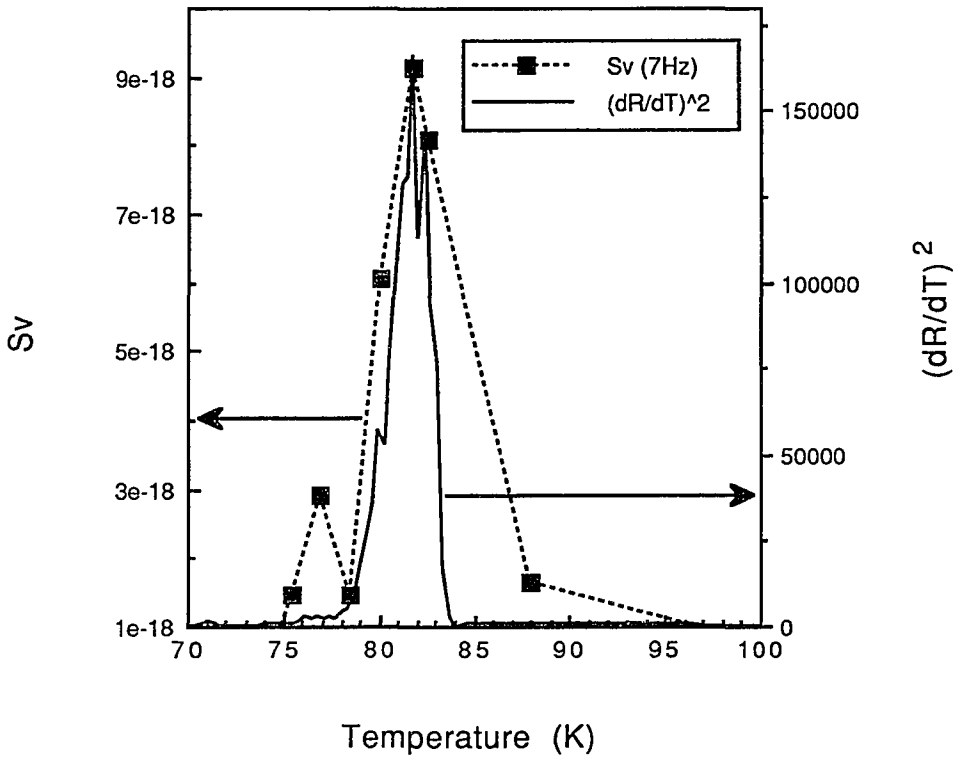

Fig. 7.5 : 1/f noise spectral density and square of temperature derivative of resistance as a function of sample temperature. The measurements are shown for single crystal of $Y_1Ba_2Cu_3O_x$ (sample #3) along the c-axis, near the transition region. It can be seen that the widths of two peaks are not the same: peak in noise density is broader than the $(dR/dT)^2$ peak.

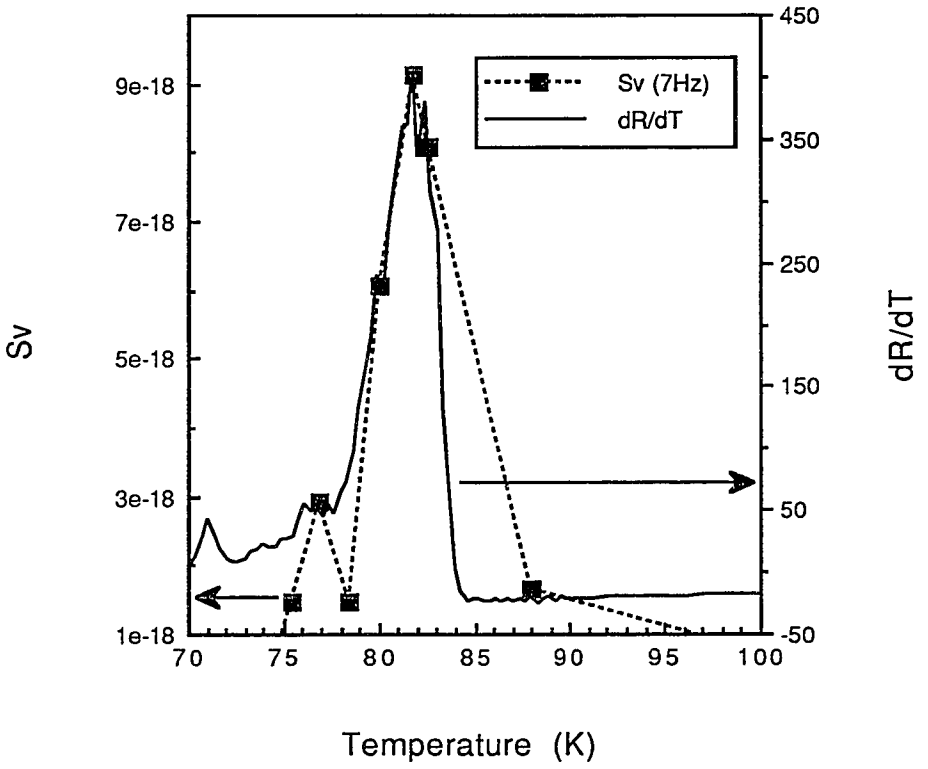

Fig. 7.6 : 1/f noise spectral density and temperature derivative of resistance as a function of sample temperature. The measurements are shown for single crystal of $Y_1Ba_2Cu_3O_x$ (sample #3) along the c-axis, near the transition region. It can be seen that the widths of two peaks are nearly the same. This would indirectly support the idea that the enhanced 1/f noise in the transition region is due to thermally activated processes.

that the activation energy for vortex hopping is low in the ab-plane and is higher in the c-direction. So if the current is flowing in the ab-plane then vortex hopping must take place in the c-direction, which requires large activation energy. This large activation energy will result in reduced vortex hopping and hence no enhancement of the noise. Whereas a current in the c-direction, can cause many thermally activated vortex hops to take place in the ab-plane causing the noise to be enhanced by a large amount. Another explanation of the observed anisotropy of 1/f noise will be discussed later in terms of the pinning mechanism of vortices.

7.5.3 Enhanced noise: comparison with thermal fluctuation model

Since the source of enhanced noise in the superconducting transition region is expected to be different from the noise source in the normal state, it is possible that this source of enhanced noise in the transition region is related to thermal fluctuations as predicted by Voss-Clarke model. Their model predicts the noise power to be proportional to square of temperature derivative of resistance

$$S_V \propto (dR/dT)^2$$

Previous studies by Testa [6] and Clark [23] on superconducting materials in the transition region have indicated a possible correlation between the 1/f noise and square of the temperature derivative of resistance $(dR/dT)^2$. Testa et al. studied bulk samples of Y_{123} and Er_{123} where they found that the correlation between noise and $(dR/dT)^2$ was imperfect in the sense that the 1/f noise peak was somewhat broader than the $(dR/dT)^2$ peak. In the case of Clark, where 1/f noise was studied in tin films, in the superconducting transition region, the correlation was even worse than found in the bulk samples of Testa et al. To check a possible correlation, a calculation was done for one

single crystal of Y_{123} used for the c-axis resistance measurement (sample #3). In Fig.7.5, both the 1/f noise power and $(dR/dT)^2$ are shown as a function of temperature. In this case too, we find that the noise peak is broader than the $(dR/dT)^2$ peak. However, it may be possible that the noise power instead of being related to $(dR/dT)^2$ through the thermal fluctuation model, is related to the thermal activation energy for flux motion which is proportional to dR/dT

$$S_V \propto D(U) \propto dR/dT$$

where the temperature dependence of the noise power may be related to either the temperature dependence of the activation energy or to the shape of the distribution function of activation energies.

Fig.7.6 shows the 1/f noise power and dR/dT of the above sample as a function of temperature. It can be seen that the correlation between the noise and dR/dT is better than the previous case. This adds support to the idea that the enhanced noise in the superconducting transition region along the c-axis of a single crystal is due to thermally activated processes.

7.5.4 The effect of twin boundaries : anisotropic 1/f noise

The observed anisotropy of 1/f noise was explained before on the basis of the difference in the values of the activation energies in two directions : ab plane and c-axis. It is possible that the observed anisotropy in the 1/f noise behavior is related to the pinning mechanism. W. K. Kwok et. al. [44] have presented evidence that twin-boundary planes in a single crystal of Y_{123} act as strong pinning centers in the flux flow regime when they are aligned parallel with the magnetic field. In their experiment, the resistivity of a single crystal was measured in the transition region as a function of angle between the magnetic field and the transport measuring current. The direction of

the transport current was in the ab-plane of the single crystal. It was found that the resistivity drops sharply whenever the applied magnetic field is parallel to the twin planes. The sharp drop in the resistivity was associated to the pinning of the entire length of the vortex lines at the twin boundaries when the field is aligned along the twin planes in contrast to pinning at only local points along the vortices in the nonaligned cases. Since the vortex spacing ($\approx$ 400Å) is only slightly smaller than the distance between twin planes ($\approx 10^3$Å), most of the vortex lines will be pinned. It was pointed out by Kwok [44] that a transition of the flux-line-lattice to a liquid state would not affect the pinning or resistivity drastically.

A direct observation, using a high resolution Bitter-pattern technique [50], of vortex pinning by twin boundaries in single crystal of Y_{123} has been reported by Dolan et. al. [51]. The Bitter-pattern technique employs fine ferromagnetic particles to "decorate" the surface of a superconductor. The resulting image of the vortices is then observed with the help of an electron microscope. Their results show twin boundaries to be the major pinning sites for the vortices. Their results also indicate pinning of vortices in defect free regions indicating the existence of other pinning mechanisms.

The presence of strong pinning of vortices by twin boundaries can prevent the enhancement of noise in the transition region. Since vast pinning will occur only when flux flow is parallel to twin boundaries one would expect no enhancement of noise when current is flowing in the ab-plane of a twin single crystal. The effect will be absent in an untwinned or detwinned single crystal. Hence, the validity of the above picture can be easily tested. Such an experiment is planned for the future work.

In an another experiment one can study the noise behavior in a single crystal of Tl-based superconductor where twinning does not occur. In the case of a highly oriented bulk sample, grain boundaries will play similar roles in the pinning process as twin

boundaries. In this case the absence of enhanced noise will be expected in the transition region whenever the current is parallel to grain boundaries. More importantly, anisotropic behavior of noise will not be observed if the grain boundaries form a rectangular pattern. A Study of 1/f noise in a highly oriented bulk sample of Y_{123}, whose grains are rectangular, is planned for the future work.

7.5.5 Flux lattice melting and 1/f noise

Melting of flux-lattice in conventional superconductors has been discussed by Fisher [47] long before the discovery of high Tc superconductors. It was shown that the thermal motion of vortices can cause melting of vortex lattice at melting temperature T_m. Recent experiments of Farrell et.al. [49] and Gammel et. al. [48] have shown that this melting of the flux lattice is observed near the transition region in single crystals of Y_{123}. In either experiment, the frequency of an oscillator attached to the crystal sample was monitored in the presence of a magnetic field. The oscillations are damped by dissipation in the sample. Below the melting temperature, the bulk modulus of the vortex lattice contributes an additional stiffness to the oscillator. As the lattice melts, the response softens. This is accompanied by a peak in the dissipation. The position of the dissipation peak gives the melting temperature of vortex lattice.

The existence of a vortex liquid state can give enhancement in the noise power; since now vortices are more mobile and less pinned. The observed anisotropy of noise in the transition region can be explained from the following argument : It is found by Gammel [48] that the melting temperature of vortex lattice is a function of magnetic field. The melting temperature decreases with the increase in the field strength. For a magnetic field perpendicular to the c-axis of a single crystal of Y_{123}, the melting temperature (T_m) extrapolates to $T_c(H=0)$. This will give an enhancement of the noise

in the transition region if the current is flowing along the c-axis. the noise power will be enhanced until T_c is reached and then the enhancement will decrease due to the formation of vortex lattice and the presence of pinning of vortices. For the case when magnetic field is parallel to the c-axis, the flux melting is found to be suppressed below H_{c2} by 3.6K and it does not extrapolate to $T_c(H=0)$. In this case the enhancement of noise will be observed in the region near a temperature 3.6K below T_c. Presence of this peak cannot be determined by our electrical measurements of noise power.

The above picture, relating flux lattice melting to enhancement of 1/f noise in the transition region, has a serious conflicting result which rules out the flux lattice melting as the cause of the enhanced 1/f noise. It was found by Gammel that the melting temperature is close to 30K for the case of a single crystal of $Bi_{2.2}Sr_2Ca_{0.8}Cu_2O_8$ which has a T_c close to 75K. Measurements of 1/f noise in this class of superconductors in single crystals and thin films have been reported by Maeda [3] and Ferrari [24]. Enhanced noise was always observed near the superconducting transition region. However, magnetic noise measurements by Ferrari in the superconducting state do show a drop in the noise level by one order of magnitude near 30K indicating the existence of melting point of vortex lattice.

7.6 Conclusions

In conclusion, the source of 1/f noise in the normal state of copper oxide superconductors is supposedly due to the motion of charge carriers through the defective regions (oxygen deficient domains, twin boundaries, grain boundaries etc.) which have characteristic energy barriers. The conduction in a defective region can be either thermally activated or through the tunneling process depending on the energy of the

charge carrier and height and thickness of the barrier. The 1/f noise in such conduction processes can be explained by the MIM model (tunneling) or the random fluctuation model (thermal activation).

In the superconducting state 1/f noise, also called "magnetic-flux noise", exists and the source of this 1/f noise is the thermally activated motion of vortices. The noise power is low due to pinning of vortices by various pinning centers. The temperature dependence of noise in the superconducting state is same as that in the normal state : noise power increases with an increase in the temperature. This behavior is a direct consequence of the increase in the thermal energy of vortices and charge carriers as the temperature of the sample is increased. The increase in the thermal energy results in a large number of thermally activated processes causing an increase in the noise level.

In the superconducting transition region, the plausible source of enhanced noise is the formation of vortices and their thermally activated motion. In this temperature region both electric and magnetic 1/f noises can be measured and it is found that they both have similar temperature dependence. 1/f noise is found to be anisotropic in single crystals of $Y_1Ba_2Cu_3O_x$ near the transition region : enhanced noise is observed only in the c-directions of the crystals. The thermal fluctuation model, which in the past was shown to be successful in explaining the enhanced noise behavior in superconducting materials, is found to be totally inadequate to explain the absence of enhanced 1/f noise in the ab-plane of single crystals, in the transition region. The observed anisotropy of 1/f noise can be explained either in terms of the difference in the values of activation energy for vortex hopping along the c-direction and that along the ab-plane or the presence of twin planes or other surface defects acting as strong pinning sites for vortices.

Recently Gross et.al. [28,29] have prepared DC SQUIDs in which the junctions

are formed by the use of a single grain boundary between two single crystals in an epitaxial film of Y_{123}. The noise characteristic of the SQUIDs in the superconducting region is dominated by the voltage noise across the junction which is thermally activated and in the transition region, noise is dominated presumably by the flux noise in the film. Their conclusion is in agreement with the conclusion of this dissertation.

References:

[1] J. D. Jorgensen, Physics Today, vol. 44, #6 (1991) p34.

[2] F.N. Hooge, T.G. M. Kleinpenning, and L.K.J. Vandamme, Rep. Prog. Phys. 44 , 479 (1981)

[3] A. Maeda, Y. Nakayama, S. Takebayashi, and K. Uchinokura, Physica C 160, 443 (1989)

[4] J. Clayhold, N.P. Ong, P.H. Hor, and C.W. Chu, Phys. Rev. B 38, 7016 (1988);

[5] P. Mandal, A. Poddar, A.N. Das, B. Ghosh, and P. Choudhury, Phys. Rev. B 40, 730 (1989)

[6] J.A. Testa, Y. Song, X.D. Chen, J. Golben, S.I. Lee, B.R. Patton, and J.R. Gaines, Phys. Rev. B 38, 2922 (1988)

[7] R. F. Voss and J. Clarke, Phys. Rev. B 13 (1976) 556.

[8] S. von Molnar, A. Torressen, D. Kaiser, F. Holtzberg, and T. Penney Physical Review B Vol. 37 No. 7 (1988) 3762.

[9] Y. Song et al., Phys. Rev. Lett. 66, 825 (1991)

[10] Y.Song et al., Physica (Amsterdam) 172C, 1 (1990)

[11] A.L. McWhorter, "Semiconductor Surface Physics", edited by R.H. Kingston (University of Pennsylvania, Philadelphia, 1957).

[12] J.C. Phillips, "Physics of High-Tc Superconductors", (Academic Press, New York, 1989).

[13] J.G. Simmons, J. Appl. Phys. 35, 2472 (1964); C.A. Neugebauer and M.B. Webb, J. Appl. Phys. 33, 74 (1962).

[14] Y. Zhu et al., Appl. Phys. Lett. 54, 374 (1989).

[15] J.C. Phillips, Phys. Rev. Lett. 64, 1605 (1990).

[16] J. V. Mantese et al. Phys. Rev. B vol. 33, #12 part 1, (1986) p7897.

[17] J. V. Mantese et al. Phys. Rev. Lett. Vol 55 #20, (1985) p2212.

[18] J.Z. Liu et al. Physics Lett. A, vol. 144, #4,5 (1990) p265.

[19] D.M. Fleetwood et al. Phys. Rev. Lett. vol 64, #5, (1990) p579.

[20] J.A.Testa, Ph.D. Thesis, Dept. of Physics, Ohio State University (1988).

[21] P. Dutta and P.M. Horn, Rev. Mod. Phys. 53, 497 (1981).

[22] P. Dutta et al. Phys. Rev. Lett. 43, (1979) p646.

[23] J. Clark et al. Phys. Rev. Lett. 34, #19 (1975) p1217.

[24] M.J. Ferrari et al., Phys. Rev. Lett. 64, 72 (1990).

[25] M.J.Ferrari et al. Nature vol 341 (1989) p723.

[26] M.J. Ferrari et al., Appl. Phys. Lett. 53, 695 (1988).

[27] V.Foglietti et al. Appl. Phys. Lett. 54 (22) (1989) p2259.

[28] R.Gross et al. Appl. Phys. Lett. 57(7) (1990) p727.

[29] R.Gross et al. Physica C, 170 (1990) p315.

[30] Charles P. Poole, Jr. et al. in "Copper Oxide Superconductors" a Wiley-Interscience Publication (1988) p24.

[31] J. Z. Sun et al., Appl. Phys. Lett. 54, 663 (1989).

[32] W.E.Farneth et al., Solid State Commun. 66, 953 (1988)

[33] M. Affronte et al., Physica C 172 (1990) 131.

[34] N. Thier et al., IEEE Trans. Mag. 25(2) (1989) 2293.

[35] Yi Song's model unpublished

[36] R. S. Kwok et al., Physica C, 152 (1988) 240.

[37] P. P. Freitas et al., Phys. Rev. B 37(7) (1988) 3657.

[38] M. F. Crommie et al., Phys. Rev. B 37(16) (1988) 9734.

[39] B. W. Veal et al., Physica C, 162-164 (1989) 97.

[40] B. Rupp et al., Physica C, 162-164 (1989) 538.

[41] T. T. M. Palstra et. al. Appl. Phys. Lett. 54(8) (1989) 763.

[42] E. Zeldov et al. Phys. Rev. Lett. 62(26) (1989) 3093.

[43] E. Zeldov et. al. Appl. Phys. Lett. 56(7) (1990) 680.

[44] W. K. Kwok et al. Phys. Rev. Lett. 64(8) (1990) 966.

[45] R. Griessen et al. Phys. Rev. Lett. 64(14) (1990) 1674.

[46] S. de Brion et al. Physica C 178 (1991) 225.

[47] D. S. Fisher, Phys. Rev. B 22(3) (1980) 22.

[48] P.L. Gammel et al. Phys. Rev. Lett. 61(14) (1988) 1666.

[49] D. E. Farrell et al. Phys. Rev. Lett. 67(9) (1991) 1165.

[50] P. L. Gammel et al. Phys. Rev. Lett. 59 (1987) 2592.

[51] G. J. Dolan et al. Phys. Rev. Lett. 62(7) (1989) 827.